Pol II degradation activates cell death independently from the loss of transcription

Nicholas W. Harper[1], Gavin A. Birdsall[1], Megan E. Honeywell[1], Athma A. Pai[3], and Michael J. Lee[1,2,*]

[1] Department of Systems Biology, UMass Chan Medical School; Worcester, MA, USA.

[2] Program in Molecular Medicine, and Department of Molecular, Cell and Cancer Biology, UMass Chan Medical School; Worcester, MA, USA.

[3] RNA Therapeutics Institute, UMass Chan Medical School; Worcester, MA, USA.

* Corresponding author. Email: michael.lee@umassmed.edu

ABSTRACT

Pol II-mediated transcription is essential for eukaryotic life. While loss of transcription is thought to be universally lethal, the associated mechanisms promoting cell death are not yet known. Here, we show that death following loss of Pol II is not caused by dysregulated gene expression. Instead, death occurs in response to the loss of Pol II protein itself, specifically loss of the enzymatic subunit, Rbp1. Loss of Pol II exclusively activates apoptosis, and expression of a transcriptionally inactive version of Rpb1 rescues cell viability. Using functional genomics, we identify a previously uncharacterized mechanism that regulates lethality following loss of Pol II, which we call the **P**ol II **D**egradation-dependent **A**poptotic **R**esponse (**PDAR**). Using the genetic dependencies of PDAR, we identify clinically used drugs that owe their efficacy to a PDAR-dependent mechanism. Our findings unveil a novel apoptotic signaling response that contributes to the efficacy of a wide array of anti-cancer therapies.

INTRODUCTION

Accurate control of gene expression is critical for all cellular processes. For nuclear protein-coding genes, expression depends on the transcriptional activity of RNA polymerase II (hereafter referred to as Pol II). Pol II activity is considered a life-essential function, and prolonged inhibition of Pol II activity is expected to be universally lethal to cells[1]. In recent years, drugs designed to target the transcriptional machinery have been investigated in clinical settings, especially in the treatment of various cancers[2]. However, despite the importance of Pol II-mediated transcription and clinical interest in drugs targeting the transcriptional cycle, the mechanisms of lethality following transcriptional inhibition remain unclear.

The mechanisms of lethality following Pol II inhibition remain molecularly uncharacterized largely due to the presumption that death in this context is not regulated. Regulated or “active” cell death refers to death induced by active signaling through specific effector enzymes or defined regulatory pathways[3]. In contrast, transcriptional inhibition is generally assumed to cause death due to passive mechanisms; this begins with mRNA decay and the subsequent loss of protein, leading to some unavoidable catastrophic event. Cell death of this type is sometimes referred to as “accidental cell death”, highlighting the use of passive mechanisms, such as decay[4].

In contrast with the notion that transcriptional inhibition causes an accidental death, recent studies highlight that cells are remarkably capable of buffering against perturbations to the mRNA pool[5–9]. For instance, in normal conditions mRNA concentration scales with cell size; variations in cell size are buffered by tuning Pol II activity or mRNA decay to maintain stable mRNA concentrations[7,10]. Likewise, in perturbed conditions with reduced mRNA production, the effects are also blunted by a reduction in mRNA degradation rates[7,8]. Thus, if cells have the capacity to buffer against the downstream effects of transcriptional inhibition, why do they instead die? To address this question, we aimed to formally characterize the mechanism(s) of

58 lethality following Pol II inhibition in different contexts. We make the unexpected discovery that
59 lethality following Pol II inhibition is not caused by the general decay of mRNA and protein, and
60 instead, is specifically activated by loss of Pol II itself, which initiates a previously
61 uncharacterized apoptotic response.

62

63 **RESULTS**

64

65 **Pol II inhibition exclusively activates an apoptotic cell death**

66 To investigate the mechanisms of cell death by transcriptional inhibition, we focused on
67 triptolide and α-amanitin, two well-validated transcriptional inhibitors that result in the
68 degradation of Pol II[11,12]. We first measured the levels of Rpb1, the largest essential subunit of
69 Pol II. As expected, U2OS cells exposed to a high dose of triptolide rapidly and completely
70 degraded Rpb1, and Rpb1 degradation kinetics could be titrated in a drug dose-dependent
71 manner (Fig. 1a,b and Extended Data Fig. 1a,b). To validate that Rpb1 protein expression could
72 be used to interpret the transcriptional state, we also measured incorporation of 5-ethynyl
73 uridine (EU) into newly synthesized RNAs, which confirmed the kinetics of transcriptional
74 inhibition following triptolide exposure (Extended Data Fig. 1c-e). Similar dose and time
75 behavior was also observed following exposure to α-amanitin (Extended Data Fig. 1f).

76 To explore cell death in response to Pol II inhibition, we used 1 μM triptolide, which
77 completely inactivated transcription within ~4 hours (Fig. 1a,b and Extended Data Fig. 1d). We
78 used the Scalable Time-lapse Analysis of Cell death Kinetics (STACK) assay, which quantifies
79 both live and dead cell populations[13]. We observed that live cells proliferated normally for only
80 the first 4 hours following triptolide exposure, followed by a complete loss of proliferation,
81 coinciding with the initiation of cell death (Fig. 1c). Cell death kinetics at lower doses of triptolide

82 were similar, but with a delay in death onset that matched the later degradation of Pol II
83 (Extended Data Fig. 2a,b). Similar results were observed with α-amanitin, suggesting that rapid
84 onset of lethality is a general feature of drugs that degrade Pol II (Extended Data Fig. 2c,d).
85 Taken together, these data reveal that Pol II inhibition activates cell death much more rapidly
86 than previously appreciated, and that cell death is the primary phenotypic outcome of complete
87 transcriptional inhibition.

88 Since inhibition of Pol II initiated cell death more rapidly than expected, we next aimed to
89 characterize which death mechanism(s) are activated by loss of transcription (Extended Data
90 Fig. 3a). At least 14 distinct forms of regulated cell death have been identified[14–16]. We reasoned
91 that if cell death following loss of transcription resulted from passive protein loss, rather than an
92 active signaling process, then inhibition of any single death pathway should fail to rescue
93 viability. To test this, we genetically or chemically inhibited each death pathway, one at a time,
94 and observed the effect on cell death following triptolide exposure. To inhibit apoptosis, we
95 knocked out the mitochondrial pore-forming proteins, BAX and BAK (*BAK1*)[17,18]. Remarkably,
96 BAX/BAK double-knockout (DKO) cells were completely resistant to the lethal effects of
97 triptolide (Fig. 1d and Extended Data Fig. 3b,c). While BAX/BAK DKO cells did not die, these
98 cells were rendered completely non-proliferative within 4 hours of triptolide exposure,
99 suggesting that triptolide had completely inhibited transcription in these cells (Fig. 1d and
100 Extended Data Fig. 3d,e). Triptolide-induced death was also suppressed using the caspase
101 inhibitor, z-VAD, whereas selective inhibitors of other death pathways did not alter the lethality
102 of triptolide (Fig. 1e). Similar effects were observed following α-amanitin treatment in U2OS cells
103 (Fig. 1e and Extended Data Fig. 3f,g). Furthermore, inhibiting apoptosis suppressed the lethality
104 of transcriptional inhibitors in a panel of genetically unrelated cell lines (Fig. 1e and Extended
105 Data Fig. 3h and Supplementary Table 1). These data reveal that transcriptional inhibition –

106 even complete and prolonged transcriptional inhibition – exclusively activates a single cell death
107 pathway, the cell-intrinsic apoptotic response.

108

109 **Apoptosis is activated prior to passive loss of apoptotic regulatory proteins**

110 Pol II was completely inhibited at the doses we used, and as expected, RNA levels
111 decreased rapidly following loss of Pol II activity (Extended Data Fig. 4a-c). However, at the
112 time of death initiation, the RNA pool was only modestly decreased, with the total abundance of
113 mRNAs decayed by ~25% (Extended Data Fig. 5a,b). Furthermore, at the protein level, we
114 observe no change in the expression of canonical apoptotic regulatory proteins 4 hours after
115 triptolide exposure (Extended Data Fig. 5c-f). Thus, the rapid initiation of apoptosis following Pol
116 II inhibition could not be easily explained from the passive loss of mRNA or downstream
117 decrease in protein expression.

118 Cellular behaviors did not appear to be dysregulated, even following a more substantial
119 loss of RNAs. For instance, we observed similar RNA decay rates in U2OS and U2OS-
120 BAX/BAK DKO cells (Extended Data Fig. 6a). However, 4 days following triptolide exposure,
121 when U2OS were completely dead, BAX/BAK DKO cells display no overt signs of dysregulation,
122 despite having lost more than 90% of the RNA pool (Fig. 1f-h and Extended Data Fig. 6a-d).
123 Even 4 days after triptolide exposure, BAX/BAK DKO cells: were capable of re-adhering to
124 plates following trypsinization, produced roughly normal levels of ATP, and could actively signal
125 following exposure to external stresses, such as DNA damage (Extended Data Fig. 7a-g).
126 Normal behaviors were maintained in BAX/BAK DKO cells through ~10 days of triptolide
127 exposure, after which, cells began dying, with the entire population dying by 24 days (Fig. 1g).
128 Notably, the passive death observed in BAX/BAK DKO cells was coincident with the complete
129 loss of all mRNAs, as evaluated using absolute mRNA quantification (Fig. 1h and Extended
130 Data Fig. 8a,b). These data reveal that accidental cell death following loss of mRNA does

131 indeed occur, but is temporally distinct from the rapid death activated by Pol II loss in cells that
132 are proficient for activating apoptosis.

133 One potential explanation for these unexpected results is that the lethality induced by
134 triptolide and α-amanitin stems from an off-target mechanism, unrelated to Pol II inhibition. To
135 address this hypothesis, we evaluated the effects Pol II degradation in HAP1 cells, in which the
136 endogenous RPB1 gene (*POL2RA*) is tagged with an auxin-inducible degron (HAP1-RPB1-AID)
137 (Fig. 1i, top)[19]. While auxin had no effect on wild-type HAP1 cells, HAP1-RPB1-AID cells
138 displayed rapid cell death that initiated shortly after Pol II degradation (Fig. 1i and Extended
139 Data Fig. 9a). Furthermore, the lethality of Rpb1 degradation could be potently suppressed by
140 co-treatment with z-VAD, consistent with the results observed for triptolide and α-amanitin (Fig.
141 1i). Taken together, these data reveal that apoptosis following Pol II inhibition occurs in
142 response to an active process that is distinct from the effects of global loss of mRNA.

143

144 **Loss of mRNA production is not correlated with the induction of apoptosis**

145 While apoptotic-proficient cells die before experiencing global loss of mRNA, these cells
146 still experience a complete loss of extremely short-lived transcripts (Fig. 1h, and Extended Data
147 Fig. 6b). Mcl-1 is a potent negative regulator of apoptosis, that is unique among apoptotic
148 regulators in that it is rapidly turned over at both the mRNA and protein levels[20–23]. Indeed, Mcl-1
149 is rapidly lost following transcriptional inhibition at both the mRNA and protein levels (Extended
150 Data Fig. 10a,b). However, U2OS cells were insensitive to chemical inhibition or genetic
151 knockout of *MCL1*, and loss of *MCL1* did not alter sensitivity to triptolide (Extended Data Fig.
152 10c,d).

153 We next sought to more generally test if loss of short-lived RNAs following transcriptional
154 inhibition causes apoptosis. One simple prediction of this model is that drugs that inhibit Pol II

155 activity faster will initiate cell death proportionally faster. Thus, coordinated variation in drug-
156 induced decay and the subsequent activation of cell death may help to identify causal events.
157 To capture variation in Pol II inhibition kinetics, we profiled transcriptional inhibitors that function
158 with different inhibition timing: flavopiridol, THZ1, triptolide, actinomycin-D, α-amanitin, and
159 ethynylcytidine (Extended Data Fig. 11a-d)[24]. To quantify the kinetics of Pol II inhibition for these
160 drugs, we used immunoblotting of Rpb1 to distinguish between the levels of active and inactive
161 Pol II. Rpb1 migrates as two distinct bands. The upper band, called Pol II-o, migrates slowly due
162 to hyper-phosphorylation of the highly conserved series of heptapeptide repeats in the
163 regulatory carboxyl-terminal domain (CTD)[25]. Importantly, Pol II-o is the actively elongating pool
164 of Pol II[26]. The lower band, called Pol II-a, represents all other inactive forms of Pol II, including
165 preinitiation complex (PIC) bound, promoter paused, early pause released, and free Pol II[27]. We
166 observed significant variation in the kinetics of Pol II inhibition, with some drugs, such as the
167 Cdk9 inhibitor flavopiridol, completely inhibiting Pol II activity within minutes, while other indirect
168 inhibitors required several hours to completely inactivate Pol II (Fig. 2a-b and Extended Data
169 Fig. 11a-d). However, the fastest-acting transcriptional inhibitors were not particularly fast at
170 activating cell death. The two fastest transcriptional inhibitors, flavopiridol and THZ1, were, in
171 fact, the two slowest activators of cell death (Fig. 2b). Overall, we found no correlation between
172 the timing of Pol II inhibition and timing of cell death (Fig. 2c,d and Supplementary Table S2).
173 These data suggest that the death induced by Pol II inhibition does not result from the loss of
174 short-lived mRNAs.

175 The effects of transcriptional inhibitors could be phenocopied by degrading Rpb1 using
176 an auxin-inducible degron (Fig. 1i). Thus, we considered other mechanisms by which loss of Pol
177 II could activate apoptotic death. While previous studies have often focused on how
178 transcriptional inhibitors target actively elongating Pol II-o, our data highlight an
179 underappreciated ability of these drugs to modulate the inactive Pol II-a pool as well (Fig. 2a).

180 Notably, while loss of Pol II *activity* was not correlated with activation of death, we observed a
181 strong positive correlation between timing of cell death and timing of degradation for the *inactive*
182 Pol II protein (Fig. 2e,f and Extended Data Fig. 11e). Furthermore, the relationship between
183 inactive Pol II decay and cell death was directly proportional, such that loss of inactive Pol II
184 consistently preceded cell death by a fixed amount of time (Fig. 2f). While only a correlative
185 result, these data propose an alternative model whereby death following transcriptional
186 inhibition is not related to the inhibition of Pol II activity and the subsequent loss of mRNA, but
187 instead may result directly from the degradation of Pol II protein.

188

189 **Loss of Pol II protein, not loss of mRNA, activates apoptosis**

190 A critical challenge for determining causality in this context is the mutual dependence
191 between Pol II protein and its enzymatic function: degrading Pol II invariably inhibits Pol II
192 activity, and the existence of Pol II protein relies on Pol II-mediated transcription. Indeed, we
193 were unable to identify any compound capable of completely inhibiting transcription without also
194 inevitably degrading Pol II protein. To overcome this challenge, we developed three
195 complementary strategies for uncoupling the inhibition of Pol II activity and the degradation of
196 Pol II protein (Fig. 3a, i-iii). First, we acutely degraded Pol II without inducing subsequent loss of
197 mRNAs, by exposing cells to triptolide while concurrently inhibiting key mediators of RNA
198 degradation (Fig. 3a-i). NUP93 and EXOSC5 have been shown to be critical mediators of
199 mRNA concentration homeostasis, and acute knockdown of these proteins leads to an
200 accumulation of mRNA[7]. As expected, the mRNA pool in cells lacking NUP93 was stabilized,
201 and significantly more resistant to triptolide-induced mRNA loss than control cells (Fig. 3b).
202 Despite the stabilized mRNA pool, however, triptolide activated cell death to similar levels – and
203 with similar kinetics – in control and NUP93-KO cells (Fig. 3c). Similar results were observed in

204 EXOSC5-KO cells (Extended Data Fig. 12a,b). These data again suggest that cell death
205 following Pol II inhibition cannot be explained by the passive loss of mRNA alone.

206 Second, we sought to buffer against triptolide-induced degradation of Pol II, while
207 maintaining transcriptional inhibition (Fig. 3a-ii). Triptolide inhibits XPB, the helicase subunit of
208 TFIIH[11]. Triptolide-induced degradation of Pol II has been shown to require Cdk7 activity,
209 presumably because Cdk7 phosphorylation of Pol II facilitates removal of the pre-initiation
210 complex, resulting in the release of Pol II from chromatin, enabling Pol II degradation[27].
211 Consistent with this, co-treatment with the Cdk7 inhibitor, THZ1, blocks Pol II degradation
212 following high-dose triptolide exposure (Fig. 3d,e). Importantly, THZ1 is itself a transcriptional
213 inhibitor, and the combination of triptolide and THZ1 was as good at inhibiting Pol II activity as
214 either drug alone (Fig. 3d,f). Despite the potently inhibited transcriptional activity, we find that
215 the addition of THZ1 suppresses the lethality of triptolide while maintaining potent transcriptional
216 inhibition (Fig. 3d,g). This paradox – in which the lethal effects of transcriptional inhibition can be
217 suppressed by adding another transcriptional inhibitor – is in line with a model whereby lethality
218 results from the degradation of Pol II protein.

219 Finally, we asked if exogenous expression of a functionally inactive Pol II mutant protein
220 was sufficient to rescue viability following degradation of the endogenous Pol II pool (Fig. 3a-iii).
221 To accomplish this, we designed a Pol II "switchover" system (Fig. 3h). This system features a
222 doxycycline-inducible *RPB1* transgene completely devoid of the regulatory carboxy-terminal
223 domain (CTD) that is required for productive transcription[28–31]. In addition, the *RBP1* fragment
224 contains a known α-amanitin resistance mutation, N792D, allowing the selective degradation of
225 endogenous Pol II[12]. Conceptually, this system allows us to directly compare cell death
226 outcomes following transcriptional inhibition, using isogenic cells that either have, or do not
227 have, a pool of non-functional Pol II protein (Fig. 3i). To test this system, we stably expressed
228 the doxycycline-inducible *RPB1*-N792D-ΔCTD construct in U2OS cells expressing a Tet-On

229 trans-activation protein. These cells were pretreated with- or without doxycycline for two days to
230 enable expression of Rpb1-N792D-ΔCTD, followed by acute degradation of endogenous Pol II
231 using 10 μM α-amanitin. As expected, complete loss of endogenous Pol II was observed
232 following α-amanitin exposure, in both doxycycline-pretreated and untreated conditions (Fig. 3j).
233 However, only cells pretreated with doxycycline expressed a truncated Rpb1 protein that did not
234 respond to α-amanitin (Fig. 3j). Expression of Rpb1-N792D-ΔCTD did not inhibit the loss of
235 mRNA following α-amanitin treatment, validating that the CTD is required for productive
236 transcription (Fig. 3k, and Extended Data Fig. 13a). Importantly, expression of Rpb1-N792D-
237 ΔCTD potently suppressed α-amanitin-induced cell death (Fig. 3l). Expression of Rpb1-N792D-
238 ΔCTD had no effect on the lethality of unrelated apoptotic agents, and rendering the Rpb1-
239 ΔCTD protein sensitive to α-amanitin abolished its ability to suppresses cell death (Extended
240 Data Fig. 13b,c). These experiments demonstrate that cell death following transcriptional
241 inhibition is caused by the degradation of Pol II protein, and not loss of Pol II activity.

242

243 **Apoptosis following Pol II degradation requires PTBP1 and BCL2L12**

244 We next aimed to characterize how decreased Pol II levels are sensed and
245 communicated to initiate apoptosis. Considering the lack of prior knowledge for which processes
246 respond to loss of Pol II protein, we evaluated this question using an unbiased genome-wide
247 screening approach. We used Cas9-expressing U2OS cells, and the TKOv3 sgRNA library, to
248 evaluate the effect of all single gene knockouts on triptolide-induced lethality[32,33]. To identify
249 genes that specifically regulate cell death, rather than proliferation, we developed a simple
250 experimental approach to mechanically separate live cells from apoptotic corpses, such that
251 both populations could be sequenced independently (Fig. 4a, Extended Data Fig. 14a-f and
252 Supplementary Table 3).

253 Our screen identified more than 100 genes whose knockout significantly reduced the
254 level of triptolide-induced cell death (Fig. 4b and Supplementary Table 4). Remarkably, this
255 cohort of genes included every gene encoding an essential pro-apoptotic regulatory protein (Fig.
256 4b,c). We also identified key negative regulators of apoptosis, such as *XIAP* and BCL-xL
257 (*BCL2L1*), which increase triptolide-induced lethality when deleted (Fig. 4b,c). Our screen also
258 identified triptolide-specific genetic dependencies, including *CDK7*, in line with our finding that
259 the Cdk7 inhibitor, THZ1, also rescues triptolide-induced cell death (Fig. 4b and 3g).

260 To clarify the mechanism by which Pol II degradation activates apoptosis, we began by
261 exploring if the regulators of triptolide-induced cell death were enriched for genes involved in
262 known stress response pathways. As expected, given that Pol II degradation exclusively
263 activates apoptosis, the hits from our screen were strongly enriched for apoptotic regulatory
264 genes (Fig. 4d); however, we did not identify any other known stress response pathways that
265 might facilitate activation of apoptosis (Extended Data Fig. 15a). Due to the proximity of Pol II to
266 DNA, we paid special attention to regulators of the DNA damage response (DDR). However, the
267 DDR did not appear to be involved in triptolide-induced cell death: no regulators of the DDR
268 were hits in our screen, triptolide failed to activate DDR signaling, and knocking out TP53, an
269 essential regulator of DDR-induced apoptosis[34], had no effect on triptolide-induced cell death
270 (Extended Data Fig. 15b-d).

271 We next explored if Pol II degradation activates apoptosis through a unique and yet
272 undescribed process. Surprisingly, the two genes whose deletion most strongly suppressed
273 triptolide-induced cell death were not core apoptotic effectors, but PTBP1 and BCL2L12 (Fig. 4b
274 and Extended Data Fig. 16a). BCL2L12 is a poorly understood protein with an undefined role in
275 apoptotic activation, even though the Bcl2 family has been extensively studied in the context of
276 apoptosis[35]. PTBP1 is a multi-functional RNA binding protein, with well-established roles in
277 alternative splicing and activation of internal ribosome entry segments (IRESs)[36–38]. To validate

278 the role of these genes in triptolide-induced cell death, we generated *PTBP1* and *BCL2L12*
279 knockout cells in the U2OS genetic background. Knocking out either *PTBP1* or *BCL2L12*
280 suppressed triptolide-induced cell death, validating the results of our screen (Fig. 4e).

281 Notably, our screen identified every essential apoptotic effector downstream of
282 mitochondrial outer membrane permeabilization; however, *BCL2L12* was the only Bcl-2
283 homology (BH) domain-containing gene that suppressed death (Extended Data Fig. 16b).
284 These data suggest that PTBP1 and BCL2L12 may play a pro-apoptotic role, specifically in the
285 context of Pol II degradation. To test this idea, we explored the effect of *PTBP1* or *BCL2L12*
286 knockout in other drug contexts. As we observed for triptolide, knocking out *PTBP1* or *BCL2L12*
287 suppressed lethality following exposure to other Pol II inhibitors, such as α-amanitin (Fig. 4f and
288 Extended Data Fig. 16c,d). In contrast, knocking out *PTBP1* or *BCL2L12* failed to suppress
289 lethality in the context of canonical apoptotic agents, such as the BH3 mimetic, ABT-199, or
290 Staurosporine (Fig. 4f and Extended Data Fig. 16e,f). As expected, all apoptotic drugs failed to
291 activate death in BAX/BAK DKO cells (Fig. 4f and Extended Data Fig. 16c-f). Together, these
292 data reveal that apoptotic death induced by Pol II degradation requires PTBP1 and BCL2L12.

293

294 **Nuclear-to-cytoplasmic translocation of PTBP1 regulates death**

295 Knocking out *PTBP1* did not alter Pol II degradation, nor the triptolide-induced loss of
296 transcriptional activity, or the decay of mRNAs following triptolide exposure (Extended Data Fig.
297 17a-c). These data rule out the trivial explanation that loss of *PTBP1* inhibits triptolide activity.
298 Furthermore, triptolide-induced changes in gene expression in U2OS and PTBP1-KO cells were
299 nearly indistinguishable, and the shared expression changes between U2OS and PTBP1-KO
300 cells included apoptotic regulatory mRNAs, such as *MCL1*, which were also rapidly lost at the
301 protein level in both cell types (Extended Data Fig. 17d-f).

302 Thus, we next explored the mechanisms by which PTBP1 could regulate apoptosis
303 following Pol II degradation. PTBP1 is an RNA binding protein. Prior studies have reported a
304 post-transcriptional function for PTBP1, which can promote TNF-induced apoptosis by activating
305 IRESs to facilitate translation of apoptotic effector proteins, such as APAF1[39,40]. However, we
306 observed that APAF1 protein expression was not altered during triptolide exposure, and APAF1
307 was expressed to similar levels in WT and PTBP1-KO cells (Extended Data Fig. 17f). The best
308 described functions for PTBP1 are in regulating alternative mRNA splicing[41–44]. Intriguingly, the
309 influence of PTBP1 on triptolide-induced lethality also does not appear to be related to its role in
310 splicing. Other regulators of alternative splicing did not rescue the lethality of triptolide
311 (Extended Data Fig. 18a). Additionally, although we observed alternative splicing of known
312 PTBP1-dependent splicing events in PTBP1-KO cells, triptolide did not affect PTBP1-dependent
313 splicing, and splicing changes induced by triptolide were unaffected in PTBP1-KO cells
314 (Extended Data Fig. 18b-f)[36].

315 Many RNA binding proteins, such as PTBP1, are localized to the nucleus, and
316 accumulate in the cytoplasm following transcriptional inhibition, though the precise reason for
317 this is unclear[45,46]. Curiously, triptolide-induced lethality was rescued by knocking out the
318 nuclear exporter *XPO1*; and conversely, knocking out nuclear import factors, *RANGAP1* or
319 *KPNB1*, sensitized cells to triptolide-induced lethality (Fig. 4g). Furthermore, we observed
320 PTBP1 translocation to the cytoplasm shortly following triptolide or α-amanitin-induced Pol II
321 degradation (Fig. 4h and Extended Data Fig. 19a,b). Finally, expression of inactive Pol II (Rpb1-
322 N792D-DCTD) blocked the cytoplasmic translocation of PTBP1 and suppressed the lethality of
323 α-amanitin (Fig. 4i and Extended Data Fig. 19c). These data suggest that the cytoplasmic
324 trafficking of PTBP1 is important for its death regulatory function.

325 We performed RNAseq on cytoplasmic and nuclear fractions separately in WT and
326 PTBP1-KO cells, and found no evidence that the altered localization of PTBP1 is associated

327 with a change in mRNA localization that can causally explain triptolide-induced cell death
328 (Extended Data Fig. 19d-f). A cross-comparison of our RNAseq and chemo-genetic profiling
329 datasets further revealed no potential PTBP1-dependent transcriptional effects that could
330 causally explain triptolide-induced cell death (Extended Data Fig. 19g,h). These data further
331 support our general finding that loss of mRNA cannot causally explain cell death following
332 transcriptional inhibition. Moreover, these data support the notion that PTBP1 is a genuine
333 regulator of apoptosis, specifically in the context of Pol II degradation, and that its mechanism in
334 this context is likely unrelated to its currently known molecular functions.

335

336 **Multiple anti-cancer drugs owe their lethality to Pol II degradation**

337 We next aimed to investigate if activation of a Pol II degradation-dependent cell death
338 could be valuable in a therapeutic context. To address this question, we focused on clinically
339 relevant compounds – including those not conventionally considered transcriptional inhibitors –
340 and determined the degree to which the lethality of these drugs depended on genes required for
341 triptolide-induced cell death. We generated a simple “Transcriptional Inhibition Similarity” (TIS)
342 score to quantitatively evaluate the functional similarity of a given drug to the canonical Pol II
343 degrader, triptolide (Fig. 5a,b). We applied this signature-based strategy across 46 diverse
344 compounds, covering 16 clinically relevant drug classes (Fig. 5c and Extended Data Fig. 20a-i).
345 Strikingly, a wide array of TIS scores were observed across the dataset, with variation both
346 across and within drug classes (Fig. 5c and Extended Data Fig. 21 and Supplementary Table
347 5). High TIS scores were observed for most, but not all, drugs that directly target Pol II or
348 transcriptional Cdk proteins (Fig. 5c). Additionally, drugs that induce proteotoxic stress, such as
349 Brefeldin A, Thapsigargin, or Tunicamycin, were quite lethal, but featured low TIS scores,
350 further confirming that Pol II degradation activates death in a manner that is distinct from
351 general dysregulation of protein levels (Extended Data Fig. 21). Collectively, these data

352 highlight that clinically relevant drugs covering disparate annotated mechanisms share the
353 genetic dependencies observed for transcriptional inhibitors.

354 Because each drug was evaluated across a range of doses, our data revealed an
355 unexpectedly large degree of variation in the TIS score across doses of a drug. To more
356 precisely identify drug-dose pairs that owe their lethality to a triptolide-like mechanism, we
357 developed a binary classifier to evaluate our TIS data. We used a conservative probabilistic
358 nearest neighbors-based classification approach, in which a drug-dose pair was classified as
359 "Transcriptional inhibition-like" only if its proximity to validated Pol II degrading drugs is within
360 the neighborhood occupied by the Pol II degraders, triptolide and α-amanitin (Extended Data
361 Fig. 22a)[47,48]. Our classifier identified significant variation in drug mechanisms of lethality,
362 particularly across drugs that induce DNA damage (Fig. 5d). For instance, Idarubicin, a
363 Topoisomerase II inhibitor, was lethal at the highest 4 tested doses, but was only "TI-like" at the
364 highest dose (Fig. 5d and Extended Data Fig. 21). Conversely, the UV radiation-mimetic, 4-
365 NQO, was lethal at nearly all tested doses, but strikingly, was only TI-like at intermediate doses
366 (Fig. 5d and Extended Data Fig. 21).

367 To validate our classifier, we next tested whether drugs classified as TI-like also
368 degraded Pol II, and if this behavior was restricted to the appropriate doses. We focused on
369 Abemaciclib, given the unexpected dose dependence, in which our classifier predicts Pol II
370 degradation at only a single intermediate dose, and paradoxically, not at high doses (Extended
371 Data Fig. 22b). Consistent with our classifier, we found that Pol II is degraded following
372 exposure to 1 μM Abemaciclib, but not when exposed to a ten-fold higher dose (Fig. 5e). These
373 distinctions are particularly surprising given that Abemaciclib is lethal at both doses
374 (Supplementary Table 5). Similar paradoxical dose-dependent Pol II degradation was observed
375 for other drugs, including 4NQO, the Cdk2/4/6 inhibitor PF-06873600 (PF3600), and Idarubicin,
376 (Extended Data Fig. 22c-i).

377 Due to its widespread clinical use, we next focused on Cisplatin, a DNA cross-linking
378 drug used in the treatment of bladder, head and neck, lung, ovarian, and testicular cancers,
379 among others[49]. Strikingly, our classifier predicts that Cisplatin has a TI-like mechanism of
380 lethality at all doses that activate high levels of cell death (Fig. 5d and Extended Data Fig. 23a).
381 This was surprising, given that DNA damage can independently activate apoptosis through the
382 DDR, which is observed for other drugs in this dataset (Extended Data Fig. 21 and 23a).
383 Consistent with our classifier, we observe Pol II degradation following Cisplatin exposure at all
384 doses that induce substantial lethality (Fig. 5f and Extended Data Fig. 23b-d). These data
385 suggest that the lethality of several DNA damaging agents may hinge upon a Pol II degradation-
386 dependent apoptotic response in both a drug- and dose-dependent manner.

387 Finally, to further validate that Pol II degradation is responsible for the lethality of TI-like
388 compounds, we explored other features that are unique to this mechanism. In addition to the
389 dependence on PTBP1, BCL2L12, and the degradation of inactive Pol II protein, death kinetics
390 represent another critical feature of this mechanism. We demonstrated that canonical
391 transcriptional inhibitors activate death with consistent timing following loss of the inactive form
392 of Pol II (Fig. 2f). For drugs classified as “TI-like”, cell death kinetics were well-correlated with
393 the kinetics of inactive Pol II degradation (Fig. 5g). Cell death kinetics for negative control drugs
394 showed no relationship, and no correlation was observed between cell death timing and loss of
395 Pol II activity (Fig. 5g and Supplementary Table 6). These data reveal that the mechanisms of
396 drug-induced lethality vary in unexpected and non-trivial ways across dose, and more
397 specifically, that Pol II degradation is a common mechanism of lethality across many unrelated
398 drug classes.

399

400

401

402 **DISCUSSION**

403 The fact that transcriptional inhibition is lethal to cells is hardly surprising. However, the
404 common assumption to date has been that prolonged loss of transcription is toxic to cells due to
405 global loss of mRNA and protein. We show that death following transcriptional inhibition initiates
406 much more rapidly than previously appreciated, well before cells are experiencing stress from
407 the loss of mRNA or protein. Furthermore, we demonstrate that death occurs in response to an
408 active signaling process, which unexpectedly, is initiated by loss of the Pol II protein, not the
409 loss of Pol II transcriptional activity, nor the general decay in mRNA or protein levels. Therefore,
410 we propose that this previously uncharacterized process be termed the **P**ol II **D**egradation-
411 dependent **A**poptotic **R**esponse (**PDAR**).

412 Why has this phenotype not been observed previously? Notably, the central issue is
413 simply related to analytical resolution. Specifically, while apoptotic-deficient cells remain 100%
414 viable following Pol II degradation, these cells also cannot proliferate. Common drug response
415 metrics misinterpret the level of lethality in this context, because a non-proliferative drug-treated
416 population is already very small when compared to a rapidly dividing untreated population
417 (Extended Data Fig. 24a)[50]. Furthermore, given the lack of mechanistic insight provided by
418 conventional analysis methods, any observed difference could reasonably have been
419 interpreted as evidence that apoptosis makes a partial and/or negligible contribution to the
420 lethality of transcriptional inhibition. Our initial evaluations of transcriptional inhibitors used the
421 drug GRADE analysis method[51], and the mechanistic clarity provided by GRADE-based
422 analysis revealed that apoptotic-deficient cells completely arrest cell proliferation without
423 activating any cell death (Extended Data Fig. 24b).

424 Our study also identifies two key regulators of this process: PTBP1 and BCL2L12.
425 PTBP1 is a ubiquitously expressed RNA binding protein with several established roles in RNA
426 and translational regulation[38,40]. Notably, these prior functions appear not to contribute to

427 lethality following Pol II degradation. Our study, however, confirms that PTBP1 can translocate
428 to the cytoplasm in response to stress, which in the context of Pol II degradation, appears to
429 communicate information about Pol II protein level from the nucleus to the cytoplasm, facilitating
430 the activation of apoptosis. Additionally, *BCL2L12* is also a ubiquitously and highly expressed
431 gene. This feature distinguishes *BCL2L12* from other members of the BCL2 family, which
432 generally have low and varied expression across cell types. Furthermore, BCL2L12 is generally
433 considered an anti-apoptotic protein, and has not been described to have any pro-apoptotic
434 functions[52]. Thus, it appears that PTBP1 and BCL2L12 have unique roles in response to Pol II
435 degradation that are distinct from their previously annotated functions. Central remaining
436 questions include developing a detailed molecular mechanism by which these proteins activate
437 apoptosis following Pol II degradation, and exploring the context in which this pathway evolved
438 to be beneficial.

439 Prior to this discovery, substantial attention had already been focused on targeting the
440 transcriptional cycle in the context of cancer treatment. New drugs that target transcriptional
441 Cdk proteins appear to be promising. However, the mechanisms allowing for the selective killing
442 of cancer cells remain unclear, and are generally presumed to be dependent on loss of rapidly
443 turned over proteins, such as Myc or Mcl-1[53]. Our study highlights that many of these drugs owe
444 their lethality to the Pol II degradation-dependent mechanism that we describe. Notably, the
445 definitions used in this study for defining a Pol II degradation-dependent cell death are
446 conservative, as a drug was only characterized as PDAR-dependent if no other backup
447 mechanisms existed to facilitate death in the absence of this pathway. Importantly, our study
448 also highlights that selective killing is possible for PDAR-dependent drugs, as we identified
449 several conventional DNA damaging chemotherapies, which have long-standing clinical utility,
450 that also unexpectedly score as PDAR-dependent using our conservative criteria. Thus, future

451 studies of the PDAR pathway are likely to reveal new biomarkers that improve our ability to use
452 a wide array of anti-cancer drugs, and also may reveal new ways to selectively kill cancer cells.

Acknowledgements

We thank M. Walhout, T. Fazzio, E. Baehrecke, R. Davis, C. Navarro, T. Naylor, M. Wesley, and all members of the Lee Lab and UMass Chan Medical School DSB community for their helpful comments and suggestions throughout the development and execution of this study. We especially thank E. Calvo-Roitberg for advice related to evaluating PTBP1-dependent splicing and RNA location. Additionally, we thank J. Dekker for providing the HAP1-RPB1-AID cells.

Funding

Funding for this project was provided by the National Institute of General Medical Sciences (NIGMS) grant R35GM152194 (to M.J.L.), and the National Cancer Institute (NCI) grant F31CA284879 (to N.W.H.).

Author contributions

N.W.H. and M.J.L. conceptualized this project, including selection of methodology, analytical strategies, data visualization, and interpretation. N.W.H. performed all experiments and analyses in this study. G.A.B. assisted N.W.H. with the evaluation of cell death mechanisms activated by transcriptional inhibitors and canonical cell death activating drugs. M.E.H. generated the materials used in the chemo-genetic profiling of triptolide, and assisted with the design and analysis of chemo-genetic profiling data. A.A.P. designed the experiments and analytical strategy used in evaluating PTBP1- and triptolide-dependent changes in RNA localization and RNA splicing. The original draft of this manuscript was written by N.W.H. and M.J.L. All authors participated in manuscript review and editing.

Competing interests

The authors declare that they have no competing interests.

Data and materials availability

RNA sequencing data generated in this study can be found as FASTQ files from the Gene Expression Omnibus (GEO) with the following accession numbers: GSE283148 (triptolide exposure time course in U2OS and BAX/BAK DKO cells), GSE283149 (triptolide exposure for 8 hours in NUP93 or EXOSC5 KO cells), GSE283150 (RNA sequencing from nuclear and cytoplasmic fractionation in U2OS or PTBP1 KO cells), GSE283151 (triptolide exposure following a-amanitin in Pol II switchover system). Chemo-genetic profiling data can be found as raw FASTQ files (GSE283147), and as sequencing counts or death rates in Supplementary Tables 3 and 4, respectively. Source data associated with Fig. 1e can be found in Supplementary Table 1. Source data associated with Fig. 2 can be found in Supplementary Table 2. Source data associated with Fig. 5c can be found in Supplementary Table 5. Source data associated with Fig. 5g can be found in Supplementary Table 6. All other data are available in the main text or supplementary materials.

Code Availability

Custom MATLAB scripts for dose-response curve fitting, lethal fraction kinetics, and drug GRADE computation are deposited on GitHub (https://github.com/MJLee-Lab). Custom scripts for all other analyses are available upon request.

Materials & Correspondence

Correspondence and requests for materials should be directed to Michael Lee.

500 **MATERIALS AND METHODS**

501 **Cell lines and reagents**

502 U2OS, HT-29, H1650, WI-38, Hs578T, MDA-MB-453, MCF7 and MDA-MB-157 cells
503 were obtained from the American Type Culture Collection (ATCC). A375 cells were a gift from
504 the Green laboratory (UMass Chan Medical School). HAP1 and HAP1-RPB1-AID cells were a
505 gift from the Dekker laboratory (UMass Chan Medical School)[19]. RPE-1 cells were a gift from
506 the Pazour laboratory (UMass Chan Medical School). PC9 cells were a gift from the Pritchard
507 laboratory (Penn State University). U2OS, MDA-MB-157, A375, Hs578T, MDA-MB-453, and
508 MCF7 cells were grown in DMEM (Corning, 10-017-CV) supplemented with 2mM glutamine
509 (Corning, 25-005-CI). HT-29 cells were grown in McCoy's 5A medium (Corning, 10-050-CV).
510 WI-38 cells were grown in MEM medium (Thermo Fisher Scientific, 10370088). H1650 and PC9
511 cells were grown in RPMI medium (Thermo Fisher Scientific, 11875119). RPE-1 cells were
512 grown in low glucose DMEM (Gibco, 11885-092) and Hams F-12 (Thermo Fisher Scientific,
513 11765054) mixed at a 1:1 ratio. HAP1 cells were grown in IMDM medium (Thermo Fisher
514 Scientific, 12440053). Each media was supplemented with 10% FBS (Peak Serum, PS-FB2, lot
515 no. 21E1202) and penicillin-streptomycin (Corning, 30-002-CI). Hs578T cells were
516 supplemented with 10μg/mL insulin (Thermo Fisher Scientific, 12585014). Cell lines were
517 cultured in incubators at 37C with 5% CO2. Cell lines were maintained at low (<25) passage
518 number from the original vial.

519 U2OS-BAX/BAK1 double knockout cells (DKO) were generated previously[54] . All
520 mKate2+ cells were generated by lentiviral infection with NucLight Red Lentivirus (Sartorius,
521 4627), followed by FACS selection. HAP1-RPB1-AID cells were treated with 450 μg/mL
522 hygromycin for one week prior to use. U2OS-Cas9 expressing and U2OS-TP53 knockout cells
523 were generated previously[34] .

524 U2OS-PTBP1 and U2OS-BCL2L12 clonal knockout cells were generated using
525 CRISPR. For each gene, the highest-scoring sgRNA was selected from the TKOv3 library
526 (PTBP1: 5' – CGAGGTGTAGTAGTTCACCA – 3'; BCL2L12: 5' –
527 AGAAGGAAGCCATACTGCGG – 3') and cloned into the pX330-puro plasmid using the single-
528 step digestion-ligation protocol from the Zhang laboratory (available on the Zhang laboratory
529 Addgene page). U2OS cells were then transiently transfected with the respective pX330-
530 sgRNA-puro constructs using the FuGENE HD Transfection Reagent (Promega, E2311).
531 Transfected cells were then selected with 1 µg/mL puromycin for 3 days, followed by replating
532 and recovery for 2 days. Single cell clones were generated using limiting dilution. Clones were
533 validated by sequencing, phenotyping, and for PTBP1 knockouts, immunoblotting.

534 U2OS-MCL1, U2OS-NUP93 and U2OS-EXOSC5 knockout cells were generated using a
535 transient transfection strategy. Briefly, sgRNA (MCL1: 5' – CATGTAGAGGACCTAGAAGG – 3';
536 NUP93: 5' – GAACTTACAGGAGATCCAGC – 3'; EXOSC5: 5' – GAAGTTCTTACCTTGCAGGA
537 – 3') were cloned into pX330-puro as described above. U2OS cells were plated in six-well plates
538 (300,000 cells per well) and left to adhere overnight. The following day, cells were transiently
539 transfected with 2 µg of respective pX330-sgRNA-puro construct using FuGENE HD
540 Transfection Reagent. Cells were then selected using 1 µg/mL puromycin for either 2 days (for
541 NUP93 and EXOSC5) or 3 days (for MCL1), followed by replating and expansion for either 1
542 day (for NUP93 and EXOSC5) or 2 days (for MCL1) prior to seeding for subsequent assays.
543 Control cells were similarly transfected with non-targeting sgRNA (NONT: 5' –
544 CGGCGGTCACGAACTCCAGC – 3').

545 For the RPB1 switchover system, a FLAG-RPB1-N792D-ΔCTD fragment was PCR
546 amplified (Forward primer: 5' –
547 CAATTCCACAACACTTTTGTCTTATACTTGGATCCATGGACTACAAGGACGACGATGACA -
548 3'; Reverse primer: 5' –

549 TAGGGGGGGGGGAGGGAGAGGGGCCGGCCGGGGCTCAGCTGGGAGACATGGCACCAC
550 – 3') from FLAG-Pol2-WT (Addgene, 35175)[55] . The PCR fragment resulted in a RPB1 mutant
551 that lacked the entire C-terminal domain (repeats 1-52) and included an N-terminal FLAG tag,
552 an α-amanitin resistance mutation, and homology regions to facilitate insertion into pLVX-
553 Tre3G-IRES (Clontech, 631362)—a lentiviral vector for doxycycline-inducible gene expression.
554 pLVX-Tre3G-IRES was digested with BamHI and NotI, gel extracted and purified. The PCR
555 product was then inserted into the MCS1 of pLVX-Tre3G-IRES using Gibson Assembly (New
556 England Biolabs, E2611). The resulting plasmid, pLVX-Tre3G-FLAG-RPB1-N792D-ΔCTD, was
557 packaged into virus using Lenti-X 293T cells (Takara, 632180), along with a vector expressing
558 the Tet-On 3G transactivator protein, pLVX-Tet3G (Clontech, 631358). U2OS cells were
559 infected with pLVX-Tet3G lentivirus, followed by selection with 600 µg/mL G418. Tet-3G
560 expressing cells were then infected with pLVX-Tre3G-FLAG-RPB1-N792D-ΔCTD virus, and
561 selected with 1 µg/mL puromycin. Single cell clones were generated using limiting dilution.
562 Clones were selected for transgene expression levels approximating endogenous Rpb1 levels,
563 determined using immunoblotting.

564 Compounds used in this study were as follows. SYTOX Green (Thermo Fisher Scientific,
565 S7020), Triptolide (Sigma-Aldrich, T3652), α-amanitin (Sigma-Aldrich, A2263), ABT-737
566 (ApexBio, A8193), RSL3 (ApexBio, B6095), Elesclomol (Sigma-Aldrich, SML2651), MNNG
567 (Biosynth Carbosynth, FM11256), TNF-α (ApexBio, P1001), SM-164 (ApexBio, A8815), IAA
568 (Sigma-Aldrich, I5148), z-VAD-FMK (ApexBio, A1902), VX765 (ApexBio, A8238), TTM (Sigma-
569 Aldrich, 323446), Rucaparib (ApexBio, A4156), Necrostatin-1 (SelleckChemicals, S8037),
570 Ferrostatin-1 (SelleckChemicals, S7243), Doxycycline Hyclate (Sigma-Aldrich, D5207),
571 Actinomycin-D (SelleckChemicals, S8964, Ethynylcytidine (MedChemExpress, HY-16200),
572 Cordycepin (Sigma-Aldrich, C3394), Flavopiridol (SelleckChemicals, S1230), DRB (Sigma-
573 Aldrich, D1916), THZ1 (SelleckChemicals, S7549), THZ531 (MedChemExpress, HY-103618),

574 YKL-5-124 (MedChemExpress, HY-101257B), Abemaciclib (MedChemExpress, HY-16297A),
575 Palbociclib (ApexBio, A8316), Ribociclib (MedChemExpress, HY-15777), PF3600
576 (SelleckChemicals, S8816), PF4091 (ChemieTek, CT-PF0710), 4-NQO (SelleckChemicals,
577 E0155), Cisplatin (SelleckChemicals, S1166), Carboplatin (Sigma-Aldrich, C2538),
578 Camptothecin (SelleckChemicals, S1288), Topotecan HCl (SelleckChemicals, B2296),
579 Idarubicin HCl (SelleckChemicals, S1228), Etoposide (SelleckChemicals, S1225), Teniposide
580 (S1787 SelleckChemicals), Niraparib (SelleckChemicals, S2741), Rucaparib phosphate
581 (SelleckChemicals, S1098), Cycloheximide (Sigma-Aldrich, C1988), Homoharringtonine
582 (Sigma-Aldrich, SML1091), Anisomycin (Sigma-Aldrich, A9789), Bortezomib (ApexBio, A2614),
583 MG-132 (SelleckChemicals, S2619), Brefeldin A (Sigma-Aldrich, B7651), Thapsigargin (Sigma-
584 Aldrich, T9033), Tunicamycin (Sigma-Aldrich, T7765), ABT-199 (ApexBio, A8194), ABT-263
585 (ApexBio, A3007), Panobinostat (ApexBio, A8178), Vorinostat (ApexBio, A4084), Torin 2
586 (ApexBio, B1640), Rapamycin (ApexBio, A8167), Mirdametinib (MedChemExpress, HY-10254),
587 Buparlisib (MedChemExpress, HY-70063), Capivasertib (MedChemExpress, HY-15431), SGI-
588 1027 (ApexBio, B1622), JQ1 (SelleckChemicals, S7110), Staurosporine (SelleckChemicals,
589 S1421), H2O2 (Fisher Scientific, BP2633500), LPS (Sigma-Aldrich, L4391), Nigericin (ApexBio,
590 B7644), copper(II) chloride (ThermoFisher Scientific, 405845000), S63845 (SelleckChemicals,
591 S8383).

592 Primary antibodies used in this study were as follows. Rpb1-NTD rabbit mAb (Cell
593 Signaling Technology, 14958, 1:1,000 dilution), β-actin mouse mAb (Sigma-Aldrich, A2228,
594 1:15,000 dilution), DYKDDDDK Tag (FLAG) rabbit mAb (Cell Signaling Technology, 14793S,
595 1:1,000 dilution), PTBP1 rabbit mAb (Cell Signaling Technology, 57246S, 1:1,000 dilution),
596 Histone-H3 rabbit mAb (Cell Signaling Technology, 4499S, 1:2,000 dilution), α-tubulin mouse
597 mAb (Sigma-Aldrich, T6199, 1:10,000 dilution), pH2A.X (Ser139) rabbit mAb (Cell Signaling

598 Technology, 9718, 1:1,000 dilution), Mcl-1 rabbit mAb (Cell Signaling Technology, 5453,
599 1:1,000 dilution), Apaf-1 rabbit mAb (Cell Signaling Technology, 8723S, 1:1,000 dilution).

600

601 **Immunoblotting**

602 Cells were seeded in 6-well plates (300,000 cells per well) or 10-cm dishes (1.5 x 10^6
603 cells per dish) and left to adhere overnight, unless otherwise stated. Cells were treated the next
604 morning. At indicated timepoints, media were removed and collected. Samples were washed
605 once with PBS, and the wash was added to the collected media. SDS-lysis buffer (50 mM Tris-
606 HCl, 2% SDS, 5% glycerol, 5 mM EDTA, 1 mM NaF, 10 mM β-glycerophosphate, 1 mM PMSF,
607 1 mM Na_3VO_4, protease inhibitor tablet and phosphatase inhibitor tablet) was used to lyse the
608 cells, along with any dead cells that were pelleted from the media and wash. Lysates were
609 centrifuged through an AcroPrep 96 well 3.0 µm glass fiber/0.2 µm Bio-Inert membrane filter
610 plate (Pall Laboratory, 5053). Protein content was quantified with a BCA assay (Thermo Fisher
611 Scientific, 23225) and normalized for equal loading. Samples were boiled for 5 minutes at 95C
612 in 6x Laemmli buffer. Denatured samples were run on hand-poured SDS-PAGE gels. Gels were
613 subsequently wet transferred onto nitrocellulose membranes and blocked in 1:1 PBS: Intercept
614 Blocking Buffer (LI-COR, 927-70003) for 1 hour at room temperature. Membranes were then
615 incubated overnight on a rocking shaker at 4C in primary antibody diluted in 1:1 PBS-0.1%
616 Tween: Intercept Blocking Buffer. The following day, membranes were incubated in primary
617 anti–β-actin antibody (diluted 1:15,000) for 1 hour at room temperature, followed by two 5-
618 minute washes with PBS-0.1% Tween. Membranes were then incubated with secondary
619 antibodies (diluted 1:15,000 in 1:1 PBS-0.1% Tween: Intercept Blocking Buffer) conjugated to
620 infrared dyes (LI-COR, IRDye 680RD, goat anti-mouse immunoglobulin G (IgG) secondary,
621 catalog no. 926-68070; IRDye 800CW, goat anti-rabbit IgG secondary, catalog no. 926-32211)
622 for 1 hour at room temperature. Following four 5-minute washes with PBS-0.1% Tween and one

623 5-minute wash with PBS, blots were visualized using a LI-COR Odyssey CLx scanner. Raw
624 protein expression levels were quantified in LI-COR's ImageStudio software, background
625 subtracted, divided by β-actin signals to normalize for loading differences, then normalized per
626 gel to a reference sample (generally, an untreated sample).
627

628 **Proteome profiler-based analysis of apoptotic proteins**

629 Proteome Profiler Apoptosis Arrays (R&D Systems, ARY009) were performed according
630 to the manufacturer's instructions. Briefly, U2OS cells were collected at 1.5 million cells per
631 condition and lysed according to instructions. An equal volume of lysate (250 µL) was loaded
632 per array. Blot arrays were visualized using a LI-COR Odyssey CLx scanner, and protein
633 expression was quantified in LI-COR's ImageStudio software.
634

635 **Labelling and measurement of nascent transcription**

636 Methods for labelling and quantification of nascent transcription were adapted from
637 methods described previously[56]. Cells treated with transcriptional inhibitors were labeled with 1
638 mM 5-ethynyl uridine (Sigma-Aldrich, 909475) for 1 hour in existing media. Cells were then
639 washed with PBS, trypsinized, pelleted, and washed with cold PBS. Cells were then fixed in 4%
640 fresh formaldehyde in PBS at room temperature for 15 minutes. Fixed cells were washed with
641 cold PBS, pelleted, resuspended in ice-cold 100% methanol, and stored at -20C overnight. The
642 following day, the methanol was removed, and the cells were washed twice with PBS-0.1%
643 Tween. Cells were then incubated for 30 minutes at room temperature with 86.5 µL Click-iT
644 reaction buffer, 4 µL $CuSO_4$ buffer, 0.125 µL Alexa Fluor-azide-488 and 10.3 µL Click-iT
645 reaction buffer additive (all from Thermo Fisher Scientific, C10329). Cells were washed once
646 with 100 µL Click-iT reaction rinse buffer (from Thermo Fisher Scientific, C10329), then washed
647 two more times with PBS-0.1% Tween. Samples were resuspended in PBS-0.1% Tween,

648 filtered, and run on a Miltenyi MACSQuant VYB cytometer with laser and filter settings
649 appropriate for reading Alexa-488. Data were analyzed using FlowJo software.

650

651 **RNA sequencing with ERCC spike-ins for absolute RNA quantification**

652 For evaluation of mRNA abundance following long-term triptolide exposure in DKO cells,
653 DKO and WT cells were seeded onto six-well plates (300,000 cells per well) and left to adhere
654 overnight. Cells were then drugged the next day (D0). To evaluate the transcriptome of WT cells
655 after 1 day of triptolide, cells were cotreated with 50 μM z-VAD to inhibit loss of material from
656 cell death. Due to the long assay length, plating and drugging was staggered for each condition,
657 such that the assay endpoint for each sample occurred simultaneously. For analyses that
658 defined the 50 shortest or 50 longest half-life RNAs, these lists of RNAs were based on prior
659 studies[57] .

660 For evaluation of mRNA abundance in the context of NUP93 or EXOSC5 knockout,
661 knockout and nontargeting cells were seeded onto six-well plates (300,000 cells per well) and
662 left to adhere overnight. Cells were then drugged the next day.

663 For evaluation of mRNA abundance in Pol II switchover cells, Rpb1-N792D-ΔCTD
664 expressing cells were seeded onto six-well plates (100,000 cells per well) and left to adhere
665 overnight. The following day, the media was removed and replaced with fresh media with or
666 without 2 μg/mL doxycycline. 48 hours later, drug or vehicle was gently added to the existing
667 media.

668 For the extraction of mRNA for the experiments above, at assay endpoint cells were
669 trypsinized, counted using a hemacytometer, pelleted, washed with PBS, and moved
670 immediately to RNA extraction. Total RNA was extracted using the RNeasy Plus Mini Kit
671 (Qiagen, 74134) according to manufacturer protocol. To facilitate absolute RNA quantification,

672 polyadenylated ERCC standards (Thermo Fisher Scientific, 4456740) were diluted 1:100 in
673 nuclease-free water, and added to each sample at 1 µL/100,000 cells. ERCC spike-ins were
674 added immediately following lysis of cells in RLT-plus buffer, and prior to all subsequent total
675 RNA extraction steps using the RNeasy Plus kit. All RNA integrity numbers (RIN) were greater
676 than 9, as measured on a 4150 Tapestation System (Agilent Technologies). mRNA was isolated
677 using the NEBNext Poly(A) mRNA Magnetic Isolation Module (New England Biolabs, E7490).
678 RNAseq libraries were prepared with the NEBNext Ultra II Directional RNA Library Prep Kit
679 using the NEBNext Multiplex Oligos for Illumina (New England Biolabs, E7765 and E7600).
680 Paired-end 2 x 50nt sequencing of libraries was performed in-house on the Illumina
681 NextSeq2000 using the NextSeq 1000/2000 P2 XLEAP-SBS Reagent Kit (Illumina, 20100987).

682 Quality control for the RNAseq datasets were performed using FastQC. Transcript
683 abundance was estimated using Kallisto (0.46.1) with parameters --bootstrap-samples 30 --
684 single-overhang --rf-stranded[58]. The Ensembl GRCh38 cDNA transcriptome build, appended
685 with ERCC control transcript sequences, was used to build a Kallisto index. Gene-level counts
686 were generated in R using the tximport package[59]. Counts were normalized to ERCC spike-ins
687 using DESeq2, implemented with the function "estimateSizeFactors" with the option
688 "controlGenes" set to the identities of the 92 ERCC transcripts[60] . Counts were filtered for
689 protein coding genes in R using AnnotationHub. Differential gene expression was performed
690 with DESeq2, and fold change shrinkage was performed using the function lfcShrink with the
691 adaptive shrinkage estimator “ashr”[61] .

692

693 **Extraction of RNA and protein from nuclear and cytoplasmic fractions**

694 Nuclear-cytoplasmic fractionation was performed in such a way to facilitate extraction of
695 RNA and protein from the same cellular lysate. A similar protocol, excluding the RNA extraction
696 steps, was used in fractionation experiments that only examined protein expression. Cells were

697 plated at 6 million cells per condition (3 million cells per 15 cm plate) and left to adhere
698 overnight. Cells were then drugged the next day. At assay endpoint cells were trypsinized,
699 counted using a hemacytometer, pelleted, washed with PBS, and moved immediately to cellular
700 fractionation. Cells were first resuspended in 900 µL hypotonic lysis buffer (50 mM HEPES pH
701 7.2, 150mM NaCl, 0.5 mM EDTA, 0.15% Triton X-100, 1 mM PMSF, protease inhibitor tablet,
702 phosphatase inhibitor tablet, 20 U/mL SUPERase-In RNase inhibitor (Thermo Fisher Scientific,
703 AM2694)). Cells were pipet up and down 10 times, 1/3 of the lysate was taken as a whole-cell
704 lysate (WCL) sample, and the cells were left to swell on ice for 10 minutes. Samples were
705 centrifuged at 12,000xg for 30 seconds at 4C. The supernatant was collected as the
706 cytoplasmic fraction (CYT). The nuclear pellet was washed once with 500 µL wash buffer (PBS
707 containing 0.1% Triton X-100, 1mM EDTA and 20 U/mL SUPERase-In), centrifuged at 12,000xg
708 for 30 seconds at 4C, and the wash buffer was completely removed. The nuclear pellet was
709 then lysed in 400µL 1x nuclear lysis buffer (50 mM HEPES pH 7.2, 150mM NaCl, 0.5 mM
710 EDTA, 1% Triton X-100, 0.5% Sodium Deoxycholate, 0.2% SDS, 1 mM PMSF, protease
711 inhibitor tablet, phosphatase inhibitor tablet, 20 U/mL SUPERase-In). 10x nuclear lysis buffer
712 was added to WCL and CYT fractions to equalize surfactant amounts to that of the nuclear
713 fraction. Each resulting lysate was divided in half to facilitate either downstream protein analysis
714 or RNA extraction.

715 For protein fractions, 100x Benzonase buffer (50 mM Tris-HCl, 20 mM NaCl, 2 mM
716 $MgCl_2$, 2000 U/mL Benzonase Nuclease (Sigma Aldrich, E1014)) was added to lysates. Lysates
717 were kept on ice for 30 minutes with periodic vortexing. The BCA assay was performed on all
718 cellular fractions, and 10 µg of each lysate was subjected to immunoblotting as described
719 above. Total protein was detected using the Revert 700 Total Protein Stain Kit (LI-COR, 926-
720 11010) prior to incubation with primary antibody.

721 For extraction of total RNA from RNA fractions, samples were subjected to the RNeasy
722 Plus manufacturer protocol with the following modifications. 3.5x sample volume of RLT-plus
723 buffer was added to cellular fractions. Prior to removal of genomic DNA using the gDNA
724 Eliminator spin column, ERCC standards (diluted 1:10) were added to each lysate at a
725 concentration of 1 µL/ 1 million cells (or similarly, 1 million nuclei or 1 million cell cytoplasm's).
726 Following genomic DNA removal, 2.5x original lysate volume of 100% ethanol was added to
727 each flowthrough, and subsequent steps of the RNeasy Plus protocol were followed as
728 standard. mRNA was isolated as above. Sequencing libraries were prepared with the NEBNext
729 Ultra II Directional RNA Library Prep Kit, using manufacturer recommended modifications to
730 generate large (~450nt) inserts. Paired-end 2 x 150nt sequencing of libraries was performed in-
731 house on the Illumina NextSeq2000 using the NextSeq 2000 P3 Reagent Kit (Illumina,
732 20040561).

733

734 **Alternative splicing analysis from RNA sequencing data**

735 To facilitate detection of splice-level events, cytoplasmic and nuclear RNAseq FASTQ
736 files corresponding to the same biological samples (above) were pooled. Regulated splicing
737 events were detected and analyzed with VAST-TOOLS[62,63] . Briefly, reads were aligned to the
738 human genome (hg38) using the align function. Differential splicing events were identified using
739 the diff function (with parameters -S 2). Events were filtered for adequate coverage using the
740 tidy function (with parameters -min_N 4, --noVLOW, --min_SD 5, and --p_IR). Splicing events
741 were considered significantly different if the VAST-TOOLS reported expected absolute ΔPSI
742 value was greater than 0.1 and if the minimum value (95% confidence) of the absolute ΔPSI
743 value was greater than 0.

744

745 **STACK assay for kinetic evaluation of drug responses**

746 The STACK assay was used to evaluate cell proliferation and cell death continuously
747 over time using microscopy, as previously described[13] . Briefly, mKate2+ cells were seeded into
748 96-well black-sided plates, and left to adhere overnight. The following day, cells were given
749 drugged media containing 50 nM SYTOX Green, and imaged over time time-lapsed images
750 were collected using an IncuCyte S3 (Essen Biosciences). Images were collected with a 10x
751 objective with acquisition in the green channel ex: 460 ± 20, em: 524 ± 20, acquisition time:
752 300ms; and red channel ex:585 ± 20, em: 635 ± 70, acquisition time: 400ms. Counts of dead
753 (green) and live (red) cells were determined using the built-in IncuCyte software (Essen
754 Biosciences) and exported for analysis using a custom MATLAB script.

755 For the long-term evaluation of BAX/BAK DKO cells following triptolide, accurate dead
756 cell measurements using STACK as described above are insufficient, as identification of a dead
757 cell from an image is no longer possible after the dead cell fully degrades away. To overcome
758 this technical confound, a modified STACK assay was used, taking advantage of the FLICK
759 assay (described in detail below), which does not rely on image segmentation for cell
760 quantification. Cells were seeded and drugged as above, at a high density (15,000 cells per
761 well). Separate plates were prepared for each timepoint, whereby cells were first imaged using
762 an EVOS FL Auto 2 automated microscope (ThermoFisher Scientific). Images were acquired
763 using a 10x objective (EVOS 10x objective, Cat #: AMEP4681). Sytox images were acquired
764 using a GFP filter cube (EVOS LED Cube, GFP, Cat #: AMEP4651, ex: 470/22, em: 525/50,
765 acquisition time: 13.5ms) Mkate2+ images were acquired using a TexasRed filter cube (EVOS
766 LED Cube TxRed, Cat #: AMEP4655, ex: 585/29, em: 628/32, acquisition time: 642.0ms).
767 Following imaging, FLICK was performed as an endpoint measurement to obtain lethal fraction
768 values, as described below. Images were linearly adjusted using a custom MATLAB script.

769

770 **Quantification of drug-induced cell death using the FLICK assay**

771 The FLICK assay was performed as described[54,64] . Briefly, 90 µL of cells were seeded
772 at a density of 2,000-5,000 cells per well in black-sided optical-bottom 96-well plates (Greiner
773 Bio-One, 655090) and left to adhere overnight. The following day, cells were treated with 10 µL
774 of media containing the indicated compound/s along with SYTOX Green, resulting in a final
775 SYTOX concentration of 2 µM. Fluorescence was monitored at various times following drugging
776 with a Tecan Spark (running SparkControl software version 2.2) microplate reader (ex: 503, em:
777 524). Gain was set to achieve a linear relationship between SYTOX signal and dead cell
778 number. To obtain the total cell number at the time of drugging, a duplicate "T0" plate was lysed
779 in 0.15% Triton X-100 and 2 µM SYTOX for 2-4 hours at 37C prior to taking a fluorescence
780 reading. Total cell number for each condition at the end of the assay was similarly determined
781 by lysing cells in 0.15% Triton X-100. From these measurements (dead cells at each timepoint,
782 along with total cell numbers at the beginning and end of the assay), live cell numbers over time
783 can be inferred and all calculations to determine LF, FV, RV and GR can be made [50]:

784 $$LF = \frac{Dead}{Live+Dead}, FV = \frac{Live}{Live+Dead}, RV = \frac{Live_{Trt}}{Live_{Unt}}, GR = 2^{\frac{\left(\frac{log_2(\frac{Live_{Trt}}{Live_{T0}})}{log_2(\frac{Live_{Unt}}{Live_{T0}})}\right)}{}} - 1$$

785 All analyses were performed using custom MATLAB scripts. Dose-response curves were fit
786 using a 4-parameter sigmoidal equation. Lethal fraction kinetics were fit using the lag-
787 exponential death (LED) equation [13]:

788 $$LF(t) = LF_0 + (LF_P - LF_0)(1 - e^{-D_R(t-D_O)})$$

789 All analyses were performed using custom MATLAB scripts. All data were fit with the "fit"
790 function in MATLAB using nonlinear least-squares.

791

792

793 **Drug GRADE-based analysis of drug responses**

794 True proliferation rates and death rates were calculated using the GRADE method, as
795 previously described[51] . Conceptually, the GRADE method infers the true, underlying cell
796 proliferation rates and death rates of cell population by cross-referencing experimentally
797 measured death rates (FV or LF) and net population growth rates (GR) with computational
798 simulations. To begin, we simulated all pairwise combinations of 500 proliferation rates and 500
799 death rates using the following equations where C_0 = initial cell number, t = assay length, τ =
800 proliferation rate, and D_R = death rate.

801 $$Live\ Cell\ Number = \left(C_0 * 2^{\left(\frac{t}{\tau}\right)}\right) - \left(C_0 * 2^{\left(\frac{t}{\tau}\right)} * D_R\right)$$

802 $$Dead\ Cell\ Number = C_0 * 2^{\left(\frac{t}{\tau}\right)} * D_R$$

803 FV and GR values (defined above) were then calculated for each simulated proliferation rate
804 and death rate pair. Next, for a given condition, experimentally determined FV and GR values
805 were calculated (as above). The simulated proliferation rate and death rate that yield the
806 empirically determined FV and GR values was then found.

807

808 **Quantification of Pol II half-life**

809 Half-lives for Pol II-a and Pol II-o were determined using temporally resolved quantitating
810 immunoblotting using an antibody recognizing the N terminal domain of Rpb1 (Cell Signaling,
811 14958S), as described above. Immunoblots were quantified in ImageStudio 3.1.4, normalized to
812 β-actin, then normalized to the untreated sample (time 0) on each gel respectively, generating
813 an abundance value relative to steady state. Data were fit to a two-term exponential decay
814 function in MATLAB, relative to the highest Rpb1 signal observed over the time course. Half-
815 lives determined from the fits, as the time at which half-maximal signal was reached. To

816 correlate Pol II half-lives with cell death timing, the LF50 time was similarly found from lag-
817 exponential death (LED) fits to STACK data. LF50 was defined as the time at which half of the
818 maximum observed LF (measured or inferred after 72 hours) was reached.

819

820 **Pol II Switch over system**

821 For experiments involving the RPB1 switchover system, cells were seeded as described
822 for the respective experiment. The following day, cells we treated with or without 2 μg/mL
823 Doxycycline (Sigma, D5207) for 48 hours to induce the expression of FLAG-RPB1-N792D-
824 ΔCTD. 10 μM α-amanitin was added to the cells without removing the conditioned media to
825 degrade the endogenous Pol II.

826

827 **Chemo-genetic profiling of triptolide-induced cell death**

828 Conventional approaches used for these "chemo-genetic profiling" studies are unable to
829 accurately identify death-regulatory genes due to the confounding effects of varied proliferation
830 rates between cells harboring different gene knockouts[34]. In general, specialized analytical
831 methods are required to identify death-regulatory genes when drug-induced lethality occurs in a
832 proliferative population, at low rates relative to proliferation, or via non-apoptotic mechanisms.
833 However, in this case, we recognized that triptolide-induced death is: 1) exclusively apoptotic, 2)
834 occurring rapidly (before the effects of varied proliferation can be observed in the population),
835 and 3) activated at high rates (such that large numbers of dead cells accumulate before
836 apoptotic corpses have decayed). Thus, we developed a simple experimental approach to
837 mechanically separate live cells from apoptotic corpses, such that both populations could be
838 sequenced independently.

839 The genome-wide CRISPR screen was performed using the Toronto KnockOut Library
840 v3 (TKOv3), which contains 4 sgRNA per gene, along with 142 non-targeting sgRNA[65] . U2OS-
841 Cas9 expressing cells were selected with 5 µg/mL blasticidin for 5 days. Following selection,
842 cells were divided into two replicates, which would be handled separately for the remainder of
843 the assay. Cells were then transduced with the TKOv3 viral library using a 'spinfection' method.
844 To maintain sufficient library coverage, more than 200 million cells were transduced per
845 replicate, at an MOI of 0.3. To do this, cells were divided into 12-well plates at a density of 2
846 million cells per along with 75 µL virus and 0.8 µg/mL polybrene (Millipore, TR1003G). Plates
847 were centrifuged at 37 °C for 2 h at 830*g*. Following spinfection, virus-containing media was
848 gently removed and replaced with fresh media, and cells were returned to the incubator
849 overnight. The following morning, cells were moved out of the 12-well plates and onto 15 cm
850 dishes. The following day, cells were treated with 1 µg/mL puromycin for 3 days, followed by a
851 two-day expansion without selection. Cells were then seeded onto 15cm plates and let to
852 adhere overnight prior to drugging. At the time of drugging, a T0 sample was taken from the cell
853 population and frozen, at a population size 650x that of the library size. The rest of the cells
854 were treated with either 1 µM triptolide or DMSO. Cells were incubated for 32 hours in drug,
855 resulting in approximately 50% cell death. Apoptotic corpses, which become non-adherent,
856 were removed and saved. Plates were washed with PBS to dislodge any remaining dead cells,
857 and PBS wash was added with the separated dead cell fraction. The adherent cells remaining
858 on the plate were the live cell population. The live cells were trypsinized and collected. Each
859 condition was collected such that a minimum of 650x library coverage was achieved per
860 replicate.

861 Genomic DNA was extracted using the Wizard Genomic DNA Purification Kit (Fisher
862 Scientific, PR-A1125). sgRNA sequences were PCR amplified out of the genomic DNA, and gel-

863 extracted and purified. A second round of PCR added sequencing adaptors and multiplexing
864 barcodes, and libraries were pooled and sequenced on a HiSeq 4000 at 500× coverage.

865 The FASTX-Toolkit (0.0.14) was used to trim reads to get just CRISPR guide sequences
866 (parameters: -f 23 -l 42). Trimmed reads were mapped to the TKOv3 library with Bowtie (1.3.0)
867 allowing for 2 mismatches (parameters: -v 2 -m 1). Samples were normalized for sequencing
868 depth using median of ratios method implemented in DESeq2. Guides with low counts
869 (approximately the bottom 2% of guides) were removed from the library. sgRNA-level $\log_2$ fold-
870 changes were determined using DESeq2, and were then z-scored to the distribution of non-
871 targeting sgRNA. The median sgRNA-level z-score was determined for each gene to collapse
872 scores to the gene level. An empiric *P* value was determined for each gene by bootstrapping
873 from the sgRNA-level fold change scores of non-targeting guides, and was FDR corrected using
874 the Benjamini–Hochberg procedure. An FDR cutoff of 0.1 was used to determine genes that
875 significantly alter the cell death rate following triptolide. Gene set enrichment using an FDR-
876 corrected one-tailed Fishers Exact test was performed to test if any apoptotic-related pathways
877 from the Molecular Signatures Database (MSigDB) were overrepresented among genes whose
878 knockout significantly reduced triptolide-induced death.

879

880 **Evaluation of drug TIS score**

881 FLICK was used to determine lethal fraction kinetics in U2OS, PTBP1-KO, BCL2L12-
882 KO, and *BAX/BAK* DKO cells across a panel of 46 drugs, across 7 half-log dilutions, and
883 spanning the following 16 classes. Pol II degraders (Triptolide, 1 – 0.001 μM; α-amanitin, 10 –
884 0.01 μM). RNA synthesis inhibitors (Actinomycin-D, 1 – 0.001 μM; Ethynylcytidine, 10 – 0.01
885 μM; Cordycepin, 100 – 0.1 μM). Transcriptional CDK inhibitors (Flavopiridol, 10 – 0.01 μM;
886 DRB, 100 – 0.1 μM; THZ1, 10 – 0.01 μM; THZ531, 10 – 0.01 μM; YKL-5-124, 31.6 – 0.0316
887 μM). Cell cycle CDK inhibitors (Abemaciclib, 10 – 0.01 μM; Palbociclib, 10 – 0.01 μM; Ribociclib,

888 10 – 0.01 μM; PF3600, 31.6 – 0.0316 μM; PF4091, 31.6 – 0.0316 μM). DNA crosslinking agents
889 (4-NQO, 31.6 – 0.0316 μM; Cisplatin, 100 – 0.1 μM; Carboplatin, 316 – 0.316 μM).
890 Topoisomerase I inhibitors (Camptothecin, 10 – 0.01 μM; Topotecan, 31.6 – 0.0316 μM).
891 Topoisomerase II inhibitors (Idarubicin, 1 – 0.001 μM; Etoposide, 31.6 – 0.0316 μM; Teniposide,
892 31.6 – 0.0316 μM). PARP inhibitors (Niraparib, 100 – 0.1 μM; Rucaparib, 100 – 0.1 μM).
893 Translational inhibitors (Cycloheximide, 100 – 0.1 μM; Homoharringtonine, 10 – 0.01 μM;
894 Anisomycin 316 – 0.316 μM). Proteasome inhibitors (Bortezomib, 1 – 0.001 μM; MG132, 10 –
895 0.01 μM). ER- and proteotoxic-stress inducers (Brefeldin A, 31.6 – 0.0316 μM; Thapsigargin,
896 31.6 – 0.0316 μM; Tunicamycin, 10 – 0.01 μM). BH3 mimetics (ABT-199, 100 – 0.1 μM; ABT-
897 263, 100 – 0.1 μM; ABT-737, 31.6 – 0.0316 μM). HDAC inhibitors (Panobinostat, 1 – 0.001 μM;
898 Vorinostat, 100 – 0.1 μM). mTOR inhibitors (Torin2, 31.6 – 0.0316 μM; Rapamycin, 10 – 0.01
899 μM). MEK/PI3K/AKT inhibitors (Mirdametinib, 31.6 – 0.0316 μM; Buparlisib, 31 – 0.0316 μM;
900 Capivasertib, 31.6 – 0.0316 μM). Others (SGI-1027, 31.6 – 0.0316 μM; JQ1, 100 – 0.1 μM;
901 Staurosporine, 10 – 0.01 μM).

902 Lethal fraction kinetics were fit to a lag exponential death (LED) equation. Non-lethal
903 conditions were defined as those having a maximum observed lethal fraction less than 0.16,
904 approximately double the death observed in untreated cells. Cells were further classified as
905 apoptotic or non-apoptotic by thresholding a 50% reduction in maximum lethal fraction in the
906 BAX/BAK DKO background compared to U2OS cells. To determine the “Transcription Inhibition
907 Similarity” (TIS) score for a particular drug-dose pair, the area under the LED fit (AUC) was
908 determined, and the baseline cell death was removed by subtracting out the AUC of untreated
909 cells. The difference in drug response between KO and U2OS cells was defined as 1 minus the
910 AUC ratio of KO over U2OS. This value, determined for PTBP1-KO and BCL2L12-KO
911 separately, was summed. Finally, scores were divided by that of 1 μM triptolide, such that a
912 score of one denotes a functional genetic signature equal to that of triptolide.

913 **Probabilistic drug classifier**

914 Drugs were classified as “triptolide-like” based on their dependency on PTBP1,
915 BCL2L12, BAX, and BAK1 for causing cell death. To perform this functional genetic
916 classification, we adapted an established approach used previously[47,48] . Briefly, for each drug-
917 dose pair, AUC ratios between each KO and U2OS were determined. This places each drug-
918 dose pair in a 3-dimensional functional genetic space. The “neighborhood” of transcriptional
919 inhibitors was calculated as the mean of pairwise Euclidean distances between validated Pol II
920 degraders (triptolide and α-amanitin) in this space. The linkage ratio describes the similarity of a
921 query compound to triptolide and α-amanitin and defines how much the neighborhood expands
922 or shrinks after the query compound is included in it. A set of negative controls, defined as a set
923 of drugs with known mechanism of action distinct from transcriptional inhibition, is then forced to
924 be included in the transcriptional inhibitor neighborhood, iteratively, causing the neighborhood to
925 expand or shrink. BH3 mimetics (ABT-199, ABT-263, ABT-737), Topoisomerase inhibitors
926 (Etoposide, Camptothecin, Idarubicin, Topotecan, and Teniposide), and ER-stress inducers
927 (Thapsigargin, Tunicamycin, and Brefeldin A) were used to generate the false expansion. This
928 process of “false expansion” generates an empirically defined null distribution of linkage ratios.
929 A linkage ratio for each drug-dose pair is then determined and compared to the null distribution
930 to derive a *P* value. *P* values are then FDR corrected using the Benjamini–Hochberg procedure.

931

932 **Data analysis and statistics**

933 Unless otherwise noted, data analysis and statistics was performed in MATLAB (version
934 R2024b) using built-in functions. Bar plots were generated in GraphPad Prism 10. ImageStudio
935 3.1.4 was used to analyze western blots. Flow cytometry analysis was performed using FlowJo
936 version 10.8.1 software.

937 **SUPPLEMENTARY TABLES**

938 **Supplementary Table 1: Mechanisms of cell death activated by Pol II degrading drugs.**
939 Raw drug response data for triptolide and a-amanitin in the presence or absence of pathway
940 specific inhibitors of certain death pathways (related to Fig. 1e). Canonical activators of
941 ferroptosis, cuproptosis, parthanatos, necroptosis, and apoptosis are included as controls. Data
942 are fractional viability measurements made using the FLICK assay.

943

944 **Supplementary Table 2: Quantification of Pol II-o inactivation and Pol II-a decay kinetics**
945 **following transcriptional inhibition.** Quantified intensities for Pol II-o and Pol II-a following
946 exposure to transcriptional inhibitors at varied doses. Data are related to Fig. 2.

947

948 **Supplementary Table 3: Raw sequencing counts from chemo-genetic profiling of**
949 **triptolide treated U2OS cells.** Raw sgRNA-level counts table from chemo-genetic profiling of
950 U2OS cells exposed to 1 μM triptolide. Data are related to Fig. 4a and b.

951

952 **Supplementary Table 4: Genetic dependencies of triptolide-induced cell death.** Gene-level
953 drug-induced growth rates and death rates from chemo-genetic profile of triptolide in U2OS
954 cells. Data are related to Fig. 4b.

955

956 **Supplementary Table 5: TIS score based classification to identify "TI-like" compounds.**
957 Raw lethality data, TIS score, and classification linkage ratio used in the identification of new
958 "TI-like" compounds. Data are related to Fig. 5a-d.

959 **Supplementary Table 6: Validation of new "TI-like" compounds.** Quantified intensities for
960 Pol II-o and Pol II-a following exposure to compounds characterized as "TI-like" or "Not TI-like"
961 at varied doses. Data are related to Fig. 5g.

962 **REFERENCES**

963

964 1. Tsherniak, A. *et al.* Defining a Cancer Dependency Map. *Cell* **170**, 564-570.e16 (2017).

965 2. Vervoort, S. J. *et al.* Targeting transcription cycles in cancer. *Nat. Rev. Cancer* **22**, 5–24
966 (2022).

967 3. Green, D. R. The Coming Decade of Cell Death Research: Five Riddles. *Cell* **177**, 1094–
968 1107 (2019).

969 4. Tang, D., Kang, R., Berghe, T. V., Vandenabeele, P. & Kroemer, G. The molecular machinery
970 of regulated cell death. *Cell Res* **29**, 347–364 (2019).

971 5. Haimovich, G. *et al.* Gene Expression Is Circular: Factors for mRNA Degradation Also Foster
972 mRNA Synthesis. *Cell* **153**, 1000–1011 (2013).

973 6. Sun, M. *et al.* Global Analysis of Eukaryotic mRNA Degradation Reveals Xrn1-Dependent
974 Buffering of Transcript Levels. *Mol. Cell* **52**, 52–62 (2013).

975 7. Berry, S., Müller, M., Rai, A. & Pelkmans, L. Feedback from nuclear RNA on transcription
976 promotes robust RNA concentration homeostasis in human cells. *Cell Syst* (2022)
977 doi:10.1016/j.cels.2022.04.005.

978 8. Slobodin, B. *et al.* Transcription Dynamics Regulate Poly(A) Tails and Expression of the RNA
979 Degradation Machinery to Balance mRNA Levels. *Mol. Cell* **78**, 434-444.e5 (2020).

980 9. Hartenian, E. & Glaunsinger, B. A. Feedback to the central dogma: cytoplasmic mRNA decay
981 and transcription are interdependent processes. *Crit. Rev. Biochem. Mol. Biol.* **54**, 385–398
982 (2019).

983 10. Swaffer, M. P. *et al.* RNA polymerase II dynamics and mRNA stability feedback scale mRNA
984 amounts with cell size. *Cell* **186**, 5254-5268.e26 (2023).

985 11. Titov, D. V. *et al.* XPB, a subunit of TFIIH, is a target of the natural product triptolide. *Nat*
986 *Chem Biol* **7**, 182–188 (2011).

987 12. Nguyen, V. T. *et al.* In Vivo Degradation of RNA Polymerase II Largest Subunit Triggered by
988 α-Amanitin. *Nucleic Acids Res.* **24**, 2924–2929 (1996).

989 13. Forcina, G. C., Conlon, M., Wells, A., Cao, J. Y. & Dixon, S. J. Systematic Quantification of
990 Population Cell Death Kinetics in Mammalian Cells. *Cell Syst* **4**, 1–18 (2017).

991 14. Galluzzi, L. *et al.* Molecular mechanisms of cell death: recommendations of the
992 Nomenclature Committee on Cell Death 2018. *Cell Death Differ* **25**, 1–56 (2018).

993 15. Holze, C. *et al.* Oxeiptosis, a ROS-induced caspase-independent apoptosis-like cell-death
994 pathway. *Nat Immunol* **19**, 130–140 (2018).

995 16. Tsvetkov, P. *et al.* Copper induces cell death by targeting lipoylated TCA cycle proteins.
996 *Science* **375**, 1254–1261 (2022).

997 17. Wei, M. C. *et al.* Proapoptotic BAX and BAK: a requisite gateway to mitochondrial
998 dysfunction and death. *Science* **292**, 727–730 (2001).

999 18. Lindsten, T. *et al.* The Combined Functions of Proapoptotic Bcl-2 Family Members Bak and
1000 Bax Are Essential for Normal Development of Multiple Tissues. *Mol. Cell* **6**, 1389–1399 (2000).

1001 19. Valton, A.-L. *et al.* A cohesin traffic pattern genetically linked to gene regulation. *Nat. Struct.*
1002 *Mol. Biol.* **29**, 1239–1251 (2022).

1003 20. Cidado, J. *et al.* AZD4573 Is a Highly Selective CDK9 Inhibitor That Suppresses MCL-1 and
1004 Induces Apoptosis in Hematologic Cancer Cells. *Clin. Cancer Res.* **26**, 922–934 (2020).

1005 21. Sancho, M., Leiva, D., Lucendo, E. & Orzáez, M. Understanding MCL1: from cellular
1006 function and regulation to pharmacological inhibition. *FEBS J.* **289**, 6209–6234 (2022).

1007 22. Widden, H. & Placzek, W. J. The multiple mechanisms of MCL1 in the regulation of cell fate.
1008 *Commun. Biol.* **4**, 1029 (2021).

1009 23. Kotschy, A. *et al.* The MCL1 inhibitor S63845 is tolerable and effective in diverse cancer
1010 models. *Nature* **538**, 477–482 (2016).

1011 24. Bensaude, O. Inhibiting eukaryotic transcription. Which compound to choose? How to
1012 evaluate its activity? *Biochem Soc Symp* **2**, 103–108 (2014).

1013 25. Zhang, J. & Corden, J. L. Phosphorylation causes a conformational change in the carboxyl-
1014 terminal domain of the mouse RNA polymerase II largest subunit. *J. Biol. Chem.* **266**, 2297–
1015 2302 (1991).

1016 26. Cadena, D. L. & Dahmus, M. E. Messenger RNA synthesis in mammalian cells is catalyzed
1017 by the phosphorylated form of RNA polymerase II. *J. Biol. Chem.* **262**, 12468–12474 (1987).

1018 27. Steurer, B. *et al.* Live-cell analysis of endogenous GFP-RPB1 uncovers rapid turnover of
1019 initiating and promoter-paused RNA Polymerase II. *Proc National Acad Sci* **115**, E4368–E4376
1020 (2018).

1021 28. Jacobs, E. Y., Ogiwara, I. & Weiner, A. M. Role of the C-Terminal Domain of RNA
1022 Polymerase II in U2 snRNA Transcription and 3′ Processing. *Mol. Cell. Biol.* **24**, 846–855
1023 (2004).

1024 29. Dahmus, M. E. Reversible Phosphorylation of the C-terminal Domain of RNA Polymerase
1025 II*. *J. Biol. Chem.* **271**, 19009–19012 (1996).

1026 30. McCracken, S. *et al.* The C-terminal domain of RNA polymerase II couples mRNA
1027 processing to transcription. *Nature* **385**, 357–361 (1997).

1028 31. Egloff, S. *et al.* Serine-7 of the RNA Polymerase II CTD Is Specifically Required for snRNA
1029 Gene Expression. *Science* **318**, 1777–1779 (2007).

1030 32. Mair, B. *et al.* Essential Gene Profiles for Human Pluripotent Stem Cells Identify
1031 Uncharacterized Genes and Substrate Dependencies. *Cell Rep.* **27**, 599-615.e12 (2019).

1032 33. Hart, T. *et al.* Evaluation and Design of Genome-Wide CRISPR/SpCas9 Knockout Screens.
1033 *G3 Genes Genomes Genetics* **7**, 2719–2727 (2017).

1034 34. Honeywell, M. E. *et al.* Functional genomic screens with death rate analyses reveal
1035 mechanisms of drug action. *Nat. Chem. Biol.* 1–10 (2024) doi:10.1038/s41589-024-01584-7.

1036 35. Kale, J., Osterlund, E. J. & Andrews, D. W. BCL-2 family proteins: changing partners in the
1037 dance towards death. *Cell Death Differ.* **25**, 65–80 (2018).

1038 36. Iannone, C. *et al.* PTBP1-activated co-transcriptional splicing controls epigenetic status of
1039 pluripotent stem cells. *Mol. Cell* **83**, 203-218.e9 (2023).

1040 37. Zhu, W. *et al.* Roles of PTBP1 in alternative splicing, glycolysis, and oncogensis. *J Zhejiang*
1041 *Univ-sc B* **21**, 122–136 (2020).

1042 38. Sawicka, K., Bushell, M., Spriggs, K. A. & Willis, A. E. Polypyrimidine-tract-binding protein: a
1043 multifunctional RNA-binding protein. *Biochem Soc T* **36**, 641–647 (2008).

1044 39. Bushell, M. *et al.* Polypyrimidine Tract Binding Protein Regulates IRES-Mediated Gene
1045 Expression during Apoptosis. *Mol. Cell* **23**, 401–412 (2006).

1046 40. King, H. A. *et al.* Remodelling of a polypyrimidine tract-binding protein complex during
1047 apoptosis activates cellular IRESs. *Cell Death Differ* **21**, 161–171 (2014).

1048 41. Kafasla, P. *et al.* Defining the roles and interactions of PTB. *Biochem. Soc. Trans.* **40**, 815–
1049 820 (2012).

1050 42. Xue, Y. *et al.* Genome-wide Analysis of PTB-RNA Interactions Reveals a Strategy Used by
1051 the General Splicing Repressor to Modulate Exon Inclusion or Skipping. *Mol. Cell* **36**, 996–1006
1052 (2009).

1053 43. Keppetipola, N., Sharma, S., Li, Q. & Black, D. L. Neuronal regulation of pre-mRNA splicing
1054 by polypyrimidine tract binding proteins, PTBP1 and PTBP2. *Crit. Rev. Biochem. Mol. Biol.* **47**,
1055 360–378 (2012).

1056 44. Llorian, M. *et al.* Position-dependent alternative splicing activity revealed by global profiling
1057 of alternative splicing events regulated by PTB. *Nat. Struct. Mol. Biol.* **17**, 1114–1123 (2010).

1058 45. Piñol-Roma, S. & Dreyfuss, G. Shuttling of pre-mRNA binding proteins between nucleus and
1059 cytoplasm. *Nature* **355**, 730–732 (1992).

1060 46. Piñol-Roma, S. & Dreyfuss, G. Transcription-Dependent and Transcription-Independent
1061 Nuclear Transport of hnRNP Proteins. *Science* **253**, 312–314 (1991).

1062 47. Pritchard, J. R., Bruno, P. M., Hemann, M. T. & Lauffenburger, D. A. Predicting cancer drug
1063 mechanisms of action using molecular network signatures. *Mol. Biosyst.* **9**, 1604–1619 (2012).

1064 48. Jiang, H., Pritchard, J. R., Williams, R. T., Lauffenburger, D. A. & Hemann, M. T. A
1065 mammalian functional-genetic approach to characterizing cancer therapeutics. *Nat Chem Biol* **7**,
1066 92–100 (2011).

1067 49. Dasari, S. & Tchounwou, P. B. Cisplatin in cancer therapy: Molecular mechanisms of action.
1068 *Eur. J. Pharmacol.* **740**, 364–378 (2014).

1069 50. Hafner, M., Niepel, M., Chung, M. & Sorger, P. K. Growth rate inhibition metrics correct for
1070 confounders in measuring sensitivity to cancer drugs. *Nat Methods* **13**, 1–11 (2016).

1071 51. Schwartz, H. R. *et al.* Drug GRADE: An Integrated Analysis of Population Growth and Cell
1072 Death Reveals Drug-Specific and Cancer Subtype-Specific Response Profiles. *Cell Reports* **31**,
1073 107800 (2020).

1074 52. Stegh, A. H. *et al.* Bcl2L12 inhibits post-mitochondrial apoptosis signaling in glioblastoma.
1075 *Genes Dev.* **21**, 98–111 (2007).

1076 53. Bradner, J. E., Hnisz, D. & Young, R. A. Transcriptional Addiction in Cancer. *Cell* **168**, 629–
1077 643 (2017).

1078 54. Richards, R. *et al.* Drug antagonism and single-agent dominance result from differences in
1079 death kinetics. *Nat Chem Biol* 1–10 (2020) doi:10.1038/s41589-020-0510-4.

1080 55. ROSONINA, E. & BLENCOWE, B. J. Analysis of the requirement for RNA polymerase II
1081 CTD heptapeptide repeats in pre-mRNA splicing and 3′-end cleavage. *RNA* **10**, 581–589
1082 (2004).

1083 56. Vervoort, S. J. *et al.* The PP2A-Integrator-CDK9 axis fine-tunes transcription and can be
1084 targeted therapeutically in cancer. *Cell* **184**, 3143-3162.e32 (2021).

1085 57. Agarwal, V. & Kelley, D. R. The genetic and biochemical determinants of mRNA degradation
1086 rates in mammals. *Genome Biol.* **23**, 245 (2022).

1087 58. Bray, N. L., Pimentel, H., Melsted, P. & Pachter, L. Near-optimal probabilistic RNA-seq
1088 quantification. *Nat. Biotechnol.* **34**, 525–527 (2016).

1089 59. Soneson, C., Love, M. I. & Robinson, M. D. Differential analyses for RNA-seq: transcript-
1090 level estimates improve gene-level inferences. *F1000Research* **4**, 1521 (2016).

1091 60. Love, M. I., Huber, W. & Anders, S. Moderated estimation of fold change and dispersion for
1092 RNA-seq data with DESeq2. *Genome Biol.* **15**, 550 (2014).

1093 61. Stephens, M. False discovery rates: a new deal. *Biostatistics* **18**, 275–294 (2017).

1094 62. Irimia, M. *et al.* A Highly Conserved Program of Neuronal Microexons Is Misregulated in
1095 Autistic Brains. *Cell* **159**, 1511–1523 (2014).

1096 63. Tapial, J. *et al.* An atlas of alternative splicing profiles and functional associations reveals
1097 new regulatory programs and genes that simultaneously express multiple major isoforms.
1098 *Genome Res.* **27**, 1759–1768 (2017).

1099 64. Richards, R., Honeywell, M. E. & Lee, M. J. FLICK: an optimized plate reader-based assay
1100 to infer cell death kinetics. *Star Protoc* **2**, 100327 (2021).

1101 65. Hart, T. *et al.* High-Resolution CRISPR Screens Reveal Fitness Genes and Genotype-
1102 Specific Cancer Liabilities. *Cell* **163**, 1515–1526 (2015).

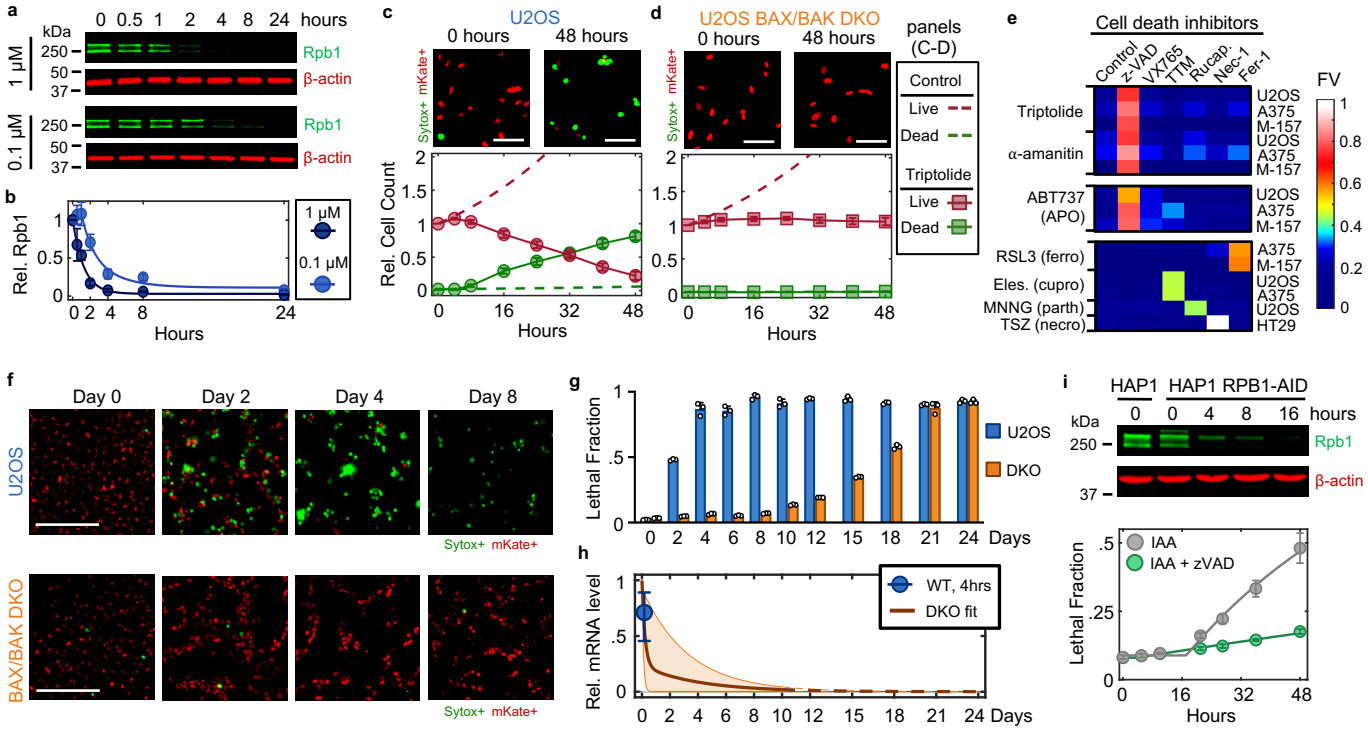

Fig. 1: Transcriptional inhibition activates apoptosis prior to dysregulation due to mRNA and protein decay. (**a**) Immunoblot of total Rpb1 protein in U2OS cells following exposure to 1 μM or 0.1 μM Triptolide. Blots are representative of 3 independent biological replicates. (**b**) Quantification of Rpb1 levels shown in panel (a). Mean ± SD are shown. (**c-d**) Live and dead cell kinetics following exposure to 1 μM triptolide for Nuc::mKate2-expressing U2OS cells. Data collected using the STACK assay. mKate+ cells are live, and Sytox+ cells are dead. (c) U2OS. (d) U2OS$^{BAX-/-/BAK1-/-}$ cells (BAX/BAK DKO). Representative images for each genotype are shown above the quantification at the indicated timepoints. Scale bar, 100 μm. Quantified cell numbers depict mean ± SD for 3 independent biological replicates. (**e**) Heatmap of fractional viability (FV) for cells treated with the indicated drugs in the presence/absence of death pathway specific inhibitors. z-VAD-FMK (z-VAD) targets apoptotic caspases; VX765 inhibits the pyroptotic initiator, caspase-1; TTM inhibits cuproptosis (cupro); Rucaparib (Rucap.) inhibits parthanatos (parth); Nec-1 inhibits necroptosis (necro); Fer-1 inhibits ferroptosis (ferro). RSL3, Elesclomol (Eles.), MNNG, and TSZ are canonical activators of the listed death pathways. M-157 = MDA-MB-157. Mean of 3 independent biological replicates is shown. (**f-g**) STACK-based analysis of live and dead cells over extended times following exposure to 1 μM triptolide. (**f**) Representative images from three biological replicates. Scale bar, 275 μm. (**g**) Lethal fraction measured using FLICK following imaging. Data are mean ± SD of 3 biological replicates. (**h**) mRNA levels following exposure to 1 μM triptolide, relative to untreated cells, measured using spike-in normalized RNAseq. Data were normalized to absolute mRNA abundance using polyadenylated ERCC spike-ins. mRNA levels were quantified only for times in which substantial lethality had not yet occurred, which was 4-hours for WT cells, and the first 10 days for DKO cells. Decay kinetics for DKO were fit to a two-term exponential decay function. Range for DKO represents the 50 longest and 50 shortest half-life mRNAs. Dashed lines denote extrapolated expectation from fits. For WT data, median, 25th, and 75th percentiles are shown. (**i**) (top) Immunoblot of total Rpb1 protein levels in HAP1 cells, or HAP1-RPB1-AID cells following exposure to 500 μg/mL auxin (IAA, 3-indoleacetic acid). (bottom) Lethal Fraction measurements for HAP1-RPB1-AID cells following 500 μg/mL IAA, in the presence or absence of 50 μM z-VAD. Data collected using the FLICK assay. Data are mean ± SD of 9 independent biological replicates.

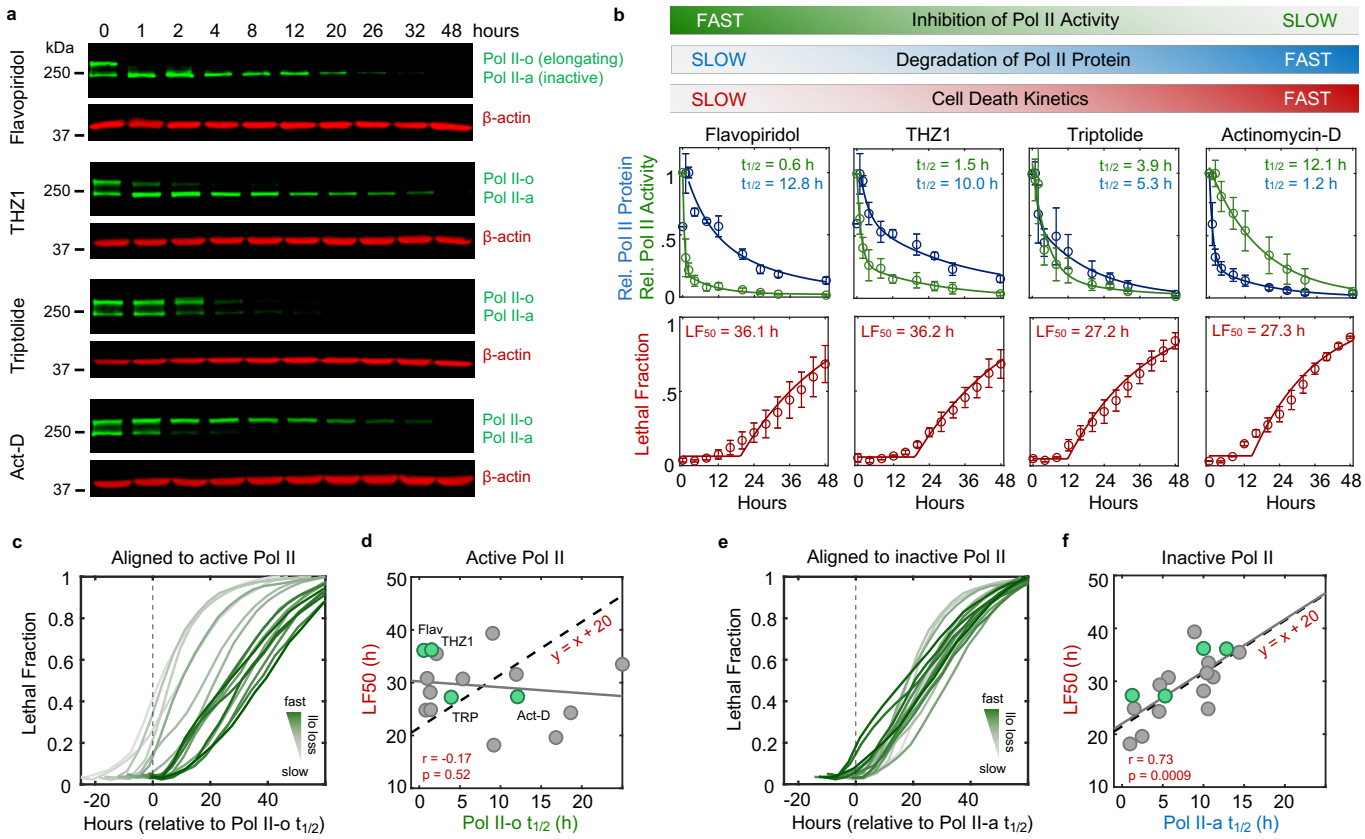

Fig. 2: Loss of Pol II protein – but not loss of Pol II activity – correlates with onset of apoptotic death. (**a**) Immunoblots of total Rpb1 protein following exposure to either flavopiridol (10 μM), THZ1 (1 μM), triptolide (0.1 μM), or actinomycin-D (Act-D, 0.1 μM). Blots are representative of three independent biological replicates. (**b**) (Top panel) Quantification of Pol II-o (elongating) and Pol II-a (inactive) decay kinetics from immunoblots described in (a). Data fit to a two-term exponential decay equation. $t_{1/2}$ denotes time to 50% decay. (Bottom panel) Cell death kinetics quantified using the STACK assay. LF_{50} denotes time to 50% max observed death. For both panels, data are mean ± SD, n = 3 independent biological replicates. (**c-d**) Relationship between loss of Pol II activity and activation of cell death. **(c)** Cell death kinetics for 17 unique transcriptional inhibitor drug-dose combinations, aligned to $t_{1/2}$ for loss of active Pol II (dashed vertical line). Cell death was quantified using the STACK assay, and the mean of 3 independent biological replicates measured every four hours is shown. (**d**) For data in (c), correlation between $t_{1/2}$ for loss of active Pol II and time to 50% lethality (LF50). Solid gray line denotes fit to a linear regression model. Black dashed line denotes a direct x = y relationship, shifted by a constant to account for a lag time between drug activity and cell death. **(e-f)** Relationship between loss of inactive Pol II and activation of cell death. **(e)** Same data as (c), except aligned to $t_{1/2}$ for degradation of inactive Pol II (dashed vertical line). **(f)** For data in (e), correlation between $t_{1/2}$ for degradation of inactive Pol II and time to 50% lethality (LF50).

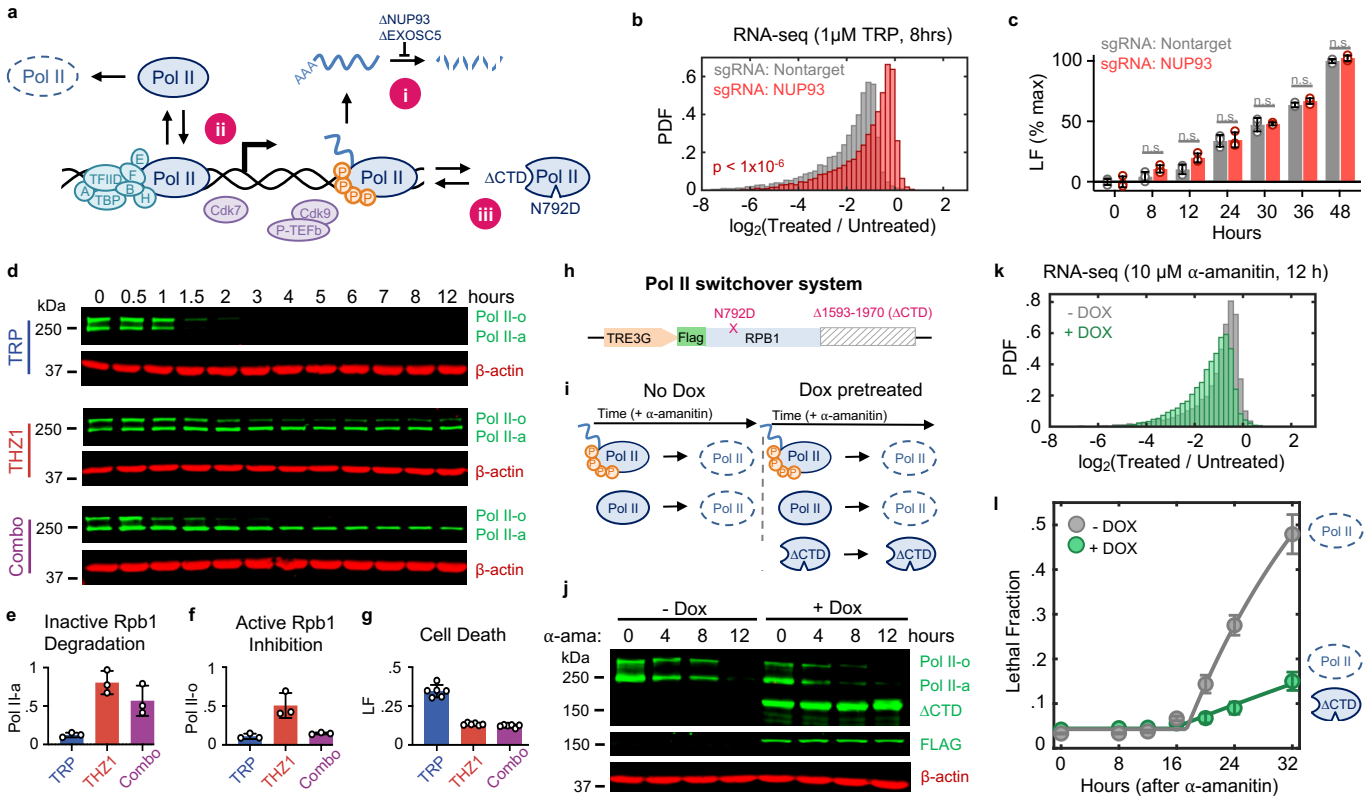

Fig. 3: Exogenous expression of inactive Pol II rescues viability following Pol II degradation. (**a**) Schematic describing three approaches (i – iii) for uncoupling inhibition of Pol II enzymatic activity from degradation of Pol II protein. (**b**) Histogram of spike-in normalized absolute mRNA fold changes following 8-hr exposure to 1 μM triptolide (TRP) in U2OS cells expressing sgRNA targeting NUP93 or nontargeting sgRNA. Two-sided KS test *p* value is shown. (**c**) Comparison of lethal fraction (LF) levels between cell types in (b) at various time points following exposure to 1 μM TRP, measured using the FLICK assay. Data normalized to max LF in cells expressing nontargeting sgRNA. Data are mean ± SD for n = 3 independent biological replicates. Wilcoxon rank sum p value shown (n.s. > 0.05). (**d**) Immunoblot of total Rpb1 levels in U2OS cells following exposure to 1 μM TRP (top), 0.316 μM THZ1 (middle), or the combination of the two (bottom). Blots shown are representative of three independent biological replicates. (**e-f**) Quantification of Rpb1 levels after 4-hr drug exposure (associated with panel d). (**e**) inactive (II-a). (**f**) active (II-o). **(g)** LF at 24-hrs, measured using the FLICK assay in identical conditions. Data are mean ± SD for n = 6 independent biological replicates. (**h-l**) Pol II switchover system used to evaluate function of inactive Pol II. **(h)** Diagram of a Pol II construct featuring a doxycycline-inducible promoter, FLAG tag, α-amanitin resistance mutation (N792D), and deletion of amino acids 1593-1970 (ΔCTD). **(i)** Experimental logic behind the Pol II switchover system. Tet-ON U2OS cells expressing the N792D/ΔCTD construct are exposed to 10 μM α-amanitin in the presence or absence of 2 μg/mL doxycycline (Dox). Dox added 48-hrs prior to α-amanitin to allow for expression of N792D/ΔCTD prior to degradation of the endogenous Pol II-o/a. (**j**) Immunoblots of Rpb1 following exposure to 10 μM α-amanitin. (**k**) Histogram of spike-in normalized absolute mRNA fold changes following 12-hr exposure to 10 μM α-amanitin. (**l**) LF kinetics following 10 μM α-amanitin. LF measured using FLICK. Mean ± SD shown, n = 5 independent biological replicates.

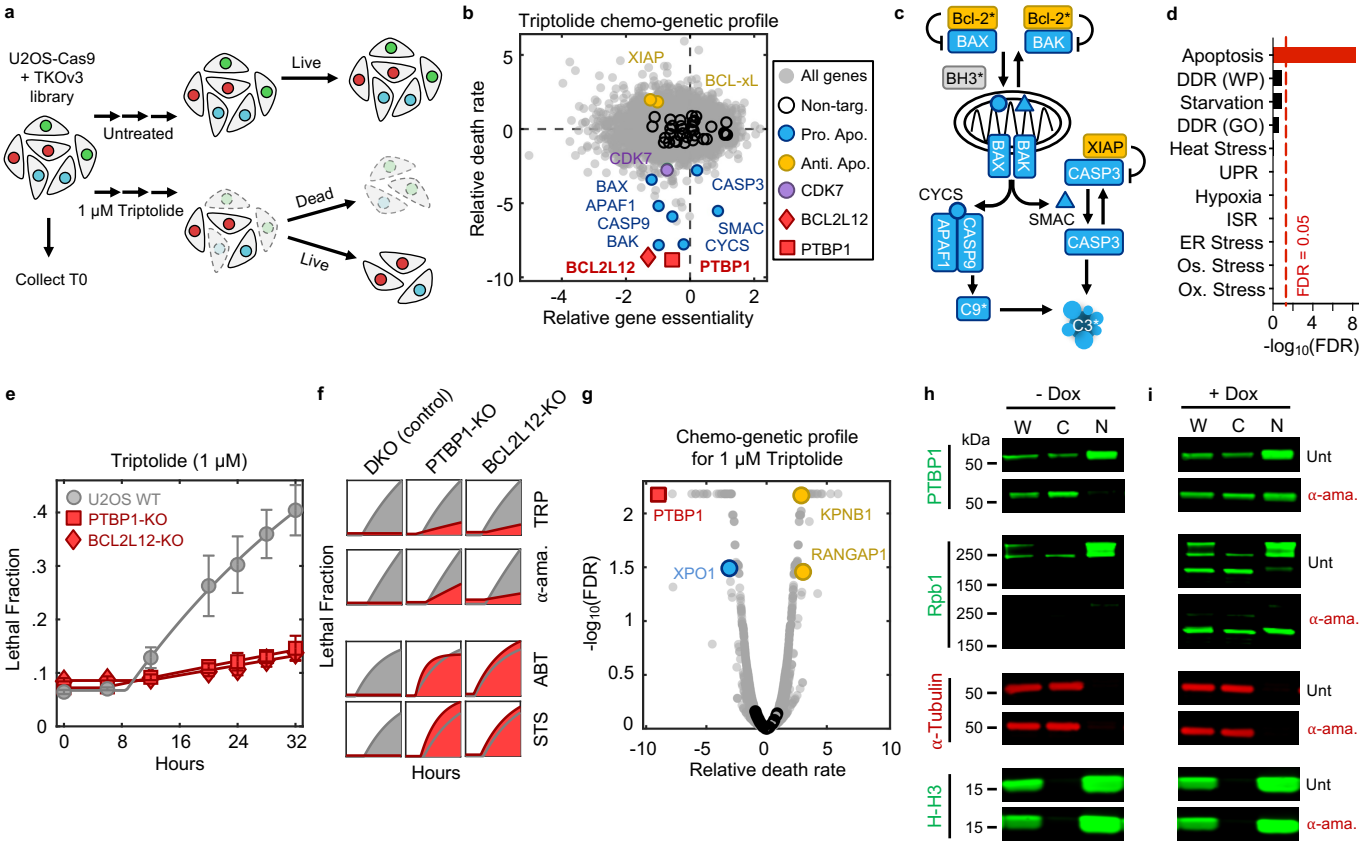

Fig. 4: Apoptosis following Pol II degradation exhibits unique genetic dependencies. (**a**) Schematic of chemo-genetic profiling to identify cell death regulatory genes. (**b**) Gene-level chemo-genetic profiling data for U2OS cells treated with 1 μM triptolide. Key death regulatory genes and non-targeting controls are highlighted. (**c**) Simplified schematic of the cell intrinsic apoptotic pathway. Bcl-2* denotes the general anti-apoptotic Bcl-2 family members, whereas BH3* denotes the pro-apoptotic BH3-only family members. Regulators in blue/yellow were identified in the chemo-genetic profiling data. (**d**) Enrichment of various stress response pathways in genes whose knockout significantly suppresses triptolide-induced cell death, as identified in the chemo-genetic profiling. Significance was determined using a one-tailed Fisher's exact test corrected for multiple comparisons using the Benjamini-Hochberg (BH) FDR. (**e**) Cell death kinetics measured using FLICK following 1μM triptolide in U2OS wild-type cells, PTBP1-KO cells (red, square), BCL2L12-KO cells (red, diamond). Data are mean ± SD for n = 6 independent biological replicates. (**f**) PTBP1 and BCL2L12 dependence for drugs that degrade Pol II, or canonical apoptotic agents: triptolide (TRP): 1 μM; α-amanitin (α-ama.): 10 μM; ABT-199 (ABT): 100 μM; Staurosporine (STS): 0.5 μM. Drugs tested in U2OS-PTBP1-KO, U2OS-BCL2L12-KO, or U2OS BAX/BAK double knockout (DKO). Lethal fraction kinetics shown with area under the kinetic curve colored: grey = wild-type cells, red = DKO, PTBP1-KO, or BCL2L12-KO cells, as indicated. Areas are based on the mean of 6 independent biological replicates. **(g)** Drug-induced death rates from chemo-genetic profiling of triptolide, with genes highlighted that regulate PTBP1 translocation: nuclear import factors in yellow; nuclear export factors in blue. Non-targeting genes in black. (**h-i**) Nuclear/cytoplasmic fractionation to assess PTBP1 localization following exposure to α-ama. W = whole cell extract; C = cytoplasmic extract; N = nuclear extract. Immunoblots for Rbp1 shown to validate α-ama. function; α-Tubulin and Histone-H3 (H-H3) shown as markers of cytoplasmic and nuclear proteins, respectively. **(h)** Data are from U2OS-RBP1-N792D/ΔCTD cells exposed to 10 μM α-amanitin for 12 hours. **(i)** As in panel (h), except samples collected from U2OS-RBP1-N792D/ΔCTD cells exposed to doxycycline (Dox) for 48 hours prior to exposure to α-amanitin.

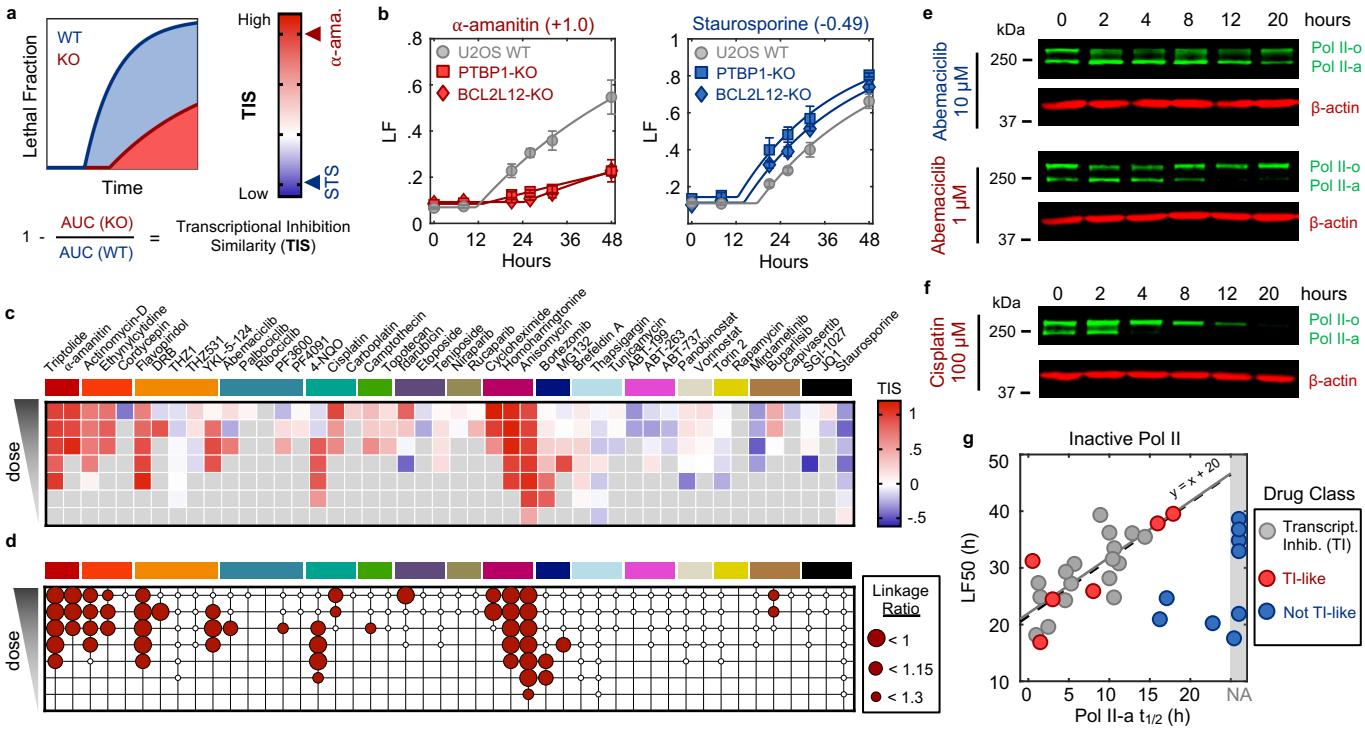

Fig. 5: Commonly used anti-cancer drugs owe their lethality to Pol II degradation. (**a**) Schematic illustrating the strategy to quantify the degree to which the lethality of a given drug is dependent on the genetic dependencies observed for Pol II degraders (*i.e.*, PTBP1 and BCL2L12). (**b**) Cell death kinetics in U2OS cells for a high scoring drug (10 μM α-amanitin, TIS = 1.0) and a low scoring drug (3.16 μM Staurosporine, TIS = -0.49). Data collected using FLICK. Data are mean ± SD for n = 3 independent biological replicates. (**c**) Heatmap depicting the Transcription Inhibition Similarity (TIS) score across a 7-point half-log dose range for 46 compounds encompassing diverse established mechanisms of action and clinical utility. Data collected in U2OS cells. Grey boxes are for non-lethal doses of each drug. Compounds are ordered and colored by drug class. See methods for exact doses tested and drug class definitions. (**d**) Binary classifier, defining each drug-dose condition as "Transcriptional Inhibition-like" (TI-like) or not. Classifier results are ordered as in (c). Red circles denote TI-like mechanism of lethality. (**e**) Immunoblot of total Rpb1 levels in U2OS cells following exposure to high dose Abemaciclib (classified as low TIS), or a ten-fold lower dose (classified as high TIS and TI-like mechanism of lethality). (**f**) Immunoblot of total Rpb1 levels in U2OS cells following exposure to high dose Cisplatin. (**g**) Relationship between timing of cell death and timing of Pol II-a loss. Data in gray denote established transcriptional inhibitors, as shown in Fig. 2f. Red and blue data points represent tested TI-like compounds and not TI-like compounds, respectively. Black dashed line denotes a direct x = y relationship, shifted by a constant to account for a lag time between drug activity and cell death.

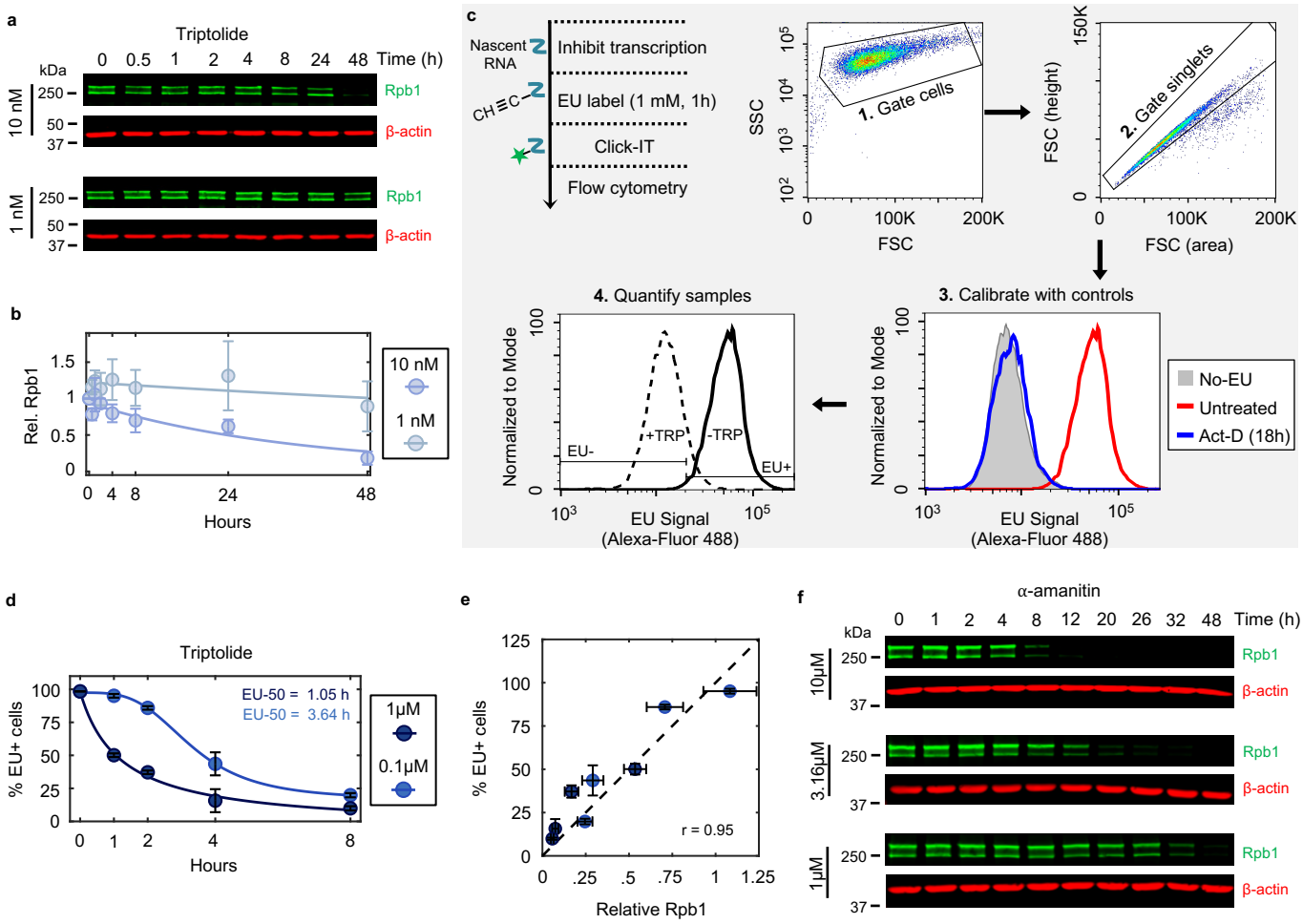

Extended Data Fig. 1: Establishing kinetics of complete transcriptional inhibition. Related to Fig. 1. (**a**) Immunoblots of total Rpb1 in U2OS cells following exposure to low doses of triptolide (10 nM or 1 nM). Blots are representative of three independent biological replicates. (**b**) Quantification of Rpb1 levels shown in panel (a). Data are normalized relative to untreated levels. (**c**) Approach for measuring incorporation of 5-ethynyl uridine (EU) into newly synthesized RNAs using flow cytometry. Following labeling of nascent RNA via incubation with EU, cells are fixed, and labeled RNA is ligated to a fluorophore using click chemistry. A high dose (1 μM) and long incubation with the pan-RNA polymerase inhibitor actinomycin-D (Act-D) is used as a control to define the signal associated with no active transcription (EU-). (**d**) EU incorporation in U2OS cells before and after triptolide. Data are mean ± SD, n = 3 independent biological replicates. (**e**) Correlation between Rpb1 protein loss (quantified by immunoblot) and nascent RNA loss (quantified by EU incorporation) following exposure to 1 μM and 0.1 μM triptolide (at 1, 2, 4 and 8 hours post drug addition). Dashed line, x = y. Pearson correlation coefficient is shown. Data are mean ± SD, n = 3 independent biological replicates. (**f**) Immunoblots of total Rpb1 protein in U2OS cells following exposure to a dose range of α-amanitin. Blots are representative of three independent biological replicates.

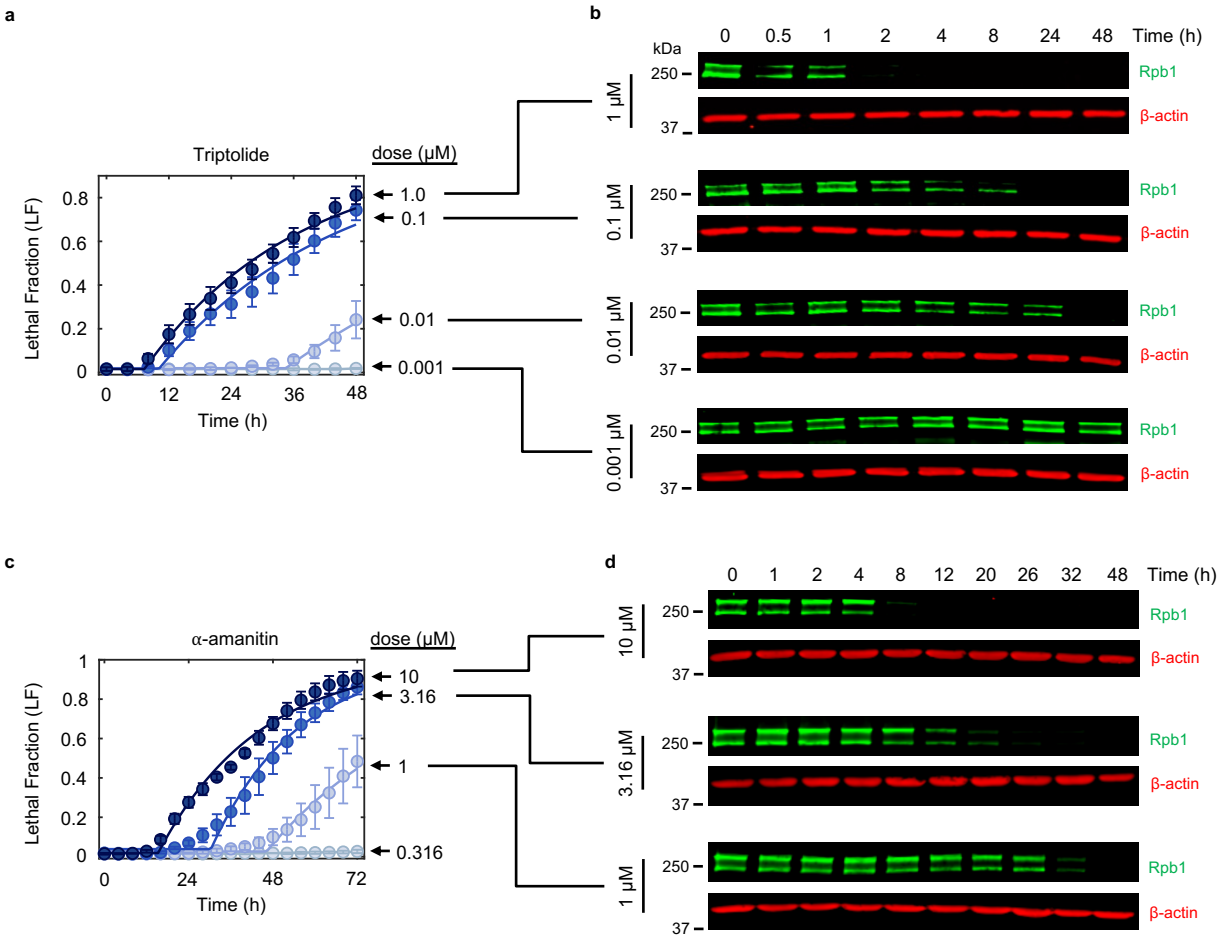

Extended Data Fig. 2: Cell death kinetics for triptolide and α-amanitin across dose. Related to Fig. 1. (**a**) Lethal fraction kinetics in U2OS cells for triptolide across dose, measured in STACK. Data are mean ± SD, n = 3 independent biological replicates. (**b**) Immunoblots of Rpb1 protein levels in U2OS cells following exposure to triptolide across dose. Dose associations with (a) are shown. Blots are representative of three independent biological replicates. (**c-d**) As in (a-b), but for α-amanitin.

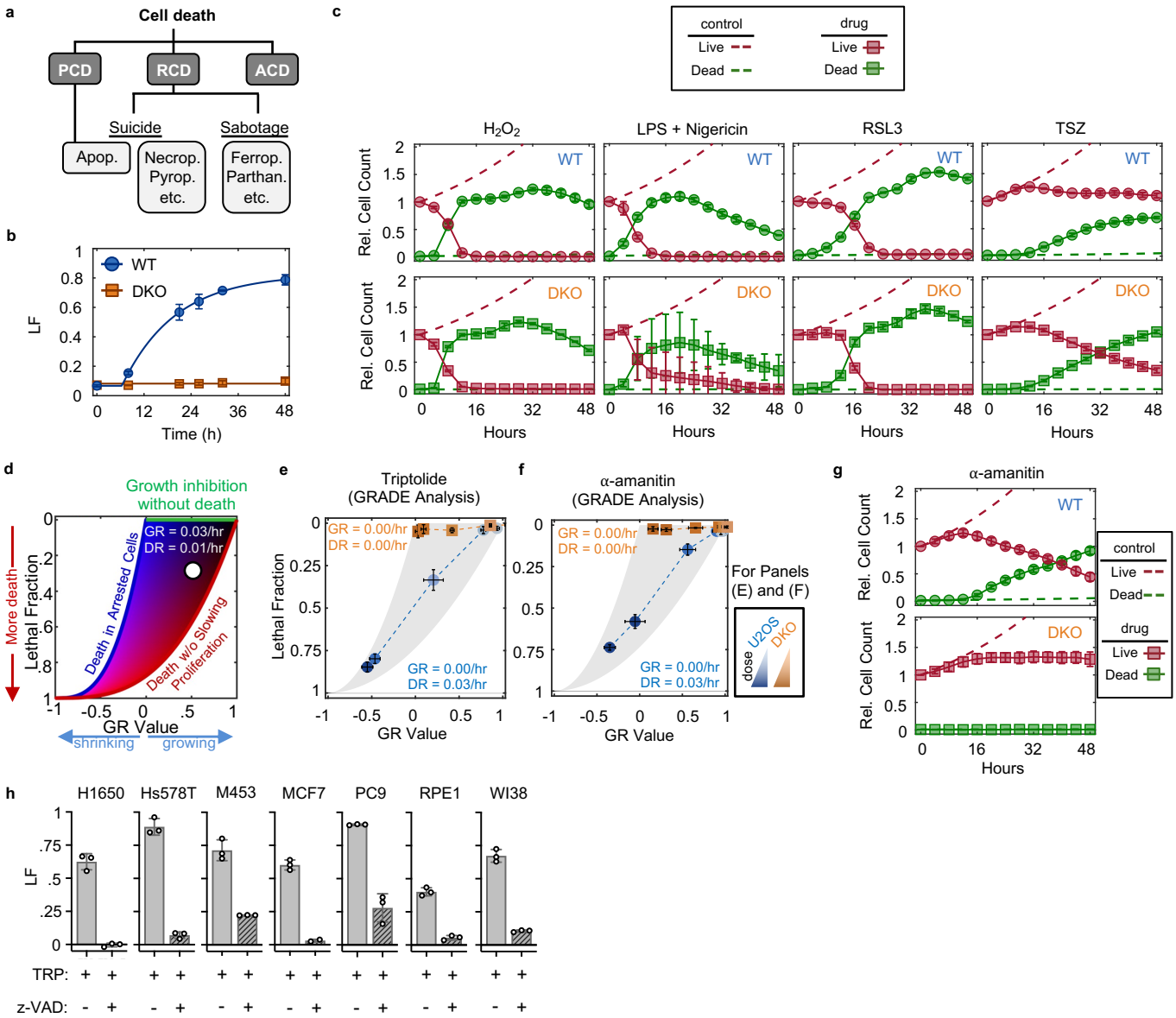

Extended Data Fig. 3: Evaluation of cell death following Pol II degradation. Related to Fig. 1. (**a**) Cell death can be broadly classified into three groups: "Accidental cell death" (ACD) results from a stress that overwhelms cellular control mechanisms; "Programmed cell death" (PCD) occurs in normal development and tissue homeostasis; "Regulated cell death" (RCD) is executed by defined signaling events and effector molecules in response to exogenous stresses. RCD is further sub-divided into cell death pathways activated via signaling (cell "suicide") or those that take advantage of cellular activities but are not necessarily due to signaling (cell "sabotage"). (**b**) LF kinetics in U2OS (WT) and U2OS$^{BAX-/-BAK1-/-}$ (DKO) cells following exposure to the apoptotic agent ABT-737 (31.6 μM), measured in FLICK. (**c**) Live and dead cell kinetics following exposure to various non-apoptotic stimuli (Oxeiptosis, 316 μM H_2O_2; Pyroptosis, 0.2 μg/mL LPS + 31.6 μM Nigericin; Ferroptosis, 31.6 μM RSL3; Necroptosis, 10 ng/mL TNFα + 10 μM SM-164 + 50 μM z-VAD). Data collected using the STACK assay. (**d**) Schematic of the GRADE method. Drug-induced growth and death rates can be inferred from GR/LF plots. (**e**) GRADE-based analysis of triptolide at 48 hours. Inference of growth (GR) and death (DR) rates for the highest dose (1 μM) are shown for both genotypes. (**f**) As in (e) but for α-amanitin. **(g)** Same as (c), for 10 μM α-amanitin. (**h**) Lethal fraction kinetics for a panel of cell lines following 72-hour treatment with 1 μM triptolide, with- or without co-treatment with 50 μM z-VAD, measured using FLICK. (b, c, e, f, g, h) Data are mean ± SD, n = 3 independent biological replicates.

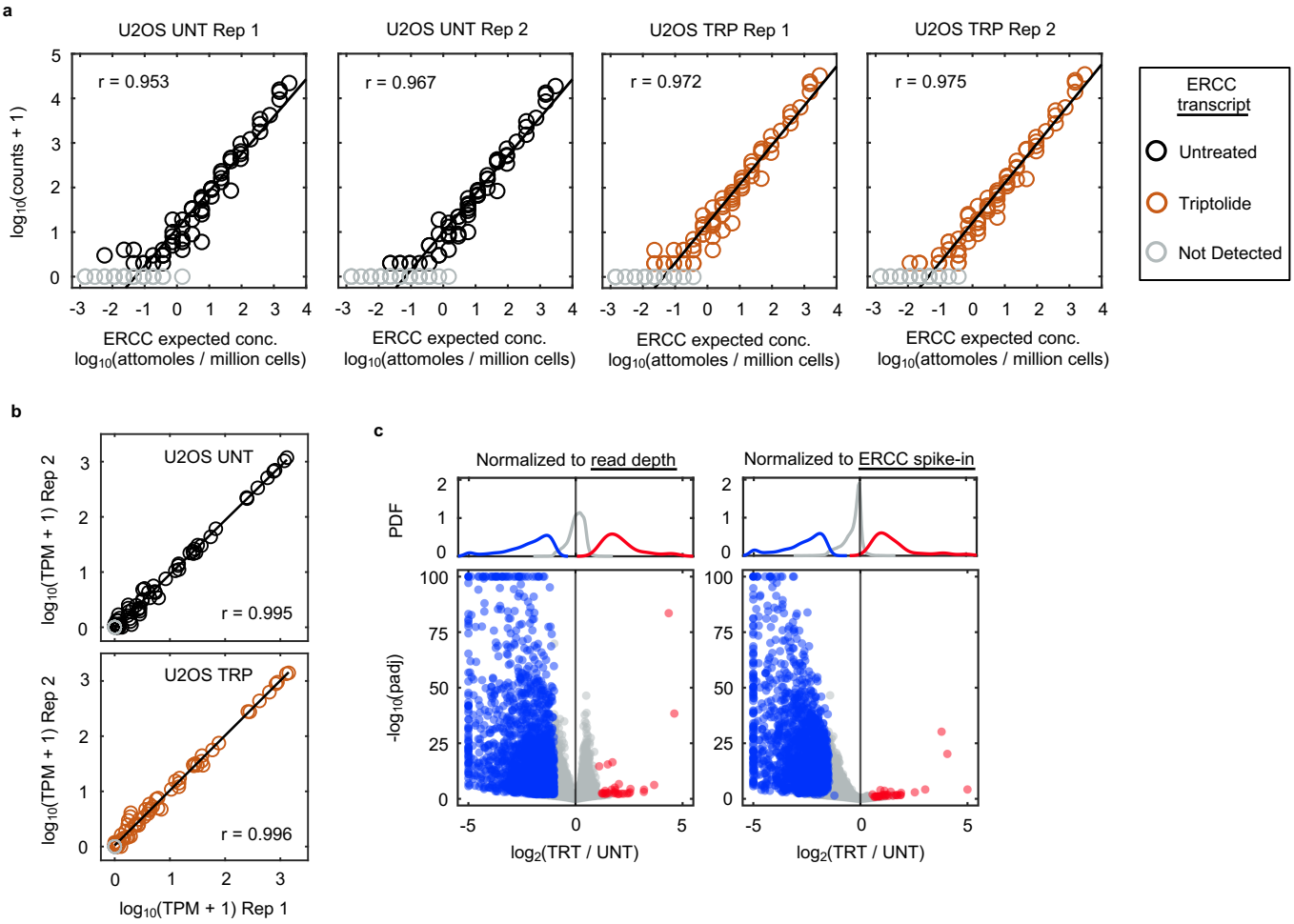

Extended Data Fig. 4: Normalization of RNAseq data to polyadenylated ERCC spike-ins. Related to Fig. 1. (**a**) The expected molar amount of RNA for each of the 92 ERCC spike-in transcript standards compared to the empirically observed read counts, for replicates of U2OS RNAseq samples untreated (UNT) or treated with 1 μM triptolide (TRP) for 4 hours. Grey circles denote ERCC transcripts with zero counts. Linear regression line is shown, along with the Pearson correlation coefficient. (**b**) Transcript abundance correlation between replicates for the 92 ERCC spike-in transcript standards (TPM, transcripts per million). (**c**) Spike-in normalization is required to measure mRNA on an absolute scale. RNA-seq profiling of mRNA expression changes following exposure to 1 μM triptolide for 4 hours. (Left) mRNA expression normalized to read depth. (Right) mRNA expression normalized to ERCC spike-ins. Genes are colored based on read depth normalization: grey: no change; blue: down regulated; red: up regulated.

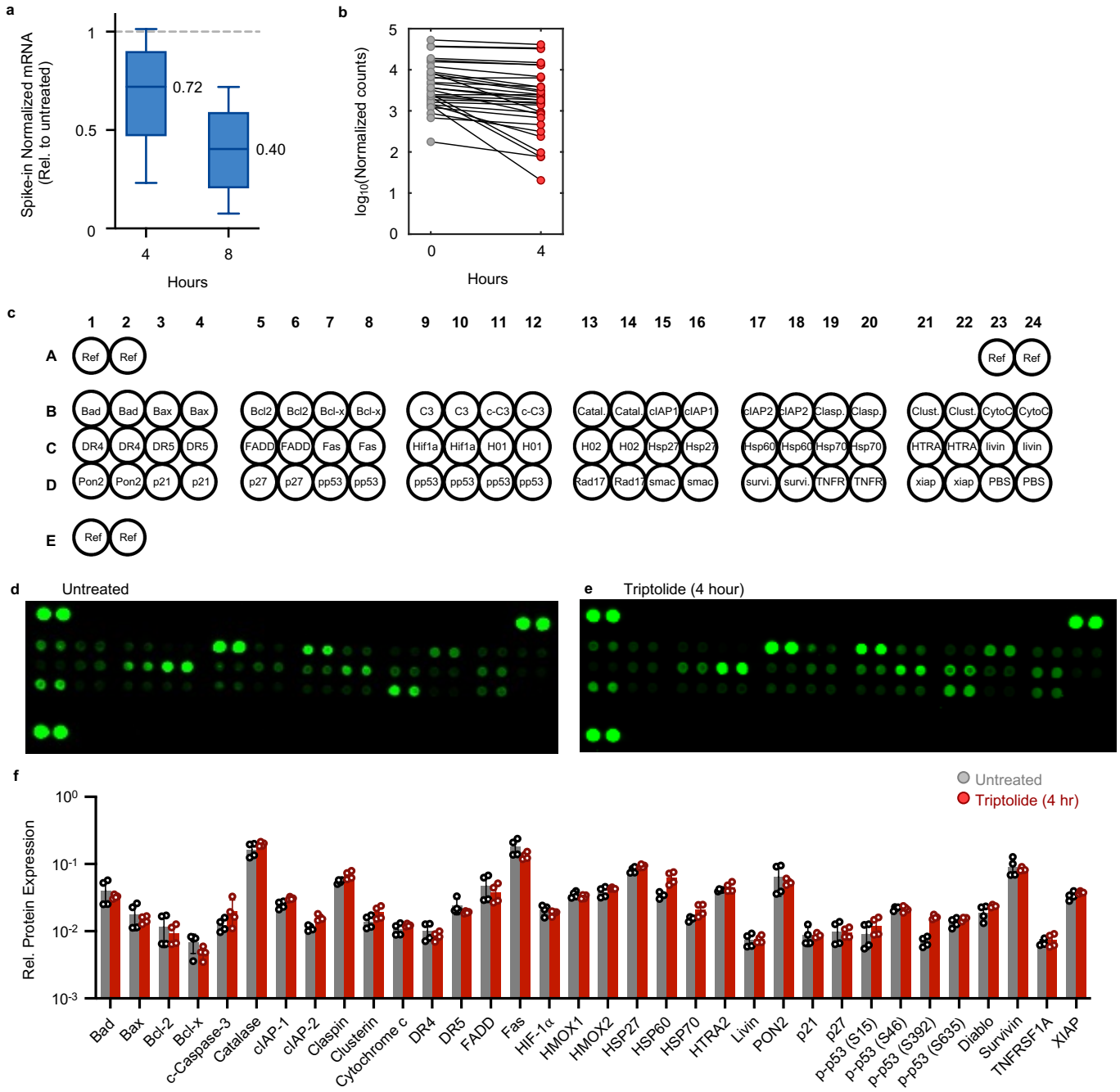

Extended Data Fig. 5: Minimal mRNA and protein decay at onset of triptolide-induced death. Related to Fig. 1. (**a**) mRNA transcript abundance following 4 or 8 hours of 1 μM triptolide, measured using spike-in normalized RNAseq. Boxplots depict 10 – 90 percentile, and the median value is stated. (**b**) mRNA expression changes following exposure to 1 μM triptolide for apoptotic regulatory genes, measured using spike-in normalized RNAseq. Genes were selected to match the proteins analyzed in (c-f) in the Proteome profiler apoptosis array. (**c-f**) Proteome profiler apoptosis array. (**c**) Proteins measured in the proteome profiler array. (**d**) Untreated U2OS cells. Data are representative of two independent biological replicates. (**e**) As in (d), for U2OS cells treated with 1 μM triptolide for 4 hours. (**f**) Quantification of (d-e). Data are means ± SD of two independent biological replicates and two technical replicates, normalized to the highest expression protein (total Pro-Caspase-3). Significant differences between treated and untreated conditions for each epitope were determined using unpaired t tests with Welch correction, and the two-stage step-up method of Benjamini, Krieger and Yekutieli was used to correct for multiple comparisons. No proteins were identified as being significantly different, except for phospho-p53 (S392) (q = 0.001).

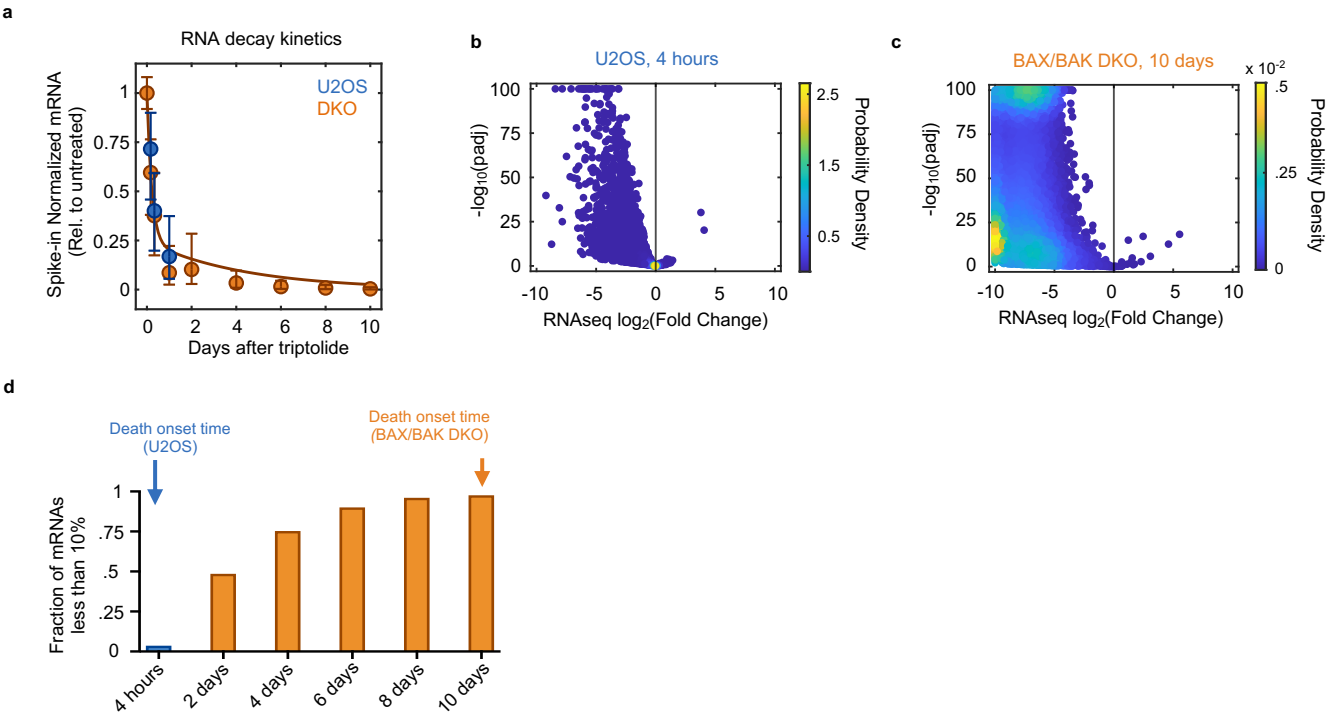

Extended Data Fig.6: mRNA decay following long-term exposure to triptolide. Related to Fig. 1. (**a**) Decay kinetics for mRNAs in U2OS and BAX/BAK DKO (DKO) after 1 μM triptolide exposure for the indicated times, measured using spike-in normalized RNAseq. Datapoints indicate median, 25th, and 75th percentiles. (**b**) Spike-in normalized mRNA fold changes in U2OS cells following 4 hours of 1 μM triptolide. (**c**) Spike-in normalized mRNA fold changes in *BAX/BAK* DKO cells following 10 days of 1 μM triptolide. (**d**) Fraction of mRNAs that have decayed beyond 90% of untreated steady-state abundance. U2OS (blue) and *BAX/BAK* DKO cells (orange) are shown, and their respective death onset times are noted.

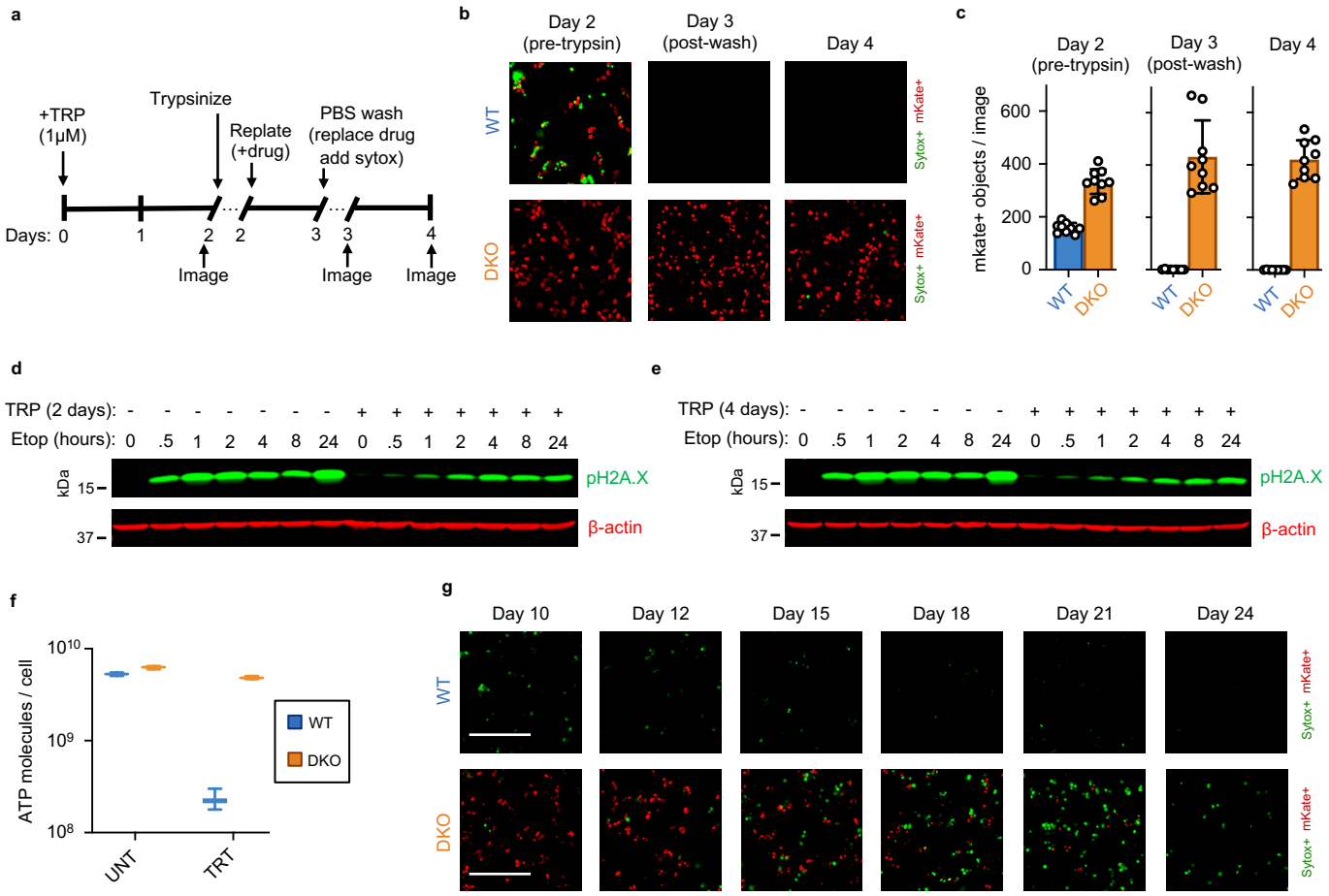

Extended Data Fig. 7: Viability of *BAX*/*BAK* DKO cells during long-term exposure to triptolide. Related to Fig. 1 (**a**) Experimental overview for testing the ability of apoptotic deficient cells to reattach to plastic following trypsinization. (**b**) Representative images of triptolide treated cells before and after trypsinization and subsequent replating. (**c**) Quantification of mKate+ nuclei per image before and after trypsinization and subsequent replating, associated with (b). (**d**) Immunoblot depicting intact DNA damage response signaling in both untreated and triptolide-treated BAX/BAK DKO cells. Cells were first treated with or without 1 μM triptolide for 2 days to induce Pol II degradation, following by addition of 31.6 μM Etoposide to induce DNA damage. pH2A.X (S139) levels were monitored over time following Etoposide. (**e**) As in (d), except BAX/BAK DKO cells were exposed to triptolide for 4 days. (**f**) ATP molecules per cell following a 4-day treatment with 1 μM triptolide in U2OS or BAX/BAK DKO cells. ATP was measured using Cell Titer Glo, and cell number was normalized using FLICK. Mean, minimum, and maximum values of n = 60 independent biological replicates are shown. (**g**) Long-term survival of BAX/BAK DKO cells following 1 μM triptolide (associated with Fig. 1f). Representative images for three independent biological replicates is shown.

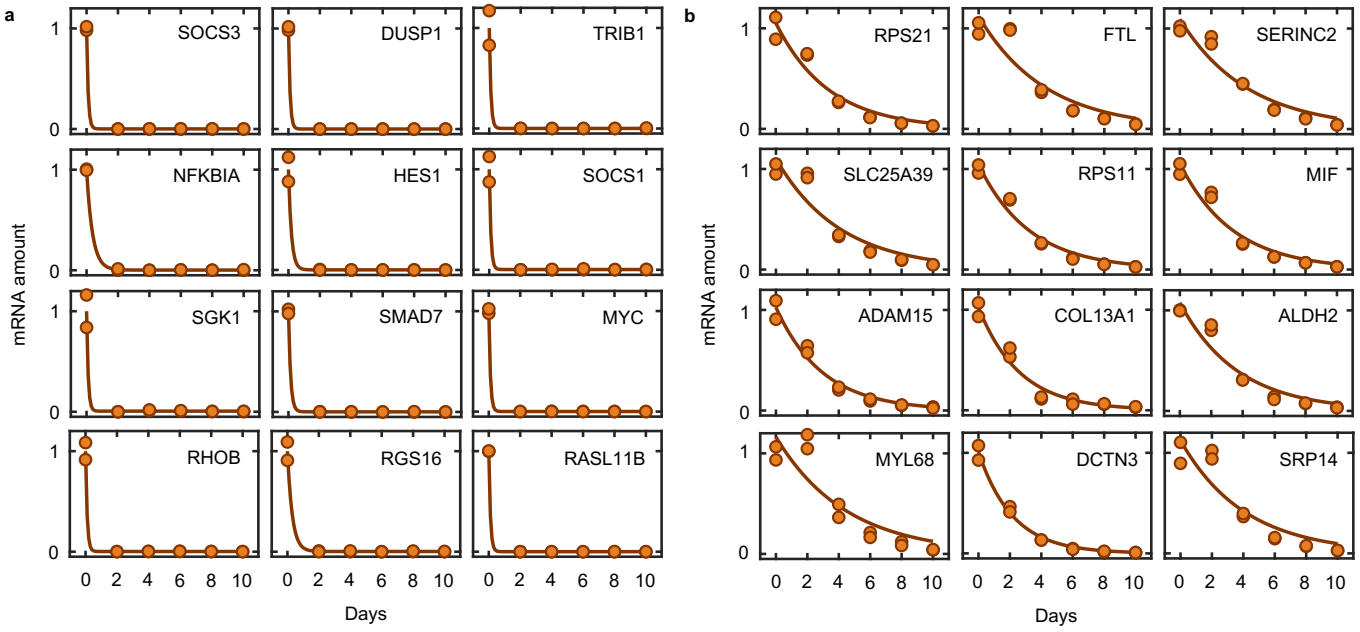

Extended Data Fig. 8: Decay kinetics of short and long-lived transcripts. Related to Fig. 1. (**a**) mRNA decay kinetics in DKO cells following long-term exposure to 1 μM triptolide, measured using spike-in normalized RNAseq. 12 shortest half-life transcripts, defined from a meta-analysis of half-life measurements Agarwal and Kelley (2022). (**b**) As in (a), for the 12 longest half-life transcripts.

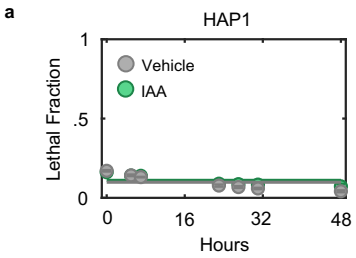

Extended Data Fig. 9: Cell death in HAP1-RPB1-AID cells is not caused by auxin itself. Related to Fig. 1 (**a**) Lethal fraction kinetics in parental HAP1 cells following exposure to 500 µg/mL auxin (IAA, 3-indoleacetic acid) or vehicle, measured in FLICK. Data are mean ± SD, n = 3 independent biological replicates.

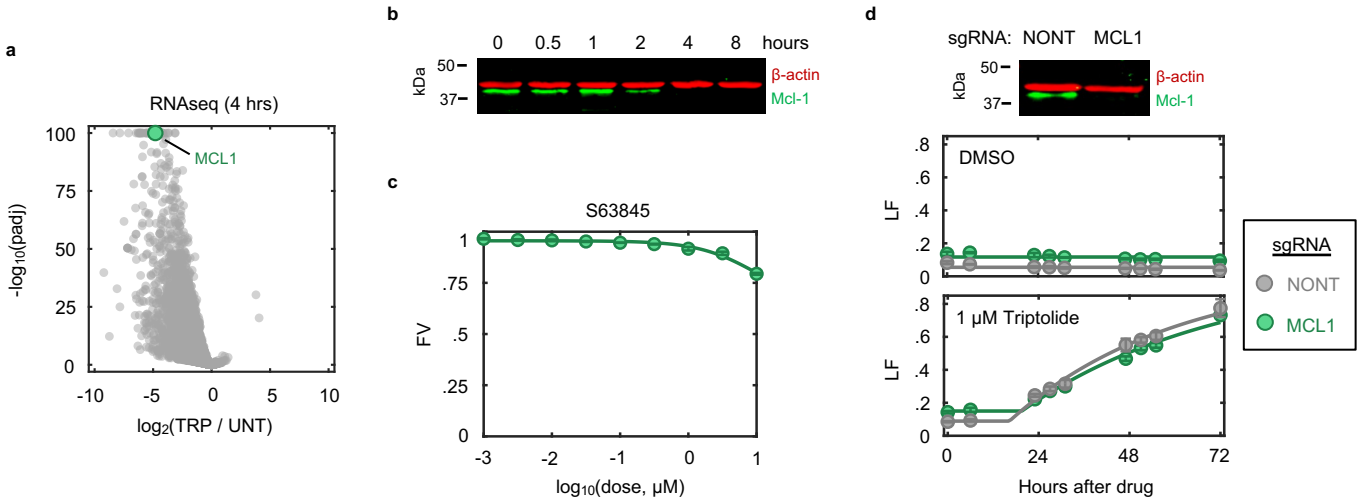

Extended Data Fig. 10: Loss of Mcl-1 protein following transcriptional inhibition is not causal for apoptosis. Related to Fig. 2. (**a**) mRNA expression following 4-hour exposure to 1 μM triptolide in U2OS cells, highlighting the rapid loss of MCL1. (**b**) Immunoblot of Mcl-1 protein levels in U2OS cells following exposure to 1 μM triptolide. (**c**) U2OS cells are insensitive to the Mcl-1 inhibitor S63845. Fractional viability (FV) measured after 72 hours of drug exposure, measured in FLICK. Data are mean ± SD for n = 3 independent biological replicates. (**d**) Knockout of MCL1 is not lethal in U2OS cells and does not impact the lethality induced by triptolide. (Top) Immunoblot of Mcl-1 protein levels in U2OS cells expressing sgRNA targeting MCL1 or nontargeting sgRNA. (Bottom) Lethal fraction (LF) kinetics between the two genotypes following exposure to triptolide or vehicle (DMSO, 0.1%). LF kinetics were measured in FLICK, and data are mean ± SD for n = 3 independent biological replicates. Protein lysates used for the immunoblot were taken from the same pool of cells used for LF measurements and were collected at the time of drugging ("0 hours").

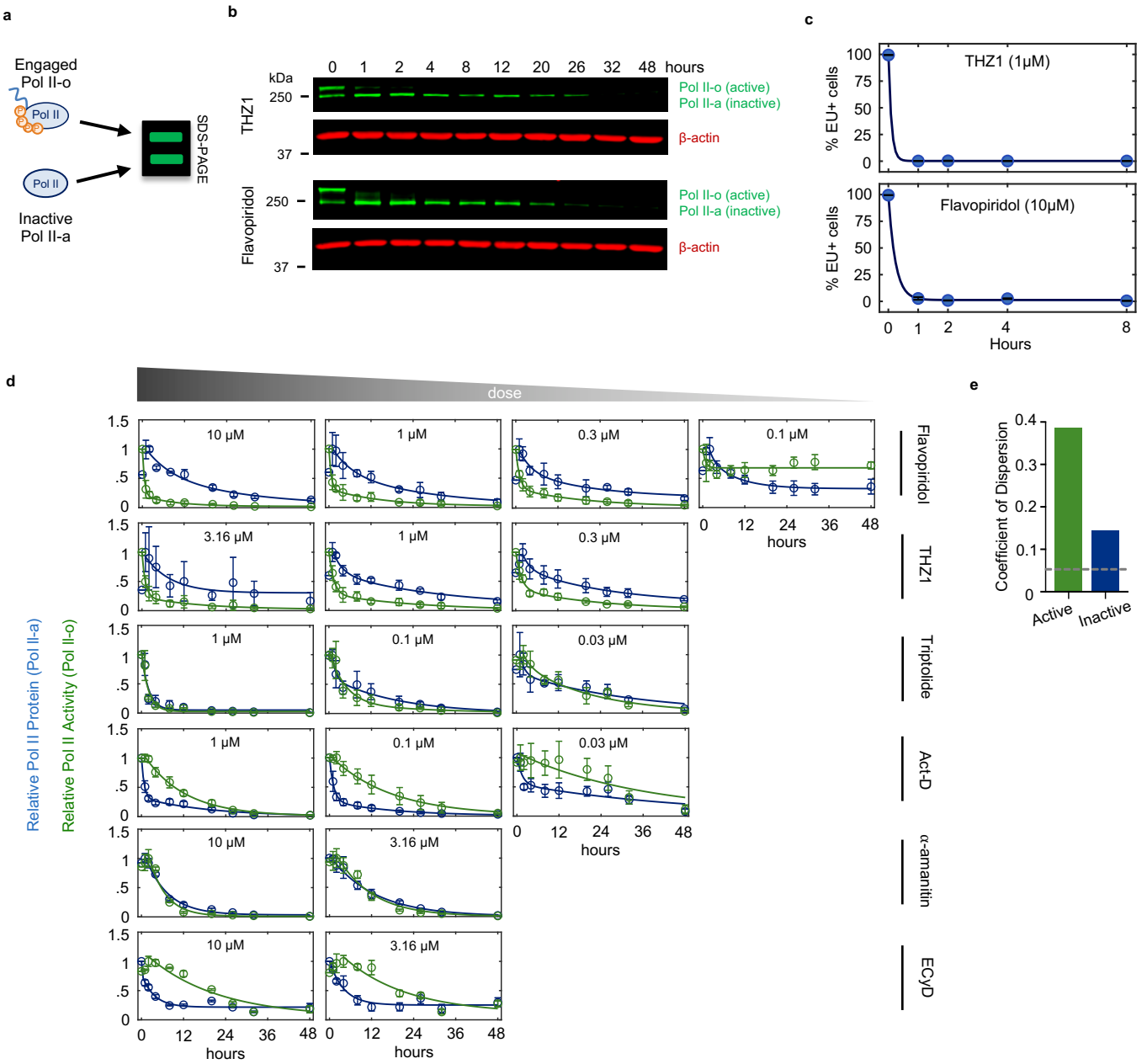

Extended Data Fig. 11: Variation in kinetics of Pol II inhibition across transcriptional inhibitors. Related to Fig. 2. (**a**) Pol II protein primarily exists in two forms. Pol II-o is hyper-phosphorylated along the carboxy-terminal domain (CTD) of the protein and is the actively elongating pool of Pol II. The hypo-phosphorylated form, called Pol II-a, represents all other inactive forms of Pol II, including preinitiation complex (PIC) bound, promoter paused, early pause released, and free Pol II. Pol II-o and Pol II-a can be distinguished by a band shift on a gel. (**b**) Example immunoblot of Rpb1 levels following exposure to two fast acting transcriptional inhibitors, THZ1 (1 μM), and Flavopiridol (10 μM). These drugs rapidly decrease Pol II-o levels. (**c**) EU incorporation into nascent RNA following fast acting inhibitors shown in (b), validating that loss of Pol II-o levels is functionally equivalent to loss of transcription. Data are mean ± SD for n =3 independent biological replicates. (**d**) Quantification of Pol II-o (green) and Pol II-a (blue) protein levels across different lethal doses of transcriptional inhibitors. Data were collected using quantitative immunoblotting and fit to a two-phase exponential decay function. Act-D, Actinomycin-D; ECyD, Ethynylcytidine. Data are mean ± SD for n =3 independent biological replicates. (**e**) Coefficient of Dispersion (CoD) of LF_{50} times for cell death kinetics aligned to active or inactive Pol II loss, as shown in Fig. 2c,e. Gray dashed line denotes the CoD for the "perfect" alignment, defined by arbitrarily shifting each kinetic curve such that maximum alignment is achieved, implemented using the MATLAB function alignsignals with method "risetime".

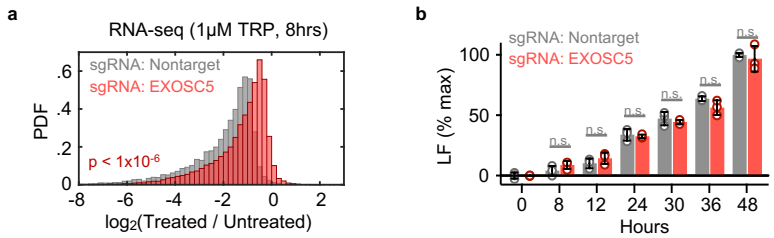

Extended Data Fig. 12: Effects of triptolide in EXOSC5 knockout cells. Related to Fig. 3. (**a**) Histogram of spike-in normalized absolute mRNA fold changes following 8-hr exposure to 1 μM triptolide (TRP) in U2OS cells expressing sgRNA targeting EXOSC5 or nontargeting sgRNA. Two-sided KS test *p* value is shown. (**b**) Comparison of lethal fraction (LF) levels between cell types in (a) at various time points following exposure to 1 μM TRP, measured using the FLICK assay. Data normalized to max LF in cells expressing nontargeting sgRNA. Data are mean ± SD for n = 3 independent biological replicates. Wilcoxon rank sum *p* value shown (n.s. > 0.05).

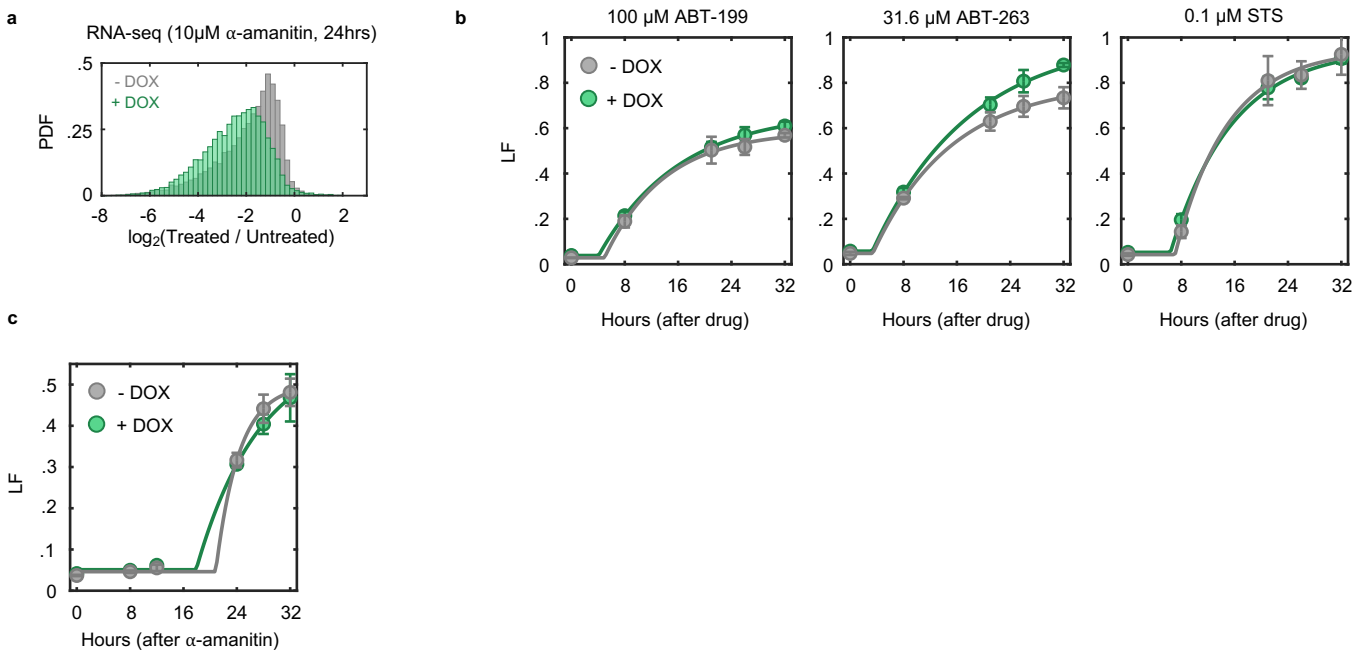

Extended Data Fig. 13: Characterization of the Pol II switchover system. Related to Fig. 3. (**a**) Histogram of spike-in normalized absolute mRNA fold changes following 24-hr exposure to 10 μM α-amanitin. (**b**) Lethal Fraction (LF) kinetics following exposure to general apoptotic agents in Pol II switchover cells with- or without doxycycline (DOX)-induced expression of RPB1-N792D-ΔCTD. LF measured using the FLICK. STS = Staurosporine. (**c**) LF kinetics in cells with- or without expression of a α-amanitin sensitive *RPB1*-ΔCTD transgene, treated with 10 μM α-amanitin and measured using FLICK. For (b-c), mean ± SD shown, n = 3 independent biological replicates.

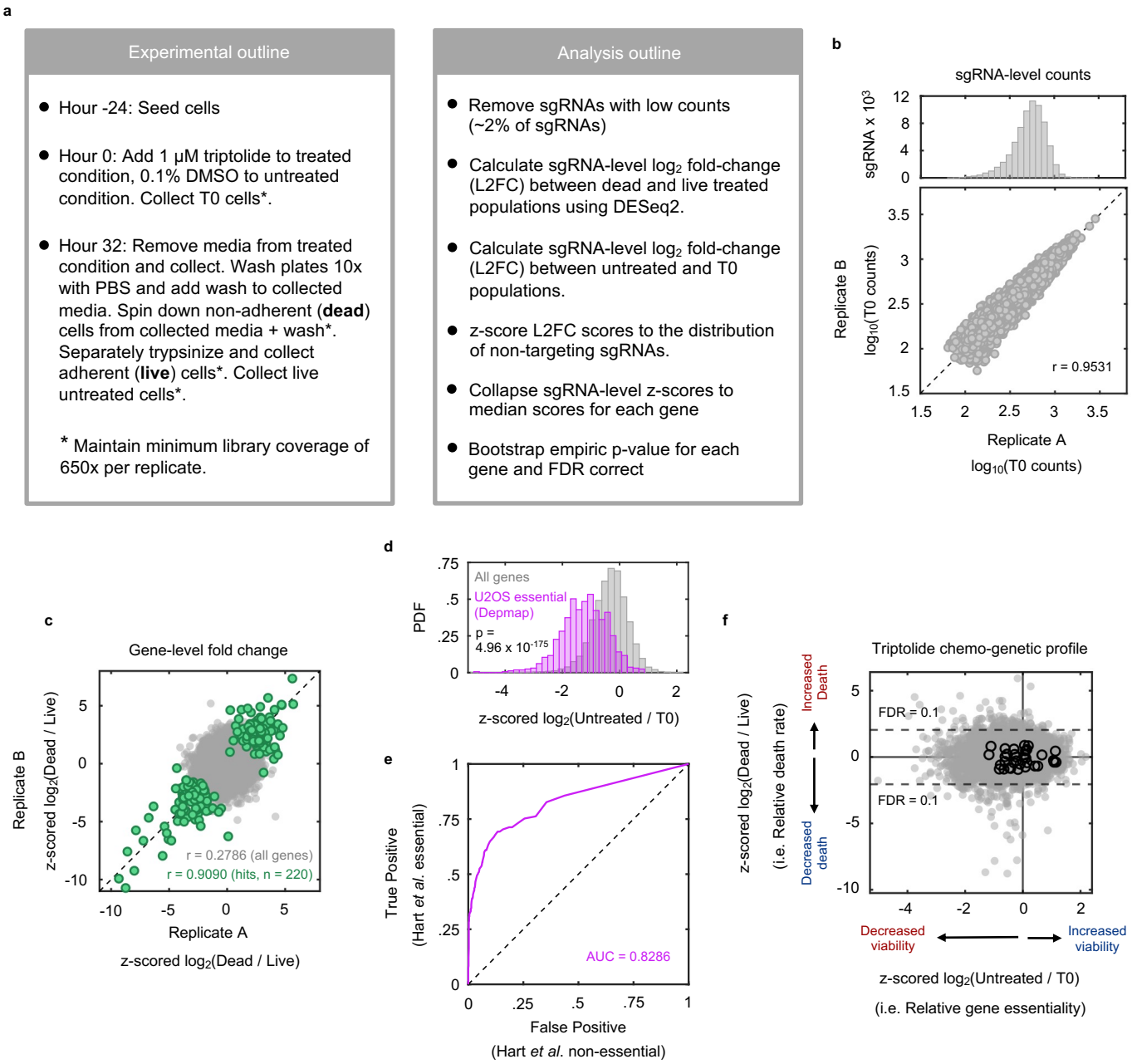

Extended Data Fig. 14: Chemo-genetic profiling strategy and quality assessment. Related to Fig. 4. (**a**) Overview of experimental and analytical process for the chemo-genetic screen. (**b**) (Top) Representative example sgRNA count distribution for replicate A of the T0 condition. (Bottom) Representative example correlation of sgRNA counts between two replicates of the same condition. Dashed line, x = y. Pearson correlation coefficient is shown. (**c**) Correlation of gene-level L2FC scores between two replicates treated with triptolide. (**d**) Distribution of gene-level L2FC scores for essential genes versus all genes in untreated vs T0 comparison. Two-sided KS test *p* value is shown. (**e**) ROC curve depicting the sensitivity and specificity of the untreated versus T0 screening comparison to classify previously established essential and non-essential genes. (**f**) Conceptual overview of metrics comprising the chemo-genetic profile of triptolide. The x-axis describes the effect a gene knockout has on the viability of a cell in untreated conditions. The y-axis describes the effect a gene knockout has on the cell death rate in the context of triptolide. Scores for all genes (gray, filled), and non-targets (black, empty) are shown.

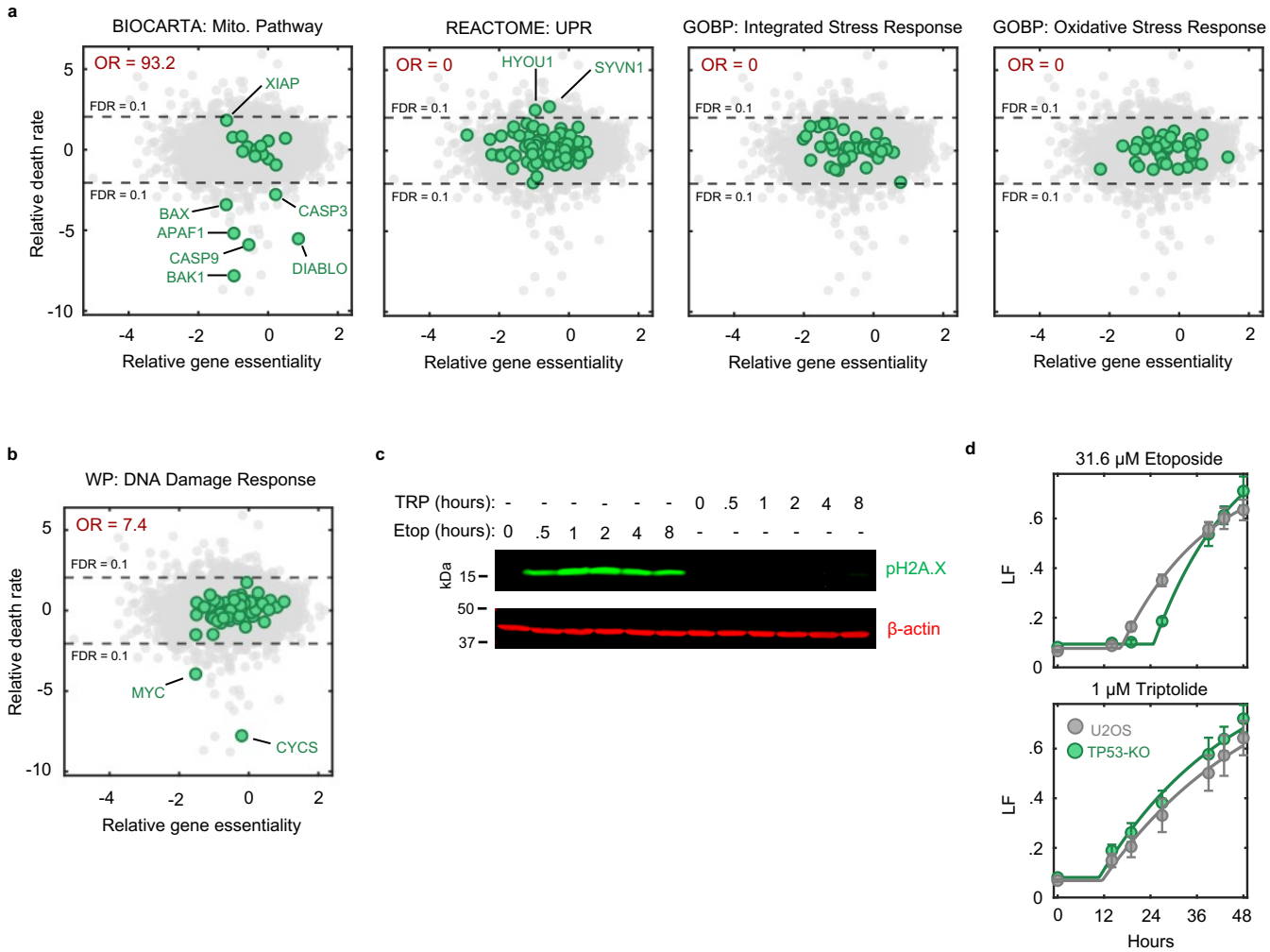

Extended Data Fig. 15: Triptolide-induced apoptosis does not depend on known stress response pathways. Related to Fig. 4. (**a**) Gene-level chemo-genetic profiling data for U2OS cells treated with 1 μM triptolide, highlighting genetic signatures associated with stress response pathways. Signatures defined from the Molecular Signatures Database (MSigDB). The mitochondrial pathway, involved in intrinsic apoptosis, are enriched (far left) among the genes whose knockout decreases triptolide-induced death. The unfolded protein response (UPR), integrated stress response (ISR), and the oxidative stress response are not enriched. Odds ratio for a one-tailed Fisher's exact test is shown (associated adjusted p-values are shown in Fig. 5D). (**b**) As in (a), but for genes associated with the DNA Damage Response (DDR). Two hits, MYC and CYCS, are more generally involved in apoptosis and are not specific to the DDR. (**c**) Immunoblot of phosphorylated H2A.X (Ser139) levels following 31.6 μM etoposide or 1 μM triptolide exposure in U2OS cells, demonstrating that triptolide does not induce DDR signaling, as compared to the DNA damaging drug etoposide. (**d**) Lethal fraction (LF) kinetics following exposure to etoposide or triptolide in U2OS cells or clonal U2OS-TP53 knockout cells, measured in FLICK. Loss of TP53 delays cell death following DNA damage, as previously described (Honeywell, et al., 2024). Loss of TP53 has no effect on cell death following triptolide. Data are mean ± SD for n = 9 independent biological replicates.

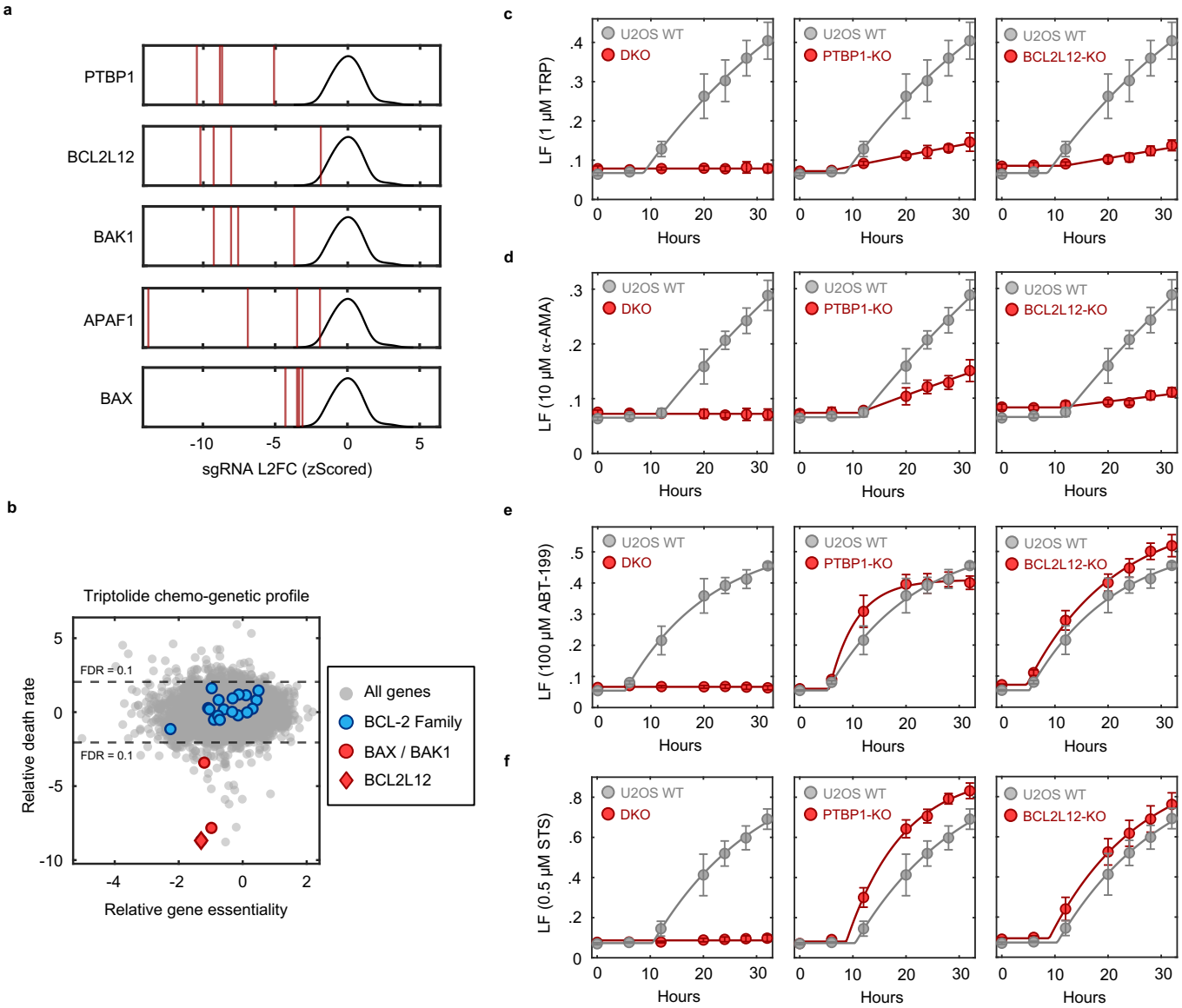

Extended Data Fig. 16: Validation of PTBP1 and BCL2L12 as unique genetic dependencies of lethality following Pol II degradation. Related to Fig. 4. (**a**) sgRNA-level log2 fold changes (dead population / live population) for PTBP1 and BCL2L12 in the context of 1 μM triptolide. BAK1, APAF1, and BAX are core apoptotic regulators and act as controls. Fold changes for 4 sgRNAs per gene (red vertical lines) were z-scored to the distribution of nontargeting guides (black). (**b**) Gene-level chemo-genetic profiling data for U2OS cells treated with 1 μM triptolide. BCL-2 family proteins regulate BAX and BAK1 activity. BCL2L12 is the only BCL-2 family protein identified that modulates cell death following triptolide (apart from BAX and BAK1 themselves). Highlighted BCL-2 family members in blue are MCL1, BCL2L1, BCL2L14, BCL2L10, BCL2A1, BCL2L2, BCL2L13, BAD, BOK, BMF, BCL2, BIK, BCL2L15, BCL2L11, and BID. (**c-f**) Cell death kinetics measured using FLICK in U2OS wild-type cells compared to BAX/BAK DKO (left), PTBP1-KO (middle), and BCL2L12-KO cells (right). **(c)** 1 μM triptolide. **(d)** 10 μM α-amanitin. **(e)** 100 μM ABT-199. **(f)** 0.5 μM Staurosporine. Data are mean ± SD for n = 6 independent biological replicates. Panels (c) and (d) are Pol II-degrading transcriptional inhibitors. Panels (e) and (f) are canonical apoptotic activators.

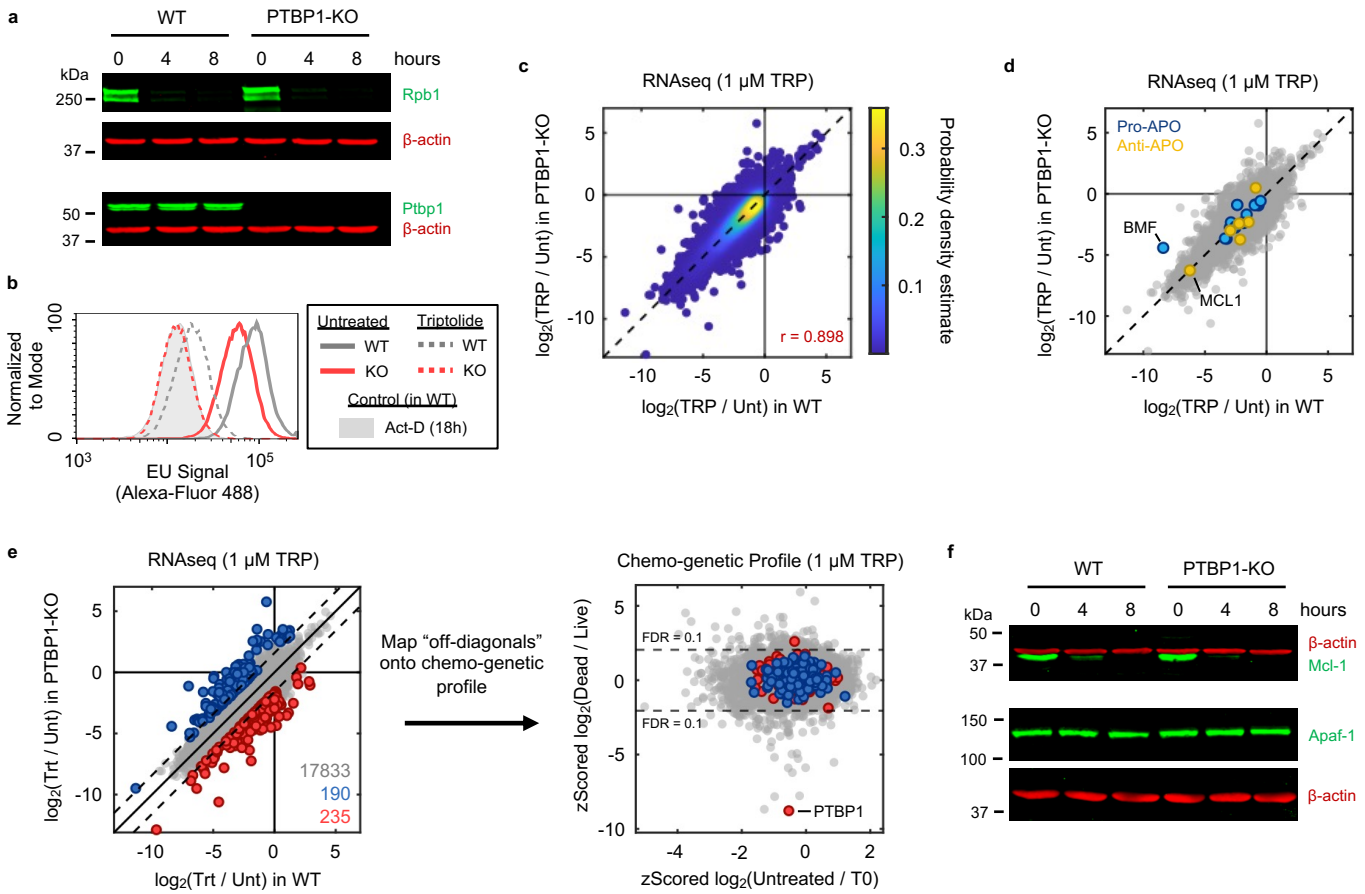

Extended Data Fig. 17: PTBP1 knockout has no effect on Pol II degradation, loss of nascent transcription, or loss of mRNA, following triptolide exposure. Related to Fig. 4. (**a**) Immunoblots for Rpb1 protein levels following exposure to 1 μM triptolide in U2OS and U2OS-PTBP1-KO. (**b**) EU incorporation into nascent RNA in U2OS and U2OS-PTBP1-KO. Cells treated with or without 1 μM triptolide for 8 hours prior to EU labeling. Populations are representative of 3 biological replicates. (**c**) RNAseq comparison of drug-induced transcriptional changes in wild-type (x-axis) and PTBP1-KO (y-axis) cells, measured 8 hours following treatment with 1 μM triptolide. Data were normalized using ERCC spike-ins. Dashed line, x = y. Correlation coefficient shown is for all genes. (**d**) RNAseq data as in (c), highlighting that established anti-apoptotic (Anti-APO) and pro-apoptotic (Pro-APO) regulators show similar expression changes following triptolide in WT and PTBP1-KO backgrounds. Anti-APO: BCL2, MCL1, BCL2L10, BCL2A1, BCL2L2, XIAP. Pro-APO: BCL2L14, BCL2L13, BAD, BOK, BMF, BIK, BCL2L11, BID, BAK1, BAX, APAF1, CASP3, CASP7, CASP8, CASP9, CYCS, DIABLO. (**e**) (Left) RNAseq data as in (c), identifying rare outlier genes whose expression is decreased more (red) or less (blue) in PTBP1-KO cells compared to WT cells following triptolide. The threshold for an "outlier" is depicted by the dashed lines, denoting 2.5 standard deviations from the identity line (x = y). Number of outliers shown. (Right) Mapping of expression outliers onto the chemo-genetic profile for triptolide. (**f**) Immunoblots for Mcl-1 and Apaf-1 protein levels following exposure to 1 μM triptolide in wild-type U2OS cells and U2OS-PTBP1-KO clones.

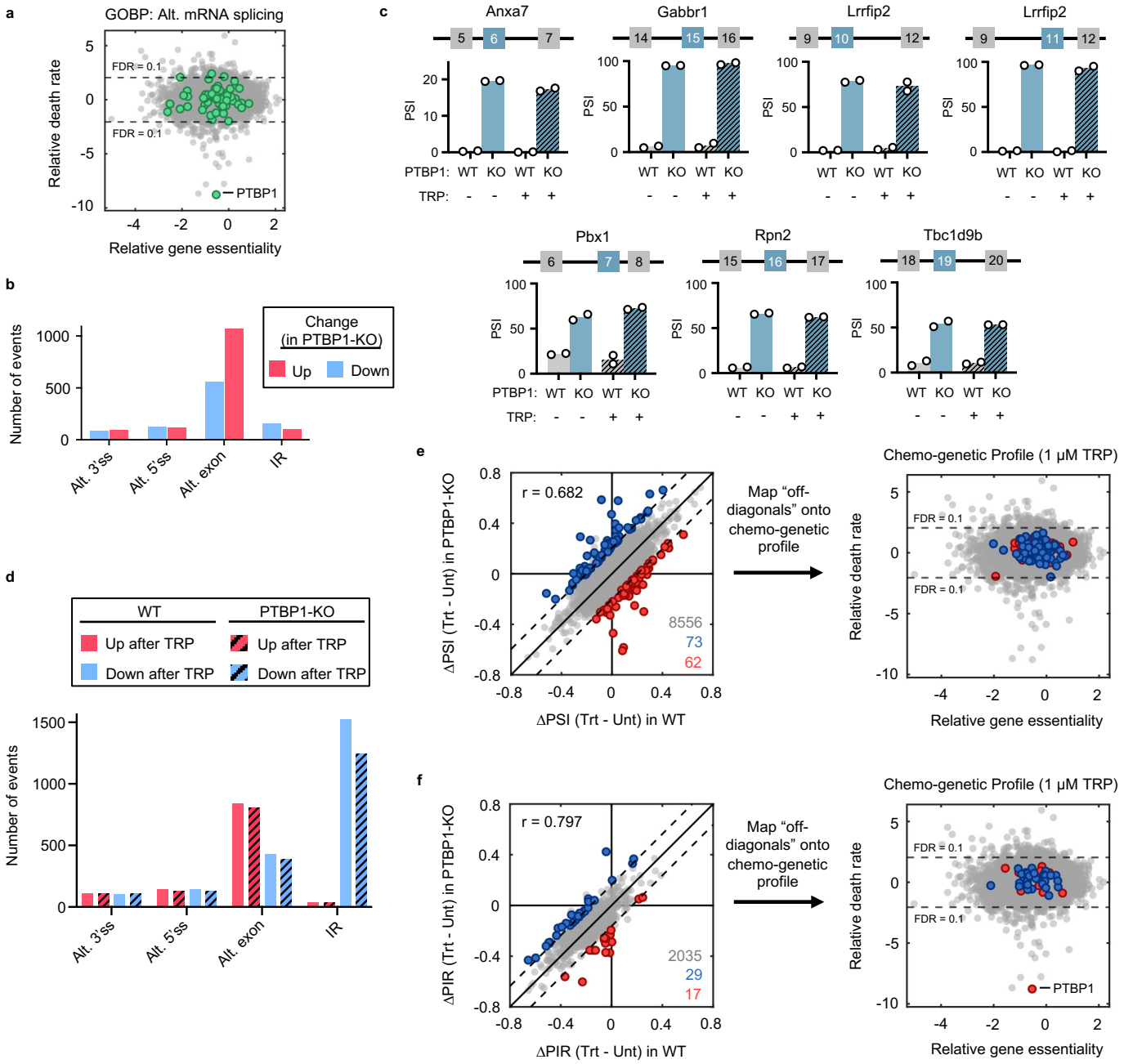

Extended Data Fig. 18: The role of PTBP1 in triptolide-induced lethality is unrelated to alternative splicing. Related to Fig. 4. (**a**) Chemo-genetic profiling data for U2OS cells treated with 1 μM triptolide highlighting genes that regulate alternative splicing, as defined by MSigDB. (**b**) Number and type of significant PTBP1-dependent splicing events identified by comparing U2OS and U2OS-PTBP1-KO RNAseq datasets. (**c**) Previously annotated PTBP1-dependent exon exclusion events. PSI: percent spliced in for the blue colored exon. Data are with- or without 1 μM triptolide for 8 hours. (**d**) Significant splicing alterations induced following 8-hour exposure to 1 μM triptolide in either U2OS (solid bars) or U2OS-PTBP1-KO (dashed bars) cells. (**e**) (Left) Comparison of drug-induced splicing changes in U2OS (x-axis) and U2OS-PTBP1-KO (y-axis) cells, measured 8 hours following treatment with 1 μM triptolide. Data include alternative 3' splice site, alternative 5' splice site, and alternative exon usage. Dashed lines denote 2.5 standard deviations from the identity line (x = y), and off-diagonals are highlighted. (Right) Mapping of outliers onto the chemo-genetic profile for triptolide. (**f**) As in (e), but specifically for intron retention (IR).

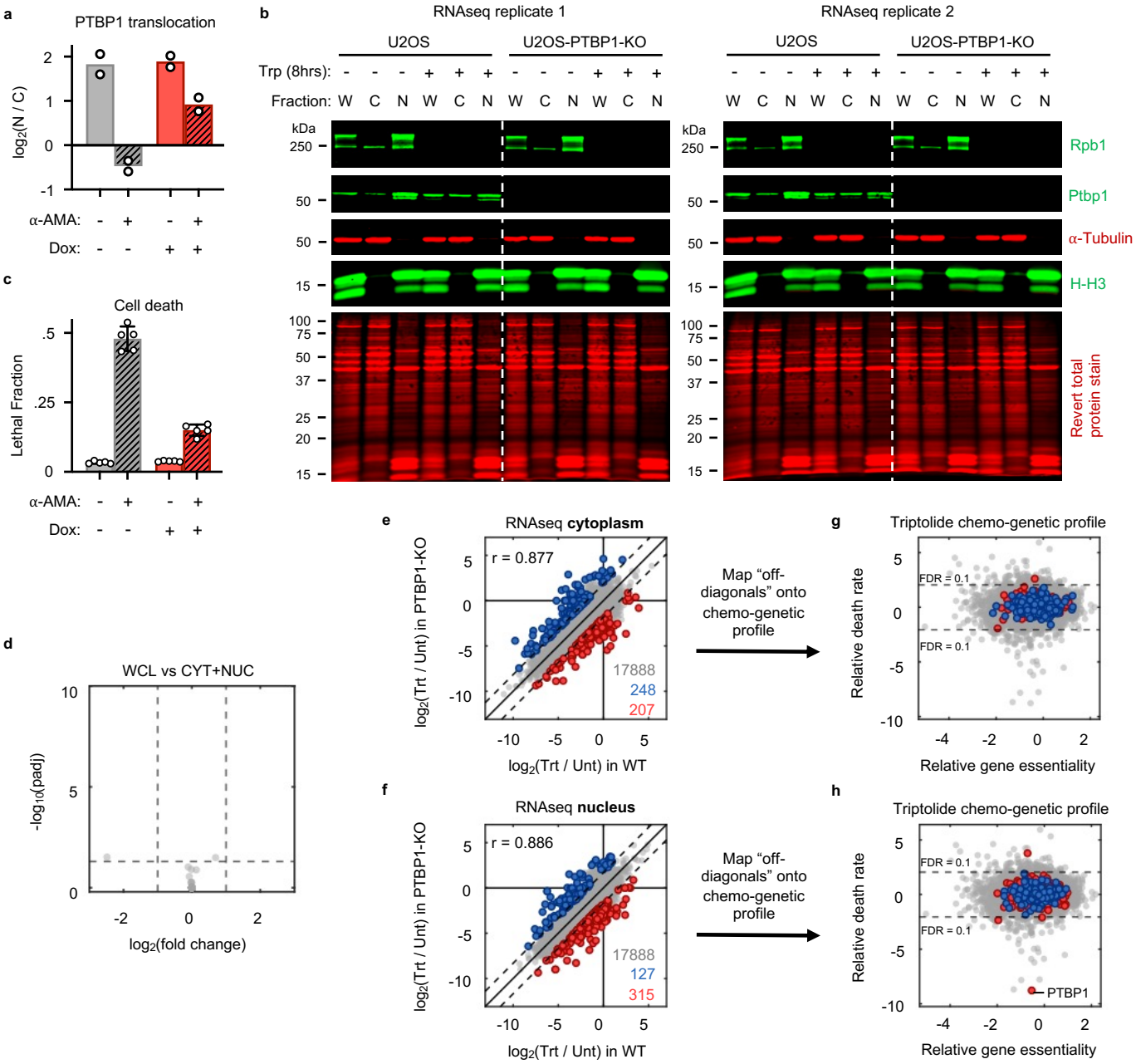

Extended Data Fig. 19: Evaluation of PTBP1 nuclear export following Pol II degradation. Related to Fig. 4. (**a**) Quantification of the nuclear-to-cytoplasmic ratio of PTBP1 protein before and after exposure to 10 μM α-amanitin for 12 hours in Pol II switchover cells, measured using immunoblotting. (**b**) PTBP1 translocation following triptolide (Trp) exposure. These samples were also used for RNA sequencing of nuclear and cytoplasmic fractions. Protein samples were simultaneously obtained from the identical cell lysates used to isolate and sequence mRNA. W: whole cell lysate; C: cytoplasmic fraction; N: nuclear fraction. (**c**) Lethal fraction measured 32 hours after exposure to 10 μM α-amanitin in Pol II switchover cells. Mean ± SD shown, n = 5 independent biological replicates. (**d**) RNAseq from cytoplasmic and nuclear fractions re-combined to recapitulate the whole cell mRNA extract, validating the quality of the fractionation. (**e**) Comparison of drug-induced expression changes of cytoplasmic mRNA in U2OS (x-axis) and U2OS-PTBP1-KO (y-axis) cells, following 8-hour exposure to 1 μM triptolide. Dashed lines denote 2.5 standard deviations from the identity line (x = y), off-diagonals are highlighted, and Pearson correlation coefficient of all genes is shown. (**f**) As in (e), but specifically for nuclear mRNAs. (**g**) Mapping of outliers from (e) onto the chemo-genetic profile for triptolide. (**h**) As in (g) but for panel (f).

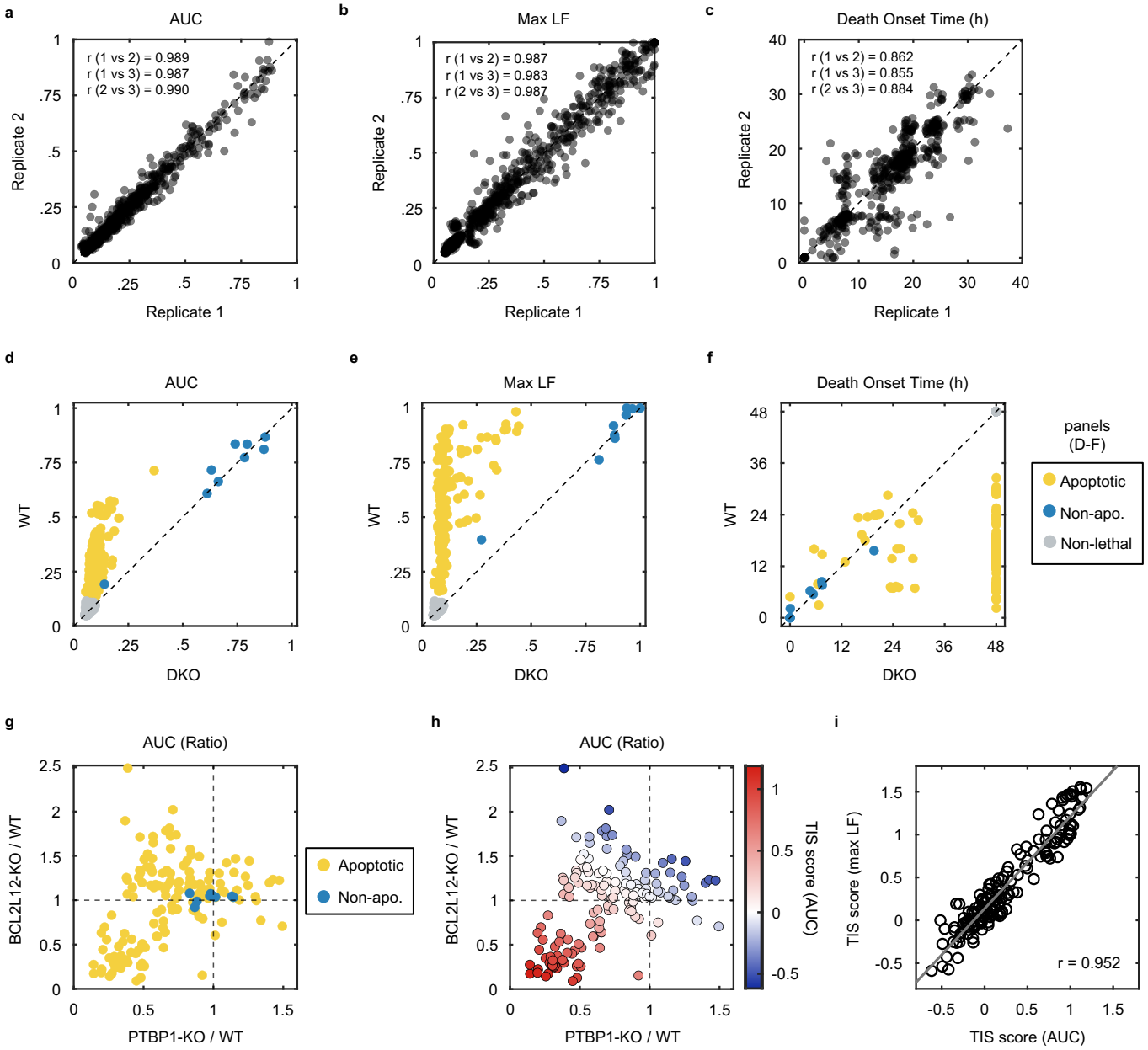

Extended Data Fig. 20: Evaluation of drug mechanism of killing using temporally resolved death kinetics. Related to Fig. 5. (**a**) Quality control for the drug screen shown in Fig. 5. Correlation of AUC values between replicates. Each point represents a single drug-dose-genotype combination, measured using FLICK. Dashed line, x = y. Pearson correlation coefficient for each pair of replicates is shown. (**b**) As in (a), but for the maximum lethal fraction observed at assay endpoint (48 hours). (**c**) As in (a), but for the onset time of death. (**d-f**) Comparison of responses between *BAX/BAK1* DKO cells and U2OS cells for each drug-dose pair. Each condition is classified as apoptotic, non-apoptotic, or non-lethal. (**g**) Comparison of the change in cell death response following knockout of PTBP1 (x-axis) or BCL2L12 (y-axis) for each lethal drug-dose pair. Values of 1 denote no difference from parental U2OS cells. (**h**) Plot depicting how TIS scores vary across the response space. (**i**) AUC is a non-biased metric for generating TIS scores. TIS scores were calculated using max LF in an identical manner as AUC, producing similar results. Linear regression line is shown, along with the Pearson correlation coefficient.

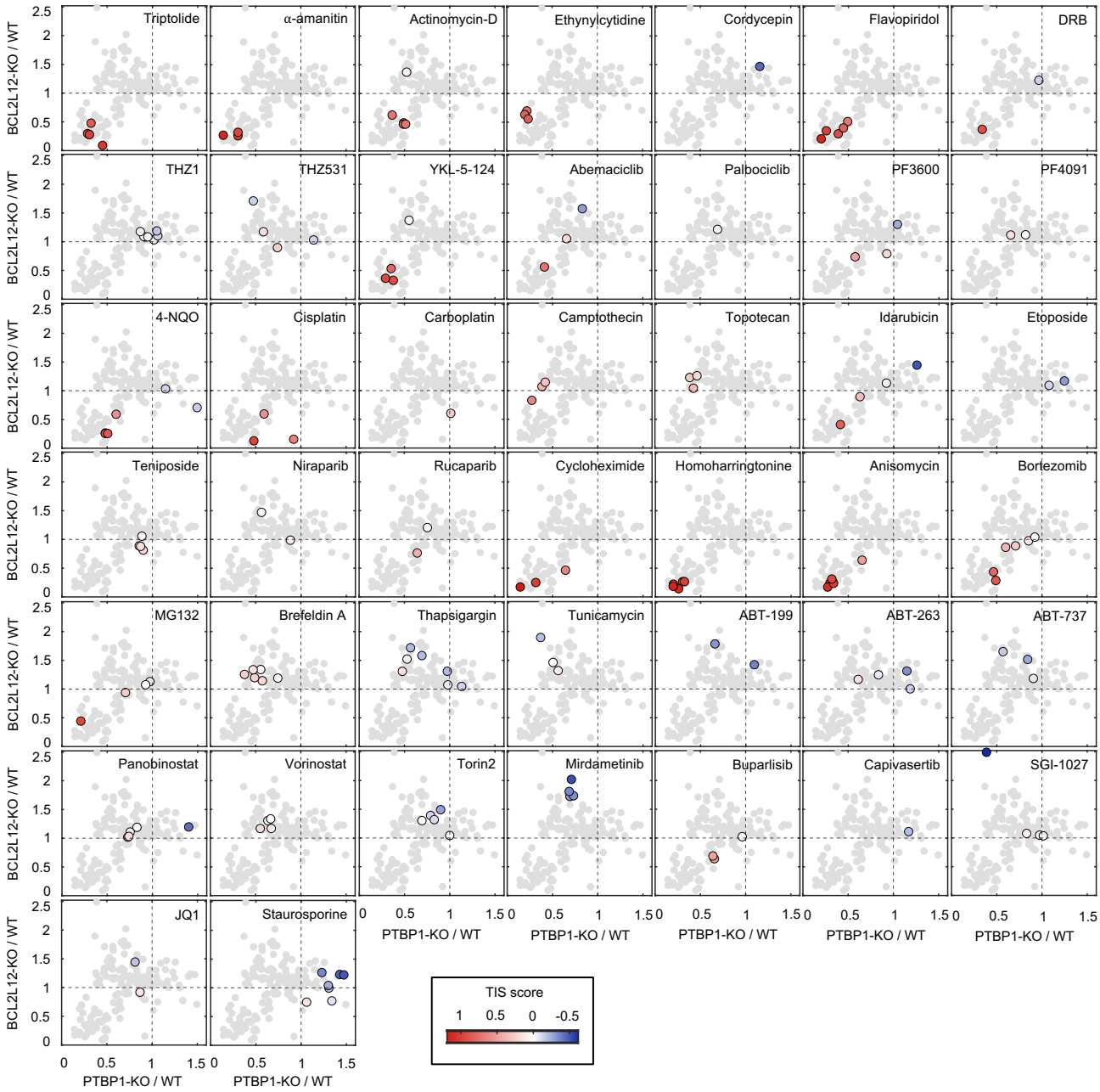

Extended Data Fig. 21: Evaluation of drug response using TIS score. Related to Fig. 5. Map of the functional effect of PTBP1 and BCL2L12 knockout on the cell killing of each drug-dose pair (gray points). For each lethal drug, lethal doses are shown and colored by TIS score. Color bar applies to all panels.

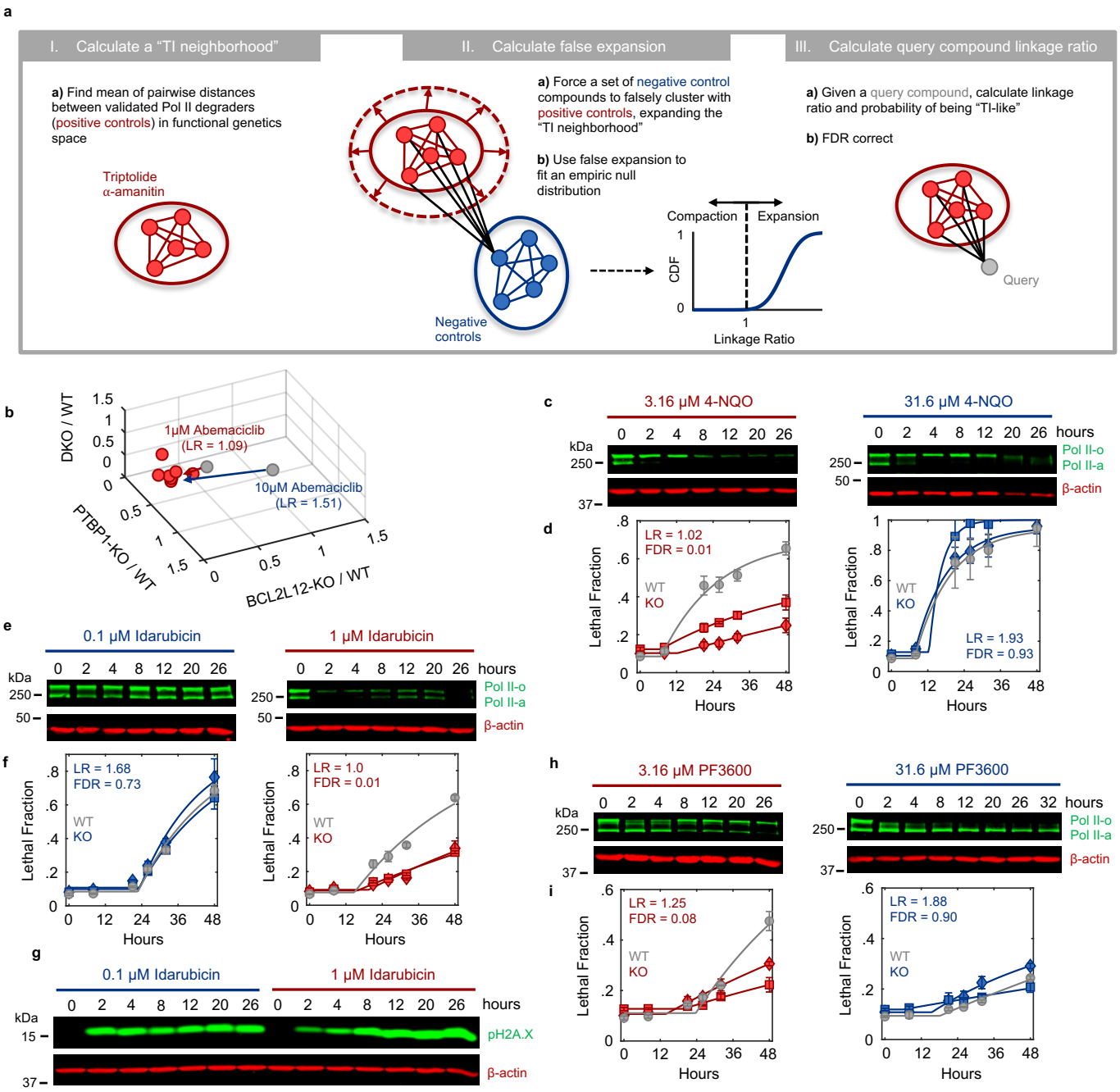

Extended Data Fig. 22: A statistical classifier to identify "TI-like" compounds. Related to Fig. 5. (**a**) Conceptual overview of the probabilistic nearest neighbors-based classification approach (adapted from Pritchard, et al., 2013). (**b**) Classification of Abemaciclib. Triptolide and α-amanitin (positive controls) are shown in red, Abemaciclib (query drug) is shown in gray. 1 μM Abemaciclib is classified as "TI-like", whereas the 10 μM dose is not. Linkage ratios (LR) are shown. (**c**) Immunoblots of Rpb1 protein levels in U2OS cells following exposure to two different doses of 4NQO (3.16 μM left, 31.6 μM right). (**d**) Lethal fraction kinetics for 1 μM Abemaciclib (left) and 10 μM Abemaciclib (right) in U2OS cells (gray circles), PTBP1-KO cells (squares) and BCL2L12-KO cells (diamonds), measured using FLICK. Linkage ratios and associated FDR values are shown. Data are associated with blots above (respectively) in (C). (**e-f**) As in (c-d) for 0.1 μM and 1 μM Idarubicin. (**g**) Similar DDR signaling, as measured by pH2A.X levels in immunoblot, are seen at both doses of Idarubicin shown in (e-f). (**h-i**) As in (c-d) for 3.16 μM and 31.6 μM PF3600. For all panels TI-like drugs are red, Not TI-like are blue. For all panels with error bars, data are mean ± SD, n = 3 independent biological replicates.

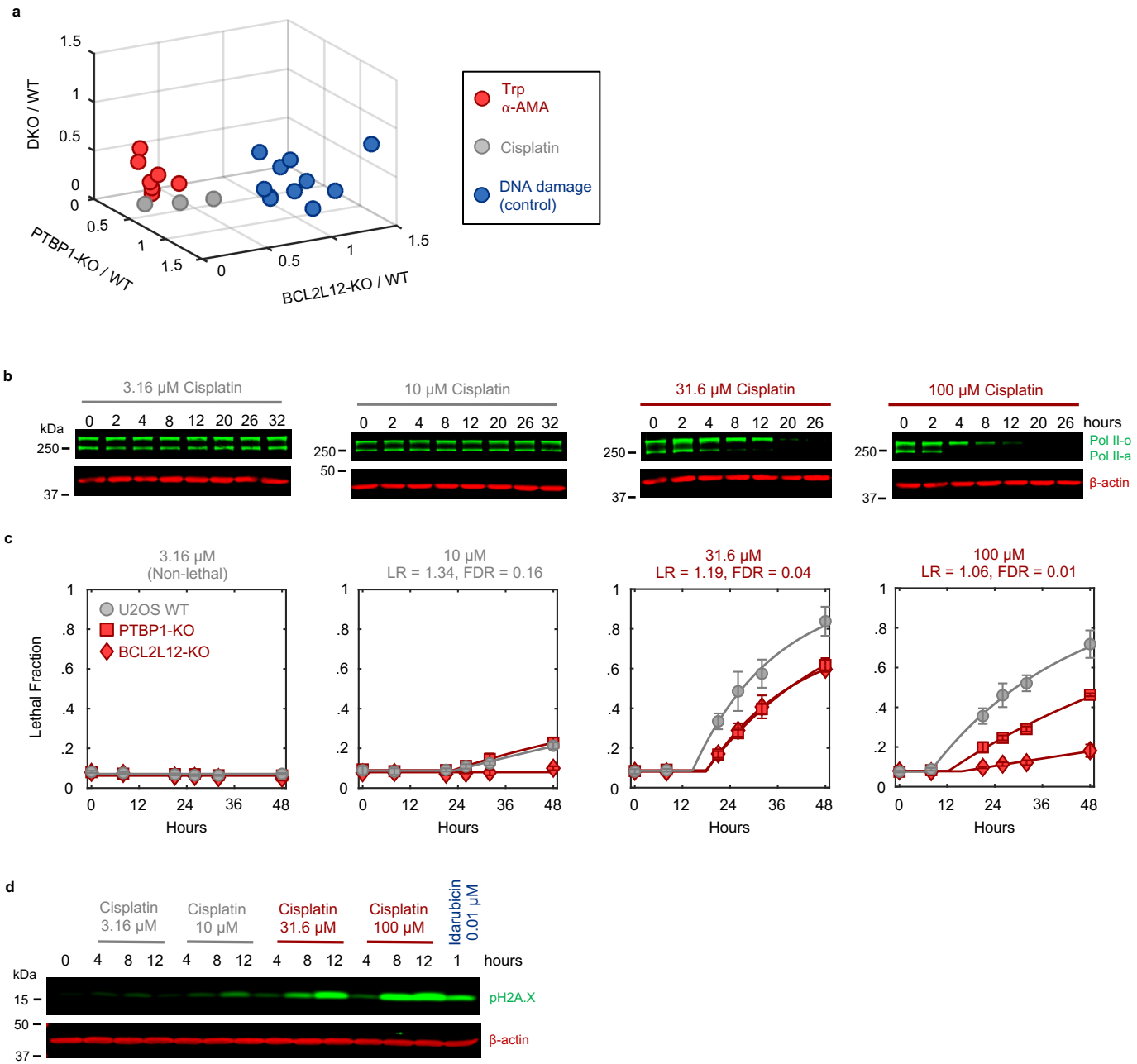

Extended Data Fig. 23: Lethal doses of Cisplatin require PTBP1 and BCL2L12 for cell killing and degrade Pol II protein. Related to Fig. 5. (**a**) Classification of Cisplatin. Triptolide and α-amanitin (positive controls) are shown in red, Cisplatin (query drug) is shown in gray. Other DNA damaging agents are shown in blue (Etoposide, Teniposide, Topotecan, and low-dose Idarubicin). (**b**) Immunoblots depicting Rpb1 protein levels over time following exposure to a range of Cisplatin doses. Images are representative of 3 independent biological replicates. (**c**) Lethal fraction kinetics of Cisplatin in U2OS, PTBP1-KO, and BCL2L12-KO cells, assessed at doses from (b). Linkage ratios and associated FDR values are shown. Data were collected in FLICK, and data are mean ± SD, n = 3 independent biological replicates. (**d**) Immunoblot of p-H2A.X levels across doses of Cisplatin. All doses of Cisplatin that induce appreciable amounts of p-H2A.X signaling are triptolide-like. A low, and non-lethal, dose of the DNA damaging agent Idarubicin is shown for comparison.

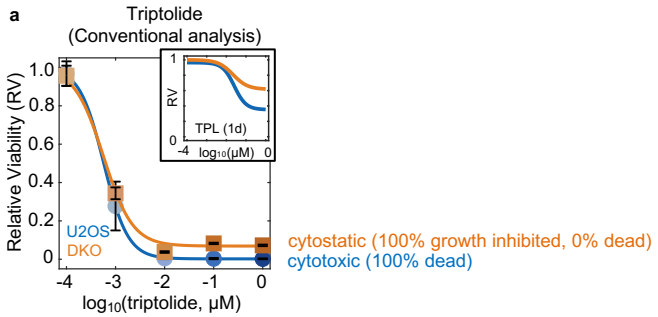

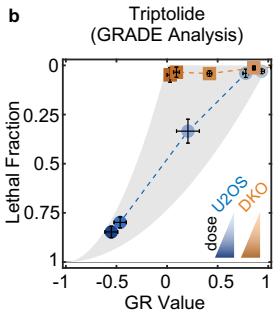

Extended Data Fig. 24: Conventional analysis metrics are insensitive to cell death and mask the existence of PDAR. (**a**) Triptolide (TPL) sensitivity in U2OS and DKO cells quantified using the conventional measure of drug sensitivity, Relative Viability (RV). RV was measured using the STACK assay 120 hours after drugging, or after 24 hours (inset). (**b**), GRADE analysis to infer the drug-induced growth rate and rate death rate from measurements of the lethal fraction and net population growth rate (GR value). Data for U2OS and DKO cells treated with triptolide for 48 hours, measured using STACK. For all panels with error bars, data are mean ± SD, n = 3 independent biological replicates.